

METABOLIC REWIRING OF MACROPHAGES PROMOTES ANTI-TUMOR ACTIVITY
IN PANCREATIC CANCER

Mingen Liu

A DISSERTATION

in

Cell and Molecular Biology

Presented to the Faculties of the University of Pennsylvania

in

Partial Fulfillment of the Requirements for the

Degree of Doctor of Philosophy

2018

Supervisor of Dissertation

Co-Supervisor of Dissertation

Gregory L. Beatty, MD, PhD
Assistant Professor of Medicine

Anil Rustgi, MD
Professor of Medicine

Graduate Group Chairperson

Daniel S. Kessler, PhD
Associate Professor of Pathology and Laboratory Medicine

Dissertation Committee

Brian Keith, PhD Kathryn Wellen, PhD
Andy Minn, MD, PhD
Todd Ridky, MD, PhD

METABOLIC REWIRING OF MACROPHAGES PROMOTES ANTI-TUMOR
ACTIVITY IN PANCREATIC CANCER

COPYRIGHT

2018

Mingen Liu

This work is licensed under the
Creative Commons Attribution-
NonCommercial-ShareAlike 3.0
License

To view a copy of this license, visit

<https://creativecommons.org/licenses/by-nc-sa/3.0/us/>

*To my aunt Cathy, who has been unwavering in her support of my endeavors, and a
constant bond for our family.*

Acknowledgment

First and foremost, I'd like to thank Dr. Gregory L. Beatty for his mentorship in my studies, through which he has help me grow professionally and personally. His relentless enthusiasm and patience in leading Team Macrophage has been invaluable for completing my dissertation research. I am also grateful for the support of Drs. Roddy O'Connor, Sophie Trefely, and Nathaniel W. Snyder as scientific collaborators, who have provided excellent guidance into new arenas of biology for me. I'd like to thank past and present members of the Beatty lab for their helpful suggestions, as well as Drs. Brian Keith, Anil Rustgi, Andy Minn, Todd Ridky, and Katy Wellen for their scientific critiques. I'd like to express my gratitude to Drs. Joseph Benci and Omkar Kawalekar for teaching me how to perform critical experiments, and many other classmates and colleagues who have helped me along the way. Finally, I am thankful for the support of Dr. Skip Brass, Maggie Krall, Maureen Kirsch, David Bittner in the Penn MSTP.

ABSTRACT

METABOLIC REWIRING OF MACROPHAGES PROMOTES ANTI-TUMOR ACTIVITY IN PANCREATIC CANCER

Mingen Liu

Gregory L. Beatty

Macrophages abound in the tumor microenvironment of pancreatic cancer and other solid malignancies. Although macrophages typically promote tumorigenesis, they also represent key targets for immunotherapy approaches, which aim to: 1) deplete macrophages, 2) inhibit their activity, or 3) redirect them toward an anti-tumor role. Redirecting macrophages is commonly described as a phenotypic shift from M2 (anti-inflammatory) to M1 (pro-inflammatory) polarization. However, macrophage phenotypes have grown increasingly diverse and only loosely describe functional roles. Here we examine the anti-tumor functions of macrophages – their ability to engulf and kill tumor cells – and the metabolic dependencies of this process, using a syngeneic and fully immunocompetent tumor model of pancreatic ductal adenocarcinoma (PDAC). In PDAC cells derived from KPC ($Kras^{LSLG12D/+}$; $Trp53^{R172H/+}$; $Pdx-Cre$) mice, the anti-phagocytic receptor CD47 was knocked out using transient CRISPR-Cas9 expression. CD47 is overexpressed by tumor cells to suppress macrophage anti-tumor activity and escape cancer immunosurveillance. Despite the critical role of CD47, we found that complete loss of CD47 in PDAC cells did not induce macrophage engulfment *in vitro*, nor did it impact tumor growth *in vivo*. We hypothesized that macrophages required an activated state, and found that ODN1826, a CpG oligonucleotide, could stimulate macrophages to

engulf tumor cells whether they expressed CD47 or not, and without inducing classical M1 or M2 markers. Moreover, CpG treatment of tumor-bearing mice induced potent anti-tumor responses that required macrophages, but not lymphocytes, natural killer cells, or dendritic cells. CpG activation was found to promote oxidative respiration dependent on fatty acid oxidation, along with rewiring of the Krebs cycle through the activity of ATP citrate lyase. Together, these changes represented a hybrid of M1 and M2 metabolisms, and were critical for macrophage engulfment of PDAC cells and anti-tumor activity. Our findings indicate that immune activation of macrophages alter their metabolic state rather than their M1/M2 phenotype to enable them to overcome inhibitory CD47 and carry out anti-tumor activity.

Table of Contents

Acknowledgment	iv
Abstract	v
List of Tables	ix
List of Illustrations	x
Chapter 1: Introduction	1
Tumor inflammation has dual roles in governing tumorigenesis.	1
Harnessing tumor inflammation for therapeutic benefit in pancreatic cancer	3
Activating tumor inflammation through PRRs (pattern recognition receptors)	4
Tumor macrophages can adopt pro-or anti-tumor phenotypes	6
Linking macrophage phenotype with macrophage metabolism	9
Pro-and anti-phagocytic immune checkpoints govern macrophage function.....	10
Dissertation Objectives	14
Figures.....	16
Chapter 2: Therapeutic Strategies for Harnessing Tumor Inflammation	18
Abstract.....	18
Introduction.....	18
Conclusion	30
Figures.....	32
Tables.....	33
Chapter 3: Metabolic rewiring of macrophages by CpG potentiates clearance of cancer cells and overcomes tumor-expressed CD47	36
Abstract.....	36
Introduction.....	37
Results.....	39
Discussion.....	49
Figures.....	57
Chapter 4: Summary and Future Directions	91
Summary	91

Optimizing phagocytic program for engulfing and degrading tumor cells.....	91
Overcoming resistance to CpG-induced anti-tumor activity: Completing the cancer immunity cycle.....	93
Integrating metabolism of effector cells, tumor microenvironment, and hosts	95
Therapeutic opportunities beyond the primary tumor	96
Chapter 5: Materials and Methods	99
Experimental Model and Subject Details	99
Method Details.....	99
Tables: Reagents	110
References	113

List of Tables

Table 1: Inflammation-based prognostic scoring systems.	33
Table 2: Active clinical studies combining FDA-approved immune checkpoint inhibitors and inflammation-directed therapies.....	34
Table 3: Flow cytometry and immunohistochemistry antibodies.....	110
Table 4: Immunohistochemistry and immunofluorescence antibodies.....	111
Table 5: Methods and software references.	112

List of Illustrations

Figure 1: Beyond M1 and M2, macrophage anti-tumor potential defined by metabolic and functional features.....	16
Figure 2: Strategies to target inflammation for cancer therapy.	32
Figure 3: Macrophage activation via TLR agonists, but not disruption of CD47, induces anti-tumor activity in a model of pancreatic cancer.....	57
Figure 4: CD47 expression in murine PDAC tumor cells.	59
Figure 5: CpG stimulates macrophage-dependent anti-tumor activity in vivo.....	60
Figure 6: Toxicity assessment of etomoxir and CpG in macrophages and PDAC cells.	62
Figure 7: In vivo delivery of CpG to tumor-bearing mice induces systemic cytokine release.	64
Figure 8: Macrophage engulfment of PDAC.1 cells in vivo.	65
Figure 9: Depletion of tumor macrophages using anti-CSF1R antibody attenuates the anti-tumor response of CpG.....	66
Figure 10: Flow cytometric and histologic quantification of tumor-associated myeloid cells in mice treated with or without a CSF1R inhibitor (CSF1Ri).....	67
Figure 11: CpG-treatment does not alter T cell activation or infiltration into tumors.....	69
Figure 12: T cells and natural killer (NK) cells are dispensable for CpG-induced anti-tumor activity.	71
Figure 13: Dendritic cells are not required for CpG-induced anti-tumor activity.	72
Figure 14: CSF1R+ F4/80+ Ly6C+ macrophages are required for CpG-induced anti-tumor response.	73
Figure 15: CpG stimulates macrophage anti-tumor activity in vitro and in vivo that is independent of the anti-phagocytic signal CD47 expressed on PDAC cells.	75
Figure 16: CpG-activation induces macrophage engulfment of tumor cells of multiple cancer types.....	77
Figure 17: Calreticulin abundance in Mock- and CpG-BMDMs.	79
Figure 18: CpG evokes metabolic changes in macrophages without polarization to M1 or M2.	81

Figure 19: Phenotypic differences in mock- and CpG-treated macrophages.	83
Figure 20: Extracellular acidification and oxygen consumption rates in TLR-activated BMDMs.	85
Figure 21: Fatty acid oxidation induced by CpG is essential for macrophage anti-tumor activity.....	87
Figure 22: Metabolic rewiring of TCA cycle supports the oxidative phenotype and anti-tumor activity of CpG-activated macrophages.	89
Figure 23: CpG-activation of macrophage metabolism leads to CD47-independent anti-tumor activity.	90

Chapter 1: Introduction

Tumor inflammation has dual roles in governing tumorigenesis.

Tumors are characterized as wounds that never heal, commonly featuring immune infiltrate that pervade the stroma of solid tumors.¹ This infiltrate includes a diverse mix of innate immune cells (e.g. macrophages, granulocytes, dendritic cells, etc) and adaptive immune cells (cytotoxic T cells, helper T cells, regulatory T cells, etc) that facilitate tumor-promoting inflammation.² Tumor inflammation supports tumorigenesis by reinforcing the hallmarks of cancer progression – including angiogenesis, metastasis, and DNA damage – although these effects can also be attenuated and reversed by altering the activity of immune cell populations.³

Under the right conditions, immune cell effectors are capable of targeting and eradicating tumor cells through cancer immunosurveillance.^{4,5} Immune-mediated clearance of tumor cells has been described as the ‘cancer immunity cycle’, a multistep process involving the concerted activity of both innate and adaptive immunity.⁶ Therapeutic advances in cancer immunotherapy aim target discrete steps of the cancer immunity cycle: 1) release of cancer cell antigens, 2) presentation by antigen presenting cells (APCs), 3) priming and activation of T cells, 4) T cell trafficking to tumors, 5) recognition and killing tumor cells. For example, clinical inhibitors of immune checkpoints, which target PD-L1 and CTLA-4, sustain T cell cytolytic activity against tumor cells.^{7,8} Other promising treatment modalities, such as cancer vaccines and oncolytic viruses, stimulate release of immunogenic components from tumor cells.^{9,10}

Understanding mechanisms underpinning each of these steps will be imperative for enacting the cancer immunity cycle.

Despite these advances, novel immunotherapies do not benefit all patients or all cancer types. Systematic profiling of immune infiltrate in tumors indicate that the heterogeneous responses of tumors to immunotherapy arise from tumor cell-intrinsic and -extrinsic properties.¹¹ Tumor cell-intrinsic properties include varying frequency of mutations across cancers, which give rise to immunogenic epitopes that can be recognized by T cells, or expression of immune checkpoint molecules that suppress cancer immunosurveillance.^{12,13} Cancers that respond to checkpoint immunotherapies (e.g. melanoma and non-small cell lung cancer) correspond with high mutational burden, but cancers that respond poorly (e.g. pancreatic cancer) lack mutational epitopes for T cells to target.^{14,15} Tumor cell-extrinsic properties include the suppression and exclusion of cytotoxic T cells, as well as the presence of myeloid cells in the stroma that contribute to an immunosuppressive milieu.¹⁶ In the tumor microenvironment, as in pancreatic cancer for example, the desmoplastic tumor stroma precludes T cell entry and the abundant myeloid infiltrate suppresses anti-tumor activity. These properties collectively render tumors as ‘hot’ or ‘cold’, which describe the composition of immune infiltrate governing therapeutic responsiveness.^{17,18}

As a hallmark feature of inflammation, macrophages dominate the tumor microenvironment of many cancers, such as pancreatic cancer.¹⁹ Macrophages commonly restrain anti-tumor activity and mediate resistance to chemotherapy, radiotherapy, and immunotherapy.^{20,21} Thus, depleting macrophages or shifting their properties represent promising therapeutic approaches for mitigating treatment resistance and complementing

strategies that target tumor cells or other immune cells.^{22,23} Understanding the critical determinants of macrophage function will be critical for achieving therapeutic effects through macrophage-directed immunotherapy.

Harnessing tumor inflammation for therapeutic benefit in pancreatic cancer

Pancreatic cancer is the fourth leading cause of cancer deaths in the United States. Without appropriate screening measures for pancreatic cancer, approximately 80% of patients have disseminated disease upon diagnosis and require systemic treatment with chemotherapy.²⁴ The five-year survival of pancreatic cancer patients remains dismal at 8.5%, despite recent clinical advances with the approval of new chemotherapy regimens such as FOLFIRINOX (Folate + 5-Fluorouracil + Irinotecan + Oxaliplatin) and the combination of nab-paclitaxel and gemcitabine.^{25,26} Thus, it is imperative to develop new treatment modalities for pancreatic cancer that can enhance standard-of-care chemotherapy.

However, immunotherapeutic agents that have demonstrated efficacy in other solid tumors have largely failed to generate clinical responses in pancreatic cancer. These agents include novel therapies targeting T cell checkpoints (e.g. CTLA-4 and PD-L1), which have improved patient survival in melanoma, non-small cell lung cancer, bladder cancer, kidney cancer, etc. Even though checkpoint inhibition has shown promise against a subset of pancreatic tumors with defective DNA mismatch repair – which gives rise to more immunogenic antigens T cell responses – pancreatic tumors more typically express few neoantigens that are conducive for checkpoint inhibition or T cell directed therapies.²⁷⁻²⁹

Despite the challenges encountered by T cell directed approaches in pancreatic cancer, several immunotherapies have shown promise as single agents or in combination with other treatments. For example, an agonistic antibody against co-stimulatory receptor CD40 has shown clinical benefit in phase I/II clinical trials.^{30,31} In part, agonistic CD40 antibodies activate macrophages to drive the degradation of the desmoplastic stroma commonly found in pancreatic tumors.³¹ Stromal degradation, in turn, enhances the effectiveness of chemotherapy and facilitate T cell responses.³²⁻³⁴ When combined with chemotherapy and checkpoint molecules, such as anti-CTLA4 and anti-PD-L1 antibodies, CD40 agonists can promote antigen presentation and potentiate durable anti-tumor responses in a murine model of pancreatic ductal adenocarcinoma (PDAC).³⁵ These studies demonstrate how immune agonists can drive a coordinated anti-tumor response by innate and adaptive immunity.

Activating tumor inflammation through PRRs (pattern recognition receptors)

The forerunner to modern immunotherapy can be traced to the development of Coley's toxins in the early twentieth century. Predating the advent of antibiotics, New York-based surgeon Dr. William Coley observed that many of his patients who developed *erysipalis*, skin infections caused by *Staphylococcus* bacteria, also experienced spontaneous regressions of unresectable tumors. To test his hypothesis that inflammation drove these tumor regressions, Dr. Coley purified crude bacterial extracts from skin lesions (known colloquially as 'Coley's toxins') and administered these to his cancer patients.³⁶ This treatment led to severe inflammatory responses in his patients and occasional long-term tumor regressions. Without molecular techniques to study the

phenomenon that Dr. Coley observed, it would be nearly a full century before immunotherapy would be considered a viable modality for cancer treatment.

The bacterial extracts that Dr. Coley isolated would have contained molecules now known to activate pattern recognition receptors (PRRs) expressed in immune cells, particularly antigen presenting cells (APCs).³⁷ Recognition of pathogen-associated molecular patterns (PAMPs), such as bacterial DNA motifs or cell wall components, stimulates PRRs to trigger maturation of APCs and a potent immune response. One such molecule is imiquimod, which activates TLR7 (Toll-like receptor 7) belonging to a family of PRRs called Toll-like receptors (TLRs). Imiquimod is used as a clinically-approved agent for treating skin tumors (i.e. superficial basal cell carcinoma and squamous cell carcinoma) by stimulating skin-resident APCs such as Langerhans cells to mobilize an immune response.^{38,39}

Multiple other activators of TLRs and PRRs have been investigated for their anti-tumor properties, particularly as adjuvants for cancer vaccines. These agonists include bacterial or viral DNA motifs known as Poly I:C and unmethylated CpG, which activate TLR3 and TLR9 respectively.^{40,41} Treatment using CpG has been examined in multiple early-phase clinical trials for lung cancer, melanoma, and lymphoma.⁴²⁻⁴⁴ Though CpG treatment exhibited promising anti-tumor activity shown in early phase studies, phase 2/3 clinical trials failed to demonstrate efficacy for CpG in combination with chemotherapy for treating melanoma, and also induced immune-related adverse events that led to discontinuation of studies.⁴⁵ Despite these clinical setbacks, ongoing investigation has indicated that the anti-tumor activity of CpG can be enhanced by addition of other modalities in preclinical models. For example, stimulation with CpG and agonists

directed against immune checkpoint OX40,⁴⁶ can potentiate potent responses that involve adaptive immunity. Additionally, blockade of interleukin-10 receptor in conjunction with CpG-treatment generated anti-tumor responses that were dependent on macrophages.⁴⁷ Inhibition of interleukin-10 receptor critically suppresses the anti-inflammatory effect of interleukin-10 generated upon immune activation. These data indicate that agents targeting Toll-like receptors, such as CpG, remain a potential therapeutic for cancer treatment, particularly for their ability to broadly activate macrophages and other immune cells.

Tumor macrophages can adopt pro-or anti-tumor phenotypes

Tumor macrophages can adopt a pro- or anti-inflammatory role, which in turn, inhibit or promote the growth of tumors. The opposing roles of macrophages are commonly described pro-inflammatory M1 and anti-inflammatory M2 phenotypes.²¹ M1 macrophages are induced by interferon- γ and lipopolysaccharide, and are typified by their ability to generate nitric oxide species through inducible nitric oxide synthase (iNOS), and secretion of interleukin-12.⁴⁸ These properties not only orchestrate a pro-inflammatory response, but also direct helper T cells toward Th1 response that supports cytotoxic responses against tumor cells. In contrast, M2 macrophages are induced by interleukin-4, and drive CD4 T cells toward a Th2 response associated with chronic inflammation conducive to tumor growth. Additionally, M2 macrophages express arginase-1 that catabolizes arginine to inhibit the production of nitric oxide.⁴⁹ Macrophages can further exert immunosuppressive effects by generating indoleamine-

pyrrole 2,3-dioxygenase, an enzyme that critically depletes the tumor microenvironment of tryptophan necessary for T cell responses.⁵⁰

The functional effect of macrophage polarization varies widely under different physiologic and pathologic contexts. In normal physiological roles, macrophages in the spleen facilitate clearance of senescent red blood cells, and osteoclasts regulate the breakdown and homeostasis of bone. However, in atherosclerotic disease, inflammation driven by M1 macrophages ultimately facilitate uptake of lipids by macrophages, leading to a foam cell phenotype associated with M2 macrophages. Macrophages in tumor microenvironments commonly adopt an M2 phenotype that not only restrain adaptive immune responses, but also enhance tumor vascularity and metastatic spread.^{21,51} In diseases such as diabetes, perturbations of nutrient availability give rise to unique states of metabolic activation that are distinct from classical M1 and M2 phenotypes.^{52,53} When using systems approaches to assess the response of human macrophages to a wide range of inflammatory stimuli, macrophages were found to exhibit a spectrum of activation, which were characterized by gene expression changes in core metabolic processes. These studies support a recent paradigmatic shift away from distinct classes of macrophage polarity, and toward an appreciation for how macrophage activation spans a spectrum of phenotypes.

The association between macrophage polarization and function is poorly understood. For example, M2 macrophages that are commonly associated with a pro-tumor role surpass M1 macrophages in performing antibody-directed cellular phagocytosis – or engulfment of tumor cells opsonized with antibodies. In macrophages cultured from human donors, this superior phagocytic ability of M2-polarized

macrophages was dependent on the Fc-receptor, as genetic variants in Fc-receptors associated with loss of augmented activity. Activation of macrophages can also coordinately regulate effector functions, such as cytokine secretion and bacterial clearance. Consequently, stimulation with LPS and CpG induces changes in a conserved network of lipid regulators that are associated with altered membrane fluidity and cytokine secretion. These data indicate that stimuli that activate phenotypic polarization also impact macrophage function, although the mechanisms underlying this relationship require further elucidation.

Macrophage activation through TLRs stimulates inflammatory functions beyond cytokine secretion, but also promote macrophage functions such as phagocytosis.^{54,55} For example, TLR activation can stimulate a unique phagocytic program in macrophages and other phagocytes known as LC3 (Light Chain 3-like protein)-associated phagocytosis (LAP).⁵⁶ Specifically, LAP is activated by TLR 1/2, 2/6, and 4 pathways, and induces the aggregation of LC3 and other autophagy-associated machinery to phagolysosomes.⁵⁷ These LC3-associated vesicles fuse with phagosomes to facilitate degradation of the phagocytic load, and demonstrate how metabolically reprogramming regulates macrophage function.⁵⁸ This process is distinct from autophagy in that LC3-vesicles facilitate breakdown of internalized loads during LAP, rather than degradation of cytosolic components as observed during canonical autophagy.⁵⁹ LAP operates during macrophage engulfment of bacteria and fungi (e.g. *Aspergillus fumigatus*), and during immunologically silent clearance of apoptotic cells.^{54,59} TLR9 stimulation has also been shown to trigger production of type I interferons dependent on the formation of LC3-associated phagosomes.⁵⁹ The ability of select TLR pathways to induce unique modes of

phagocytosis indicates that TLR-based therapies may likewise modulate macrophage function in the setting of cancer.

Linking macrophage phenotype with macrophage metabolism

The phenotypic shift accompanying macrophage activation also corresponds changes to metabolic alterations. For example, M1 macrophages often adopt a glycolytic phenotype upon stimulation to bacterial lipopolysaccharide (LPS).⁵¹ Metabolic features of M1 macrophages include increased glycolytic flux and lactate production, accompanied by decreased oxidative phosphorylation and oxygen consumption.^{60,61} Pharmacologic inhibition of these glycolytic processes also inhibited generation of interleukin-1 β , indicating an intricate link between metabolic phenotype and macrophage function.⁶⁰

In contrast, M2 macrophages are often characterized by enhanced oxidative phosphorylation and lipogenesis, which are stored as lipid droplets.⁶¹⁻⁶³ However, other studies contend that this oxidative phenotype is dispensable for M2 polarization using interleukin-4.⁶⁴ When assessed using approaches such as gene expression and metabolite tracing, M1 and M2 macrophages are distinct in a range of metabolic pathways. In addition to differences in glycolysis and Krebs cycle intermediates, M1 macrophages exhibit elevated production of itaconate, whereas M2 macrophages upregulate *de novo* synthesis of nucleotides.⁶⁵ Another hallmark feature of M2 activated macrophages is their elevated usage of glutamine-derived substrates,⁶⁶ in which glutaminolysis leads to incorporation of carbons from glutamine into the Krebs cycle. Activation of this pathway is critical for the function of M2 macrophages in clearing microbial infection *in vitro* and

in vivo. Thus, not only do classical M1 and M2 macrophage phenotypes exhibit distinct metabolic profiles, but they also integrate multiple substrate pathways to support their functions.

The association between macrophage phenotype and metabolism resembles the link observed in other immune cells. T cell activation can direct phenotypic and functional shifts that are underpinned by metabolic changes. For example, effector T cells show an increased reliance on glycolytic metabolism,⁶⁷ as opposed to memory T cells, which exhibit a dependence on fatty acid metabolism, acetate consumption, and autophagy.⁶⁸⁻⁷⁰ Similarly, for myeloid derived suppressor cells in cancer, fatty acid oxidation is critical for their immunosuppressive function.⁷¹ The metabolic shift of immune cells can also be elicited by TLR stimulation; plasmacytoid dendritic cells treated with CpG can activate fatty acid oxidation to enhance production of type 1 interferons.⁷² Together, these findings underscore how metabolic changes in immune cells can broadly regulate their phenotype and function.

Pro-and anti-phagocytic immune checkpoints govern macrophage function

Macrophage function is governed immune checkpoints. The phagocytic function of macrophages is determined by the balance of pro- and anti-phagocytic signals.^{73,74} Pro-phagocytic cues include Fc-receptor signaling upon engagement of macrophage Fc-receptors by antibodies bound to cells targeted for phagocytosis.^{75,76} Another major pro-phagocytic signal regulating macrophage phagocytic function are oxidized phospholipids on the cell membrane of senescent cells (e.g. red blood cells).^{77,78} As phospholipids accumulate on the outer cell membrane, mediated by the activity of flippase enzymes,

these phospholipids are recognized by TIM4-receptors expressed by macrophages and stimulate phagocytosis.⁷⁹⁻⁸¹ Similarly, calreticulin is a second major pro-phagocytic signal present on the surface of apoptotic and tumor cells, which engages lipoprotein receptor-related protein on macrophages and promote phagocytosis.^{55,73} Finally, a third pro-phagocytic signal can be induced by MerTK (Mer Tyrosine Kinase) expressed by phagocytes, which can bind multiple ligands and promote clearance of apoptotic cells.^{82,83} The mechanisms by which multiple pro-phagocytic pathways integrate in macrophages to coordinate their activity remains unclear.

These pro-phagocytic signals are counterbalanced by negative regulators such as CD47.⁸⁴ CD47 is a ubiquitously expressed receptor on all cells, and suppresses phagocytic activity by binding SIRP α (Signal Regulatory Protein α)-receptor found on phagocytes. Upon binding, SIRP α triggers phosphorylation and activation SHP1 phosphatase.⁷⁷ SHP-1 activation in turn suppresses the phosphorylation of myosin-IIa, which represents a critical step required to form a phagocytic cup around cells targeted for engulfment.⁸⁵ CD47 has also been implicated in conferring protection from radiation damage in tissues and cellular stemness as well.^{86,87}

The anti-phagocytic role of CD47 is coopted by multiple types of tumors as a mechanism of immune escape. Tumor cells can evade cancer immunosurveillance by the immune system through overexpression of CD47, which can function as a prognostic of survival for patients with these cancers.⁸⁸ In preclinical models, inhibition of CD47 and SIRP α binding using a CD47-blocking antibody can generate potent anti-tumor responses in xenograft human tumors implanted into NSG (NOD *scid* gamma) mice lacking natural killer, B, and T cells.⁸⁹ Similar agents, such as a fusion SIRP α -Fc protein containing

SIRP α analog fused to an Fc domain, can block CD47-SIRP α binding while simultaneously providing a pro-phagocytic signal through the Fc-receptor.⁹⁰ The efficacy of these agents can be bolstered by concomitant treatment with tumor binding antibodies – including clinically available antibodies (e.g. rituximab, cetuximab, etc) directed against surface proteins found to be commonly overexpressed in tumors.⁹¹ These CD47-targeting treatment combinations can eradicate cancer stem cells and significantly enhance survival in preclinical studies.⁸⁹

Administration of CD47-blocking antibody can elicit pleiotropic anti-tumor effects. In xenograft models of glioblastoma, CD47-blockade induces macrophage anti-tumor activity that is characterized by polarization of tumor macrophages toward an M1 phenotype associated with anti-tumor activity.⁹² The pro-phagocytic role of CD47-blockade can be similarly enhanced by stimulating macrophages with agonists of Toll-like receptors (TLRs).⁵⁵ In particular, multiple TLR agonists, including activators of TLR 4, 7, and 9 enhanced the phagocytic capacity of macrophages in conjunction with CD47 blockade. The pro-phagocytic effect of TLR stimulation on macrophages was preserved with genetic ablation of tumor-expressed CD47, indicating independent of the role Fc-receptor engagement. Rather, TLR-stimulation of macrophages promotes their secretion of calreticulin that provide a pro-phagocytic signal for tumor cell engulfment. CD47-blockade not only elicits phagocytosis by macrophages, but also induces antigen presentation to T cells and a memory response against tumors. The ability of CD47-blockade to stimulate antigen presentation to T cells is not limited to macrophages, however, but can also extends to dendritic cells.⁹³ In syngeneic murine tumor models, administration of anti-CD47 antibody led to inhibition of immunogenic tumors mediated

by DC activation of T cells. These findings highlight how the broad effects of CD47-blockade and how it may potentially complement immune agonists in novel therapeutic regimens.

The therapeutic benefit of targeting macrophage checkpoints such as CD47 has also elicited concern about the potential safety and escape mechanisms of using these approaches in cancer. For example, CD47 is also a critical regulator of engulfment and clearance of red blood cells by splenic macrophages; thus, systemic inhibition of CD47-SIRP α may give rise to anemia from accelerated destruction of red blood cells. Preclinical evidence suggests that anemia is transient, with red blood cell counts rebounding and stabilizing after sustained treatment with CD47-blocking antibodies.⁸⁹ Tumor cell resistance to CD47 treatment also remains a concern for translational applications.⁹⁴ Recent studies indicate that CD47-blockade is particularly effective against subsets of lymphomas (e.g. T-cell lymphoma), but may be less effective against other tumor types, including many solid tumors. This finding is consistent with xenograft models of pancreatic cancer, in which CD47-blockade alone failed to stimulate anti-tumor responses against human tumors.⁹⁵ Rather, the addition of gemcitabine and nab-paclitaxel was required to eliminate cancer stem cells in pancreatic tumors and generate robust anti-tumor responses. Other mechanisms by which tumors escape macrophage phagocytosis, include downregulation of MHC I on tumor cells, which can provide an additional pro-phagocytic signal. Collectively, this evidence underscores how macrophage anti-tumor activity is governed by multiple inputs, and that combination approaches to elicit this activity and overcome resistance.

Dissertation Objectives

Cancer immunotherapies have the potential to harness tumor inflammation for therapeutic benefit. A major driver of tumor inflammation is macrophages in the tumor microenvironment, which can be stimulated to mediate anti-tumor activity by treatment with immune agonists (e.g. TLR agonists) or inhibitors of macrophage checkpoints (e.g. blockade of tumor-expressed CD47). Although macrophage anti-tumor activity is associated with polarization toward classical M1 and M2 phenotypes, it is increasingly understood that macrophages span a spectrum of activation states with distinct metabolic features. The goal of this thesis is to understand how metabolic changes underlying macrophage anti-tumor function (i.e. phagocytosis) can be leveraged for enhancing immune-based treatments for cancer through the following specific aims:

1. Understand how CpG stimulation potentiates macrophage anti-tumor activity against pancreatic cancer cells that are resistant to CD47-inhibition

The majority of studies examining the impact of CD47-inhibition on macrophages focus on xenograft human tumors in immunocompromised NSG mice. Data on CD47-inhibition in immunocompetent models of cancer are lacking. Here, we examine the role of CD47-inhibition using antibody blockade and genetic knockout in a syngeneic model of PDAC. Surprisingly, PDAC tumor growth can resist CD47-blockade as well as complete loss of CD47. Thus, we hypothesize that tumor macrophages may lack an activated anti-tumor phenotype and require additional stimuli.

Using *in vitro* co-culture assays, we show that macrophage activation with CpG can promote phagocytosis of PDAC cells expressing or lacking CD47, which was

generalizable to other cancers, including immunologically ‘hot’ and ‘cold’ tumors. We also demonstrate that administration of CpG generates anti-tumor activity *in vivo*, which was revealed to be dependent on macrophages in depletion studies. These findings demonstrate that inducing an activated phenotype in macrophages can overcome CD47 expressed by tumor cells as a mechanism of immune escape.

2. Determine the metabolic changes imbued by CpG that support macrophage anti-tumor activity against PDAC cells.

Immune activation shapes the metabolism and phenotype of macrophages and other cell types (DCs, T cells, MDSCs, etc). For example, TLR activation with CpG rewires the metabolism of lipids in DCs and macrophages. However, the role of cellular metabolism in regulating macrophage function in the setting of cancer remains poorly understood. We hypothesize that stimulating an anti-tumor phenotype in macrophages with CpG will promote metabolic changes that critically support their phagocytic capacity.

To understand the cellular effects of CpG activation, we assess phenotypic changes of macrophages with respect to glycolytic flux and oxidative respiration. We further interrogate the central carbon metabolism of CpG-activated macrophages by examining the pools of short chain CoA-labeled metabolites. From these findings we find pleiotropic changes elicited by CpG that are essential for anti-tumor function, as demonstrated by pharmacologic inhibition.

Together, our findings underscore how metabolic rewiring of macrophages through CpG activation coordinates engulfment of tumor cells. This approach for enhancing macrophage anti-tumor function represents a therapeutic strategy that

could complement CD47-inhibitory agents or other immunotherapies in immunologically ‘hot’ and ‘cold’ tumors. Finally, the association between macrophage metabolism and function may impact other aspects of cellular biology (e.g. membrane biology, epigenetics, etc) that deserve to be assessed in the context of macrophage-based immunotherapies.

Figures

Figure 1: Beyond M1 and M2, macrophage anti-tumor potential defined by metabolic and functional features.

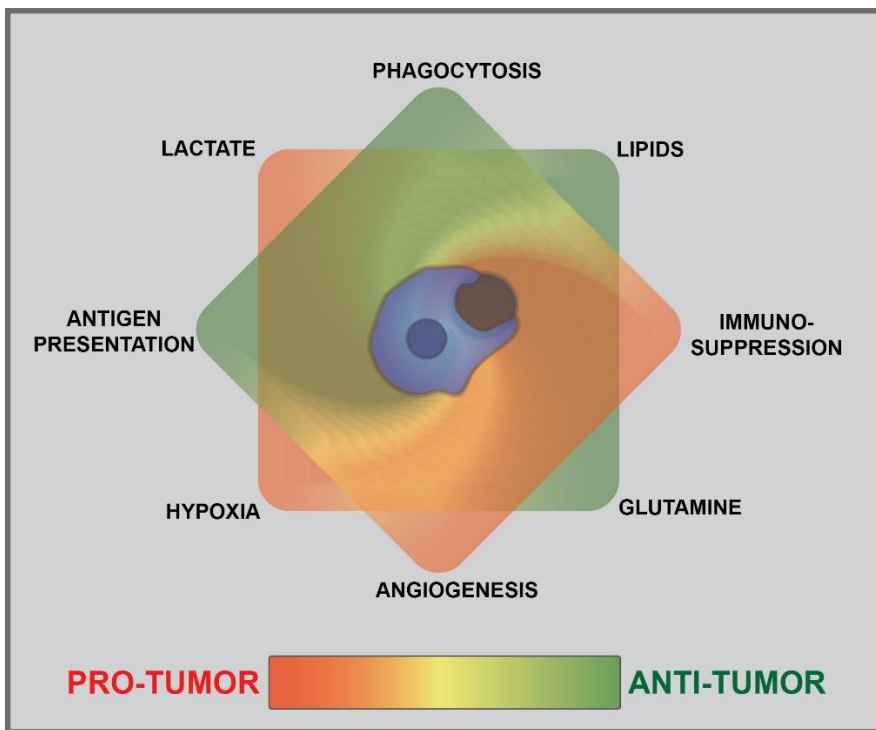


Figure 1: Macrophages regulate tumor growth through multiple functions (e.g. phagocytosis of tumor cells, angiogenesis, producing anti-inflammatory cytokines, etc). In turn, these pro- and anti-tumor roles of macrophages are modulated by metabolic cues – including hypoxia, glucose, lactate, lipids, and amino acids present in the tumor microenvironment.

Chapter 2: Therapeutic Strategies for Harnessing Tumor Inflammation

Abstract

Tumor, calor, rubor, and dolor describe four cardinal signs of inflammation. The fifth—*functio laesa*, or loss of function—was promulgated by Rudolf Virchow, who, in the 19th century, also noted an intricate link between inflammation and cancer. However, the role of cancer inflammation in driving loss of therapeutic efficacy has only recently been fully appreciated, as a result of molecular and immunohistochemical approaches applied in clinical medicine and the availability of novel agents for modulating inflammation. This review focuses on clinical evidence from solid malignancies that have shaped our view of how the immune system regulates cancer development, progression, and response to treatment. Understanding the multifaceted relationship between inflammation and patient outcomes has the potential to advance prognostic tools and uncover therapeutic opportunities for improving clinical outcomes.

Introduction

Since Virchow's early observations in the 19th century associating inflammation with malignancy, clinical studies have identified inflammatory conditions (e.g. colitis, gastritis, pancreatitis, hepatitis, and esophagitis) as key risk factors for the development of cancer.⁹⁶ Inflammation marked by the recruitment of leukocytes, particularly neutrophils, macrophages, and eosinophils, is a near universal hallmark of cancer that is directed by malignant cells which seek to establish a microenvironment that is conducive to survival, growth, and metastasis. This inflammatory reaction can also act as a barrier to

the efficacy of cytotoxic and immunotherapeutic interventions. As a result, increasing attention has been placed on strategies designed to ablate or redirect tumor-infiltrating inflammatory cells in order to improve clinical outcomes. In this review, we discuss the clinical implications of cancer inflammation and emerging interventions that disengage elements of therapeutic resistance imparted by inflammation in cancer.

Prognosis: Linking inflammation with oncology outcomes

Inflammation is a negative prognostic factor across multiple cancers and has been associated with cachexia, muscle wasting, fatigue, decreased cognitive ability and a reduced quality-of-life.^{97,98} Given the link between inflammation and cancer, several large clinical studies have evaluated biomarkers of inflammation for their prognostic value. For example, C-reactive protein (CRP) has been extensively studied as a marker of inflammation. Similarly, albumin is an acute phase reactant which decreases in the setting of a systemic inflammatory response. Together, elevated CRP and hypoalbuminemia are defining measures of the modified Glasgow Prognostic Score (mGPS) which has been validated across more than 70 studies involving over 31,000 cancer patients with a wide-range of malignancies.⁹⁹ Increased CRP (>10 mg/l) and decreased albumin levels (<35 g/l) – and consequently, a higher mGPS score – is associated with worse overall survival in patients with inoperable non-small cell lung cancer, independent of tumor staging and performance status. Higher mGPS scores also correlate with poorer quality-of-life and decreased nutritional status in multiple malignancies.⁹⁹ In addition, mGPS has recently been explored for its value in predicting therapeutic response. In patients with rectal cancer undergoing neoadjuvant chemotherapy, mGPS was strongly associated with pathologic response to treatment.¹⁰⁰ A

post hoc analysis of patients with gemcitabine-resistant metastatic pancreatic cancer, treated with capecitabine and ruxolitinib on a randomized Phase II study, also demonstrated a positive correlation between overall survival and mGPS.¹⁰¹ However, a subsequent Phase III study investigating this same treatment combination and incorporating mGPS as an inclusion criteria was terminated early due to a lack of data confirming a role for CRP in selecting patients most likely to respond to therapy.¹⁰² Thus, mGPS is a strong prognostic determinant for cancer patients but its role as a predictor of treatment response and in guiding anti-inflammatory interventions remains ill-defined.

Another measure of cancer inflammation with clinical significance is the neutrophil-to-lymphocyte ratio (NLR).¹⁰³ In patients with solid malignancies, a high NLR correlates with a poor prognosis. The NLR has also been shown to predict outcomes in advanced colorectal cancer patients receiving chemotherapy and has been used as a predictor of tumor recurrence and progression.^{104,105} However, the prognostic potential of the NLR may not apply to all therapeutic scenarios. For example, in an unplanned secondary analysis of patients with muscle-invasive bladder treated on a randomized Phase 3 study with or without neoadjuvant chemotherapy, the NLR was not found to be prognostic of overall survival benefit from neoadjuvant chemotherapy.¹⁰⁶ In general, though, the NLR describes a balance between innate and adaptive immunity, wherein an accumulation of neutrophils and/or diminution in lymphocytes portends an immune state that is less effective in controlling tumor progression.

The quality of the immune response to cancer has also been explored as a prognostic marker. Among the many cell types observed in tumors, high densities of CD3⁺ CD8⁺ T cells displaying a CD45RO⁺ memory phenotype correlates with improved

clinical outcomes.^{2,107} Taking advantage of this observation, the Immunoscore is a prognostic factor that can be incorporated into routine testing and involves immunohistochemical analysis to detect the density and location of CD3⁺ and CD8⁺ cells in tumor tissue.¹⁰⁸ An increased density of CD3⁺ and CD8⁺ cells in the core versus invasive margin of the tumor correlates with the best prognosis. Compared to the AJCC/UICC TNM-classification system, the Immunoscore has demonstrated improved prognostic significance.¹⁰⁷ In addition, it was recently found to be a better predictor of overall survival than microsatellite instability.¹⁰⁹ Moreover, CD3⁺ CD8⁺ T cell infiltration in melanoma is associated with treatment response to PD1/PDL1 checkpoint immunotherapy.¹¹⁰ An ongoing international effort is underway to validate the Immunoscore metric for colorectal carcinoma.

Together, the laboratory-based metrics described above and summarized in **Table 1** underscore the prognostic utility of the immune reaction to cancer, ranging from features of systemic inflammation detected in the peripheral blood to the quality of the cellular immune infiltrate detected in tumors. Moving forward, efforts are underway that aim to apply molecular profiling and multiplex imaging analyses to identify unique features of the inflammatory reaction to cancer for guiding treatment and predicting subsequent clinical outcomes.

Inhibiting inflammation for cancer prevention and treatment

The link between inflammatory markers and treatment resistance obviates the potential for targeting key inflammation pathways and improving patient outcomes. Strategies to intervene on cancer inflammation may (i) *deplete* elements of the inflammatory response or *block* its recruitment to tumors, (ii) *inhibit* components of the

pro-tumorigenic and immunosuppressive phenotype of inflammation, or (iii) *redirect* inflammation with properties that are tumor inhibitory, immune stimulatory, or both (**Figure 2**).¹¹¹

Targeting inflammation for cancer prevention. Early evidence for clinical benefit achieved with targeting inflammation was seen in a prospective cohort study of aspirin use among colon cancer patients, for whom low-dose aspirin use correlated with reduced fatality.¹¹² Aspirin irreversibly inactivates the cyclooxygenase (COX) enzyme that is required for prostaglandin synthesis, an important mediator of inflammation. This prophylactic effect seen with aspirin in colon cancer has been extended to randomized controlled studies comparing aspirin versus placebo among carriers of Lynch syndrome, a hereditary condition with high predisposition for colorectal cancer. In the randomized CAPP2 trial, daily aspirin use for at least 2 years significantly reduced the incidence of colorectal cancer as well as other Lynch syndrome cancers after almost 5 years of follow-up.¹¹³ An observational study of patients with Lynch syndrome included in the Colon Cancer Family Registry also showed a reduced risk for colorectal cancer among patients taking aspirin.¹¹⁴ The ongoing CAPP3 randomized double-blinded trial is currently evaluating the dose of aspirin needed for chemoprevention in Lynch syndrome (NCT02497820).

The prophylactic effect of suppressing inflammation may extend beyond colon cancer to other malignancies such as breast, prostate, and lung cancers.¹¹⁵ In a population-based case-control study, the frequency and duration of using non-steroidal anti-inflammatory agents (i.e. aspirin and ibuprofen) was associated with reduced risk for hormone-receptor positive breast cancer.¹¹⁶ However, the most pronounced beneficial

effect of aspirin has been observed in gastrointestinal malignancies, including esophageal, stomach and colon cancer.¹¹⁵ For colon cancer, NCCN guidelines suggest considering low-dose aspirin for secondary chemoprevention based on the strong data indicating that this therapy decreases risk of recurrence and death.¹¹⁷

Selective COX-inhibitors may exhibit similar benefits as aspirin. For example, COX-2 is overexpressed in many cancers including colorectal adenomatous polyps, precursors to the development of colorectal cancer. An inhibitor against COX-2, celecoxib, was shown to decrease the incidence of precancerous colorectal adenomas in phase III clinical trials.^{118,119} Celecoxib has also been shown to reduce the risk of colon adenocarcinoma in patients with familial adenomatous polyposis.¹²⁰ However, COX-2 inhibitors are not recommended routinely at this time for sporadic or familial adenomatous polyp prevention due to their increased risk of cardiovascular events and current lack of phase IV data.¹²¹

Targeting inflammation for improving cytotoxic therapy. Multiple cues present within the tumor microenvironment, including hypoxia, extracellular matrix components, and soluble factors, can shape cancer cell biology and in turn, ignite an inflammatory response that promotes chemoresistance. For example, the stiffness of the extracellular matrix surrounding malignant cells can stimulate focal adhesion kinase (FAK) activity which drives cancer cell release of chemoattractants that are important for the recruitment of myeloid cells.¹²² Inhibition of FAK signaling can decrease myeloid cell infiltration into tumors, delay tumor progression, and sensitize tumors to chemotherapy. Thus, cross-talk between malignant cells and their surrounding microenvironment is critical to defining therapeutic resistance.

Malignant cells respond to cytotoxic stress by releasing chemoattractants (e.g. CCL2) and damage-associated molecular patterns, or danger signals, that attract myeloid cells to the tumor microenvironment where they support malignant cell survival, suppress immunosurveillance, and promote subsequent tumor outgrowth. Tumor-infiltrating myeloid cells can mediate resistance to cytotoxic therapies including chemotherapy and radiation.^{123,124} Disrupting myeloid cell recruitment by blocking chemokine/chemokine receptor interactions (e.g. CCL2/CCR2) or myeloid growth factors (e.g. CSF-1/CSF-1R) improves the efficacy of cytotoxic therapies in mouse models of cancer. Early promising results also support the merit of inhibiting myeloid cell recruitment for enhancing therapeutic efficacy in patients. In a Phase I study of patients with borderline resectable or locally advanced pancreatic adenocarcinoma, treatment with chemotherapy in combination with a CCR2 antagonist produced encouraging objective responses in 16 (49%) of 33 evaluable patients with local tumor control seen in 32 (97%) patients.¹²⁵

Inflammatory cells may mediate chemoresistance through multiple pathways. By releasing soluble factors (e.g. IL-6 and soluble IL-6 receptor), inflammatory cells activate signal transducer and activator of transcription (STAT) signaling in malignant cells.¹²⁶ In models of spontaneously arising pancreatic ductal adenocarcinoma, inflammation-directed STAT signaling in cancer cells is critical for tumor development.¹²⁶ Moreover, pharmacologic inhibition of STAT signaling sensitizes tumors to chemotherapy.¹²⁷ Tumor-associated macrophages can also release insulin-like growth factors that activate IGF signaling in malignant cells and in doing so, reduce the sensitivity of cancer cells to chemotherapy.¹²⁸ Moreover, macrophages can be key orchestrators of revascularization

after cytotoxic therapy, which promotes tumor regrowth.¹²⁹ Thus, myeloid cells recruited to the tumor microenvironment can regulate cancer cell sensitivity to cytotoxic therapies.

Based on strong preclinical data supporting a role for inflammation in therapeutic resistance, multiple early phase clinical trials are underway investigating strategies designed to manipulate inflammation with the intent of conditioning tumors for enhanced responsiveness to cytotoxic therapies. Targets being explored to disrupt inflammation include chemokine receptors (e.g. CCR2, CXCR1/CXCR2), cytokines (e.g. IL-6, IL-6R, TNF- α , IL-1), and cellular signaling pathways (e.g. FAK, JAK1/2, CSF1R).

Targeting inflammation to restore T cell immunosurveillance in cancer. Although chronic inflammation predisposes to cancer and can promote tumor growth and therapeutic resistance, the immune system is inherently pliable, such that under the appropriate conditions, it can also mediate strong anti-tumor activity. In recent years, strategies designed to harness the therapeutic potential of the immune system have emerged as new treatment options for some patients across a wide range of malignancies. The robustness and durability of treatment responses produced with immune-directed interventions has incited a revolution in cancer therapy. However, not all patients respond to immunotherapy and in some cases, treatment responses can be transient due to mechanisms of adaptive immune resistance, a process in which cancer cells adapt to immune pressure.¹²⁹

Anti-tumor immunity induced with immunotherapy is dependent on the existence of tumor-specific T cells capable of infiltrating tumors and then recognizing and eliminating malignant cells.⁶ This highly regulated process relies on productive and coordinated interactions between innate and adaptive immunity. Specifically, innate

immune cells (e.g. dendritic cells) must capture and present tumor-associated antigens in order to prime antigen-specific T cells and stimulate their entry into tumor tissue and subsequent effector activity. However, chronic inflammation can impair both the priming of T cells and their subsequent effector activity by limiting effective antigen presentation and suppressing T cell activation in tumor tissues, respectively.

Chronic inflammation can suppress the development and productivity of T cell dependent immunosurveillance in cancer through multiple mechanisms including the release of immunosuppressive molecules (e.g. TGF- β , IL-10, and nitric oxide), expression of immune checkpoint molecules (e.g. PD-L1), and metabolism of amino acids (e.g. arginine and tryptophan) that are important for T cell phenotype and survival.¹³⁰⁻¹³² Inflammatory cells can also regulate T cell entry into tumors by establishing a physical barrier and upregulating immune checkpoint molecules including indoleamine 2,3 dioxygenase (IDO) and PD-L1, as has been seen in colorectal cancers with microsatellite instability.¹³³ The co-expression of T cell immune checkpoint molecules in tumor tissues at the interface between innate and adaptive immunity has suggested redundancy in mechanisms of peripheral tolerance established within the tumor microenvironment and represents the impetus for ongoing studies combining multiple immune checkpoint inhibitors (e.g. IDO inhibition plus PD-1/PD-L1 blockade and CTLA-4 plus PD-1/PD-L1 blockade).

In preclinical mouse models of cancer, releasing immune suppression imposed by chronic inflammation can enhance the efficacy of T cell directed immunotherapies including adoptive T cell therapy, immune checkpoint inhibitors, and vaccines.¹³⁴⁻¹³⁷ These findings form the basis for early phase clinical trials evaluating immune

checkpoint inhibitors in combination with strategies designed to inhibit the recruitment of myeloid cells (e.g. inhibitors of FAK, CCR2, and CXCR2) or deplete myeloid cells (e.g. CSF1R antagonists) (**Table 2**). Combining multiple immune modulatory agents, though, poses challenges in determining the contribution of each therapeutic intervention to observed clinical responses. Determining the benefit of combination therapy over monotherapy is particularly critical in early therapeutic development and relies on effective biomarkers, identification of patients unlikely to respond to monotherapy, or both. However, biomarker development for immunotherapy has been particularly challenging in contrast to targeted therapies which rely on the presence or absence of activating mutations in driver oncogenes. For example, immunological biomarkers can vary with time of assessment, anatomical site and even within a single lesion due to heterogeneity of the immune reaction. Overall, the dynamic nature of the immune reaction to cancer has made immunological biomarkers a “moving target” which is exemplified by the difficulties encountered with standardizing assays for PD-1/PD-L1 checkpoint therapy.¹³⁸ Potential biomarkers for monitoring therapies targeting cancer inflammation include immunohistochemical and flow cytometry analyses that quantify: (i) the presence and activation status of inflammatory cell subsets in tumor tissue and the peripheral blood, (ii) the presence or absence of effector T cells in tumors, (iii) activation of oncogenes (e.g. *KRAS*¹³⁹) and loss of tumor suppressor genes (e.g. *PTEN*¹⁴⁰) associated with increased inflammation, (iv) signaling pathway activation in malignant and stromal cells (e.g. phosphorylation of STAT3¹⁴¹ and FAK molecules¹²²), and (v) quantification of the matrix including vascularity and fibrosis.³² In general, biomarker development for therapies targeting cancer inflammation will need to be informed by mechanisms of

action of the pathways, molecules, or cell types targeted. However, benefit achieved with inflammation-directed therapies will ultimately rely on demonstrating improvement in standard clinical measures of response including response rates, progression free survival, and overall survival. Nonetheless, efficiently maximizing information acquired from tissues, peripheral blood and clinical observations during early phase studies will be important to the development of therapies targeting inflammation, especially given the unlikelihood that single agents targeting cancer inflammation will produce significant clinical benefit in the advanced disease setting.

Redirecting cancer inflammation for clinical benefit

Although inflammation is most commonly considered an obstacle in cancer therapy, the ability of innate immune cells to also acquire anti-tumor properties has propelled the possibility that cancer inflammation may be an opportunity that can be harnessed and redirected for therapeutic benefit. Indeed, while T cells are touted as potent “killers” capable of seeking out malignant cells with exquisite efficiency and specificity, actual tumor shrinkage requires removal of dead cells and matrix remodeling which is a hallmark of innate immunity and in particular, macrophages. Macrophages demonstrate remarkable plasticity with their biology defined by signals received from their surrounding microenvironment.¹³² To this end, while macrophages can inhibit T cell immunosurveillance in cancer, preclinical models have also demonstrated their importance for mediating anti-tumor activity directed by tumor-infiltrating effector T cells.¹⁴²

Macrophages can be important effectors of cancer therapy through release of cytotoxins (e.g. reactive oxygen species) and via engulfment of malignant cells.¹³²

These mechanisms are tightly regulated by a balance of stimulatory and inhibitory signals. Similar to immune checkpoint molecules (e.g. PD-L1) that are upregulated on malignant cells to evade T cell immunosurveillance, macrophage-inhibitory molecules (e.g. CD47) can also be upregulated on malignant cells and thwart the potential of innate immunosurveillance in cancer.^{132,143} Multiple clinical grade antagonists have been developed to disrupt one of these negative regulatory signals that involves CD47 interaction with SIRP α on macrophages.¹⁴⁴ SIRP α signaling inhibits macrophage engulfment of antibody-opsonized malignant cells and in preclinical models, disrupting CD47-SIRP α interactions enhances the therapeutic benefit of antibody based therapies, such as anti-CD20 antibodies (i.e. rituximab) used in the treatment of B cell lymphomas.⁹⁰

Macrophages can also be activated with anti-tumor activity using Toll-like receptor agonists and in response to systemic activation of the CD40 pathway.³¹ However, in general, strategies that merely redirect cancer inflammation have demonstrated minimal clinical benefit when translated from the laboratory to the clinic, perhaps due to a lack of immunological memory associated with innate immunity. This does not preclude, though, the potential of these approaches which may be particularly relevant for tumor debulking and stabilizing disease activity. For example, redirecting myeloid cells in cancer has recently been demonstrated to “condition” tumors for enhanced sensitivity to chemotherapy. This finding was dependent on cytokines and chemokines (i.e. IFN- γ and CCL2) released in response to treatment with a CD40 agonist that subsequently stimulated a subset of peripheral blood monocytes to rapidly infiltrate tumors and facilitate the degradation of the collagen-based extracellular matrix that

surrounds malignant cells and can impede the efficacy of chemotherapy.³² Redirecting myeloid cell biology in cancer has also been found to enhance the efficacy of PD-1/PD-L1 blocking antibodies, illustrating the potential of redirecting myeloid cells for enhancing T cell dependent anti-tumor immunity.¹⁴⁵ Thus, redirecting cancer inflammation holds promise as an approach for remodeling tumors with enhanced sensitivity to chemotherapy and stimulating productive T cell dependent anti-tumor immunity.

Conclusion

From Virchow's observations to studies connecting inflammation with cancer, clinical evidence supports both permissive and inhibitory roles for the immune system in regulating cancer development, progression, and therapeutic resistance. The inflammatory reaction to cancer, characterized using routine laboratory-based protocols, has demonstrated prognostic utility. Moreover, clinical studies investigating daily aspirin use for cancer prevention have provided a strong rationale for therapeutic strategies that intervene on cancer inflammation. To this end, preclinical models of cancer have highlighted the inherent plasticity of the immune system and identified novel targets for depleting, inhibiting, and redirecting cancer inflammation. These therapeutic maneuvers have the potential to enhance the efficacy of cytotoxic therapies and to restore an effective communication between innate and adaptive immunity that is necessary for productive cancer immunosurveillance. The clinical translation of agents directed at manipulating cancer inflammation will be benefited by biomarkers based on mechanisms of action for the signaling pathways and cellular subsets targeted. However, as cancer

inflammation is only one element of a complex network of signals that can regulate tumor biology, combination studies will be paramount for effectively leveraging the potential of inflammation to serve as a therapeutic target in cancer.

Figures

Figure 2: Strategies to target inflammation for cancer therapy.

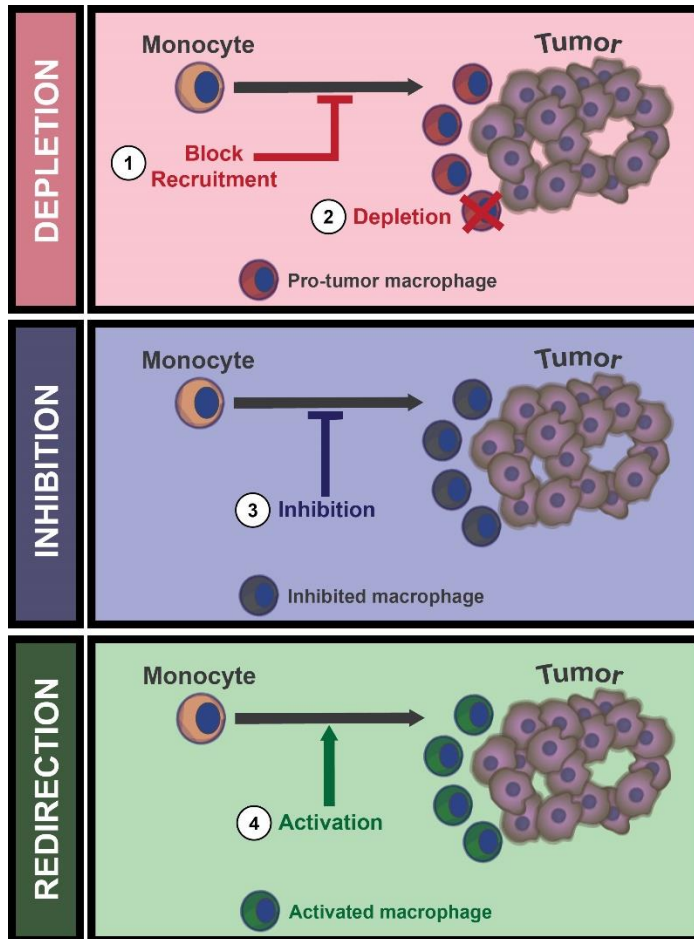


Figure 2: Inflammatory cells (e.g. monocytes) can be targeted in cancer using therapeutics that (1) *block* their recruitment to tumors (e.g. CCR2 inhibitors), (2) *deplete* inflammatory cell subsets (e.g. trabectedin and CSF1R antibodies), (3) *inhibit* pro-tumorigenic signaling pathways (e.g. inhibitors of BTK, CSF1R, FAK, HIF-2 α , IDO, JAK, PI3K δ , TGF- β), and (4) *redirect* tumor-infiltrating inflammatory cells with anti-tumor properties (e.g. CD40 agonists, CD47 antagonists, dectin-1 agonists, and TLR agonists).

Tables

Table 1: Inflammation-based prognostic scoring systems.

Scoring system	Approach
Modified Glasgow Prognostic Score ⁹⁹	0 – Albumin > 3.5 g/dL <u>and</u> CRP < 10 mg/l 1 – Albumin < 3.5 g/dL <u>or</u> CRP > 10 mg/l 2 – Albumin < 3.5 g/dL <u>and</u> CRP > 10 mg/l mGPS > 0 predicts decreased survival
Neutrophil-to-lymphocyte ratio ¹⁰³	Based on investigator-defined cut-off (e.g. NLR = 4). NLR > cutoff predicts decreased survival.
Immunoscore ¹⁰⁸	Scale ranging from 0 to 4 describing low to high densities of CD3 ⁺ and CD8 ⁺ cells in the center of the tumor and invasive margin. 0, low densities in both regions; 4, high densities in both regions. Immunoscore = 0 displays worst overall survival

Table 2: Active clinical studies[§] combining FDA-approved immune checkpoint inhibitors and inflammation-directed therapies.

Immune Checkpoint Target	Inflammation Target	Active Clinical Trials
PD-L1	CSF1R	NCT02323191
	CD40	NCT02304393
	IDO	NCT02298153, NCT02471846
CTLA-4	c-kit	NCT01738139
	IDO	NCT02073123
	TLR9	NCT02668770
CTLA-4 + PD-1	TLR9	NCT02644967
PD-1	BTK	NCT02362035
	CD40	NCT02706353
	CSF1R	NCT02526017, NCT02452424, NCT02713529, NCT02880371
	CXCR4	NCT02923531, NCT02907099, NCT02826486, NCT02823405
	Dectin-1	NCT02981303
	FAK	NCT02758587
	HIF-2 α	NCT02293980
	IDO	NCT02073123, NCT02327078, NCT02862457, NCT02752074, NCT02178722
	IL-10	NCT02553499
	JAK1	NCT02646748
	PI3K δ	NCT02862457
	TGF β R1 kinase	NCT02423343

	TLR3	NCT02834052
	TLR9	NCT02680184, NCT02521870

§ Active studies were identified on clinicaltrials.gov as of December 8, 2016 by searching for open studies including FDA-approved immune checkpoint inhibitors in combination with an inflammation-directed therapy.

Chapter 3: Metabolic rewiring of macrophages by CpG potentiates clearance of cancer cells and overcomes tumor-expressed CD47

Abstract

Macrophages enforce anti-tumor immunity by engulfing and killing tumor cells. Although these functions are determined by a balance of stimulatory (e.g. Toll-like receptor agonists) and inhibitory signals (e.g. CD47), the role of macrophage metabolism in defining the anti-tumor potential of macrophages is unknown. Here, we study the capacity of macrophages to circumvent inhibitory activity mediated by CD47 expressed on malignant cells. We show that stimulation with CpG oligonucleotides, a TLR9 agonist, evokes changes in the central carbon metabolism of macrophages that enable their anti-tumor activity, including engulfment of cancer cells that express elevated levels of CD47. These changes occur without requirement for a phenotypic shift toward classical M1 or M2 states of macrophage polarization. Rather, activation by CpG engenders a hybrid of M1 and M2 metabolisms, featuring a dependence on elevated fatty acid oxidation (FAO) and shunting of tricarboxylic acid (TCA) cycle intermediates for de novo biosynthesis of lipids. This integration of multiple metabolic inputs is underpinned by the activity of carnitine palmitoyltransferase 1A (CPT1A) and ATP citrate lyase (ACLY), which together, impart macrophages with anti-tumor potential that can overcome inhibitory activity from CD47 expressed on tumor cells. Our findings reveal central carbon metabolism to be a novel determinant and potential therapeutic target for harnessing the anti-tumor functions of macrophages.

Introduction

Macrophages govern the immune landscape of many cancers and are key proponents of tumor growth.²¹ However, macrophages can also enact anti-tumor functions. These opposing roles are explained by the phenotypic polarity of macrophages, which are often classified as either pro-inflammatory M1 macrophages that enforce anti-tumor immunity or immunosuppressive M2 macrophages that promote tumor progression.⁶² While macrophages most commonly adopt a phenotype that is supportive of tumor growth,¹⁴⁶ their biology is pliable. As a result, under the appropriate conditions, macrophages can be redirected with anti-tumor activity.^{32,147,148} The mechanisms that determine pro- versus anti-tumor functions of macrophages, though, are still being elucidated.

One mechanism governing pro- and anti-tumor roles of macrophages is the balance of stimulatory and inhibitory signals. For example, a key negative regulator of macrophage activity is CD47, a membrane-bound protein overexpressed by many cancers.^{88,90} CD47 is a “don’t eat me” signal that suppresses the phagocytic activity of macrophages upon binding SIRP α (signal regulatory protein α)-receptor present on phagocytes.¹⁴⁹ Blocking CD47-SIRP α binding promotes macrophage engulfment of tumor cells and induces anti-tumor responses in multiple xenograft models.^{89,91} However, in models of pancreatic ductal adenocarcinoma (PDAC), CD47-blockade as a monotherapy has shown modest anti-tumor efficacy,⁹⁵ which may be explained by the limited pro-phagocytic effect of CD47-blockade seen in non-hematopoietic tumor models.¹⁵⁰ These findings suggest that additional stimuli are required to potentiate anti-tumor activity by macrophages.

Macrophage stimulation is directed by cytokines and agonists of pathogen recognition receptors, such as Toll-like receptors (TLRs), which together determine macrophage phenotype.⁵² Unique combinations of stimuli have been used *in vitro* to define classical phenotypic states of macrophages, such as M1 and M2. However, in pathological settings, such as cancer, macrophages more commonly acquire phenotypes that span a spectrum of differentiation states.^{53,151}

When examined using systems-based approaches, macrophage phenotypes can be distinguished by their core metabolic processes.^{65,151} For example, M1 macrophages rely on glycolytic metabolism and reduced oxidative phosphorylation, whereas M2 macrophages perform *de novo* lipogenesis and glutaminolysis to support fatty acid oxidation (FAO).^{63,152,153} Additional studies support an association between M2-macrophage polarity and FAO, but indicate that these can also occur independently.⁶⁴ In particular, FAO and lipid metabolism underpin the anti-tumor functions of multiple myeloid subsets (e.g. dendritic cells and myeloid-derived suppressor cells).^{71,154,155} Similarly, lipid availability can modulate macrophage engulfment of red blood cells and macromolecules.^{156,157} Together, these findings underscore the potential role of metabolism in defining myeloid cell biology, and suggest that lipid metabolism may likewise coordinate macrophage function.

To understand the metabolic determinants that govern macrophage anti-tumor function, we utilized metabolomic approaches and a syngeneic model of PDAC to study macrophage engulfment of PDAC cells upon TLR stimulation. Further, we leveraged targeted knockout of CD47 in PDAC cells to understand how macrophage activation acts in concert with inhibition of anti-phagocytic signals present in cancer. Our studies reveal

a novel role for metabolic pathways in regulating macrophage anti-tumor functions, and underscore the potential of targeting macrophage metabolism for overriding inhibitory signals used by cancer cells to evade elimination by innate immunity.

Results

Macrophage activation, but not loss of inhibitory CD47, is sufficient for anti-tumor activity in PDAC

Macrophages can be induced with therapeutic and anti-tumor functions by activating pro-inflammatory signaling pathways such as CD40 and TLRs.³¹ However, macrophage biology is ultimately determined by a balance of stimulatory and inhibitory signals that are sensed within the tumor microenvironment (**Fig 3a**). One major inhibitory signal that is involved in suppressing macrophage anti-tumor activity is CD47, which is overexpressed on cancer cells across a wide range of solid malignancies.⁸⁹ Elevated levels of CD47 can be detected in both mouse (**Fig 4a-b**) and human PDAC.⁹⁵ Therefore, we initially studied the role of CD47 as a macrophage-inhibitory signal in a murine model of PDAC. To do this, we administered a CD47-blocking antibody via intratumoral delivery to mice implanted with *Kras*^{G12D/+} *Trp53*^{R172H/+} mutant PDAC tumors.¹⁵⁸ In this fully syngeneic and immunocompetent model, antibody blockade of CD47 did not alter tumor growth (**Fig 3b**). To address possible limitations in bioavailability or insufficient blockade, expression of CD47 was ablated in PDAC cells using transient expression of CRISPR/Cas9 (**Fig 4c-d**). Surprisingly, unlike models of leukemia where CD47 overexpression is a key determinant of immune escape,⁸⁸ deletion of CD47 in PDAC cells did not impact tumor engraftment or growth (**Fig 3c**). This observation suggested

that mechanisms other than CD47 can regulate macrophage-dependent anti-tumor responses in PDAC, consistent with xenograft models of this disease and other non-hematopoietic malignancies.^{95,150} In support of this finding, we also found that antibody blockade of CD47 on PDAC cells did not enhance *in vitro* phagocytosis by murine bone-marrow derived macrophages (BMDMs) (**Fig 3d**).

We next hypothesized that PDAC cells may not provide sufficient activating signals to stimulate macrophages with anti-tumor functions, and that delivery of discrete stimuli may be necessary to induce macrophages with anti-tumor activity. We tested a panel of Toll-like receptor (TLR) pathway agonists for their capacity to stimulate macrophages with anti-tumor functions, such as phagocytosis. In the absence of TLR stimulation, mock-treated BMDMs lacked the capacity to phagocytose tumor cells upon co-culture with PDAC cells (**Fig. 3e**). Further, the phagocytic capacity of BMDMs increased only modestly with 24-hour pretreatment with Pam3CSK4, Poly(I:C), lipopolysaccharide (LPS), flagellin, and imiquimod – which stimulate TLR1 & TLR2, TLR3, TLR4, TLR5, and TLR7, respectively (**Fig 3e**). In contrast, ODN1826, a Class B CpG oligonucleotide that preferentially stimulates TLR9 expressed by macrophages and B-cells, was found to be a potent activator of macrophage phagocytosis of PDAC cells (**Fig 3e-f**). Upon increasing the duration of CpG pretreatment, CpG-activated macrophages (CpG-BMDM) exhibited enhanced phagocytic capacity relative to mock-stimulated macrophages (mock-BMDM) (**Fig 3g**). To ascertain the potential of CpG-activation to produce anti-tumor activity, we also performed an extended co-culture of pretreated macrophages with PDAC cells for 48 hours. We found that CpG-activation rendered macrophages with potent anti-tumor activity leading to a decrease in tumor cell

survival in comparison to co-culture with mock-BMDMs (**Fig 3h**). Together, these data show loss of inhibitory CD47 alone to be insufficient for unleashing anti-tumor activity by macrophages in PDAC, and that an activated phenotype is also necessary for macrophages to engage in anti-tumor functions.

Tumor-associated macrophages are essential for CpG-activated anti-tumor responses

We next evaluated the *in vivo* anti-tumor activity of CpG on established murine PDAC tumor growth. Treatment was initiated with intraperitoneal injection of vehicle (PBS) or CpG on day 10 with repeated administration every other day for a total of five doses (**Fig 5a**). CpG treatment potently suppressed tumor growth in two independent PDAC tumor models (**Fig. 5b**), without inducing gross toxicity or lethality. This effect was also independent of any direct cytotoxic activity of CpG on tumor cells, as treatment of PDAC cells *in vitro* with supratherapeutic concentrations of CpG did not affect tumor cell survival (**Fig 6**).

Repeated dosing of CpG to non-tumor bearing mice has been found to stimulate a macrophage activation syndrome.¹⁵⁹ Therefore, we examined the impact of treatment on the systemic release of inflammatory cytokines. We found that *in vivo* delivery of CpG to tumor-bearing mice increased pro-inflammatory cytokines in the serum, including TNF- α , IFN- γ , and CCL2 (**Fig 7**). Consistent with this increase in inflammatory and chemotactic factors, we observed an increase in tumor-associated macrophages following CpG treatment (**Fig 5d-e**). In addition, we detected an increase in F4/80+ macrophage phagocytosis of tumor cells in CpG-treated tumors (**Fig 8**). To ascertain the role of

tumor-associated macrophages in the response to CpG treatment, we depleted distinct macrophage populations using GW2580, an inhibitor of colony stimulating factor 1-receptor (CSF1Ri), and clodronate encapsulated liposomes (CEL), which target phagocytes residing outside of the tumor microenvironment.¹⁶⁰ Depletion with either CEL or CSF1Ri alone did not affect tumor outgrowth in the vehicle-treated groups (**Fig 5f**). In contrast, CSF1Ri abrogated the anti-tumor effect of CpG, whereas CEL did not (**Fig 5f**). Similarly, we found that administration of an anti-CSF1R antibody attenuated the CpG-induced anti-tumor response (**Fig 9**). These findings implicated a CSF1R⁺ population of macrophages, which are not targeted by liposomes, in mediating the anti-tumor response by CpG. Consistent with this observation, we found that CEL did not alter macrophage presence within tumors, whereas both CSF1Ri (**Fig 5d-e, Fig 9**) and anti-CSF1R antibody (**Fig 8**) treatment decreased the abundance of tumor-associated macrophages.

To ascertain the possible contribution of other immune effectors, we considered a role for lymphocytes in CpG-induced anti-tumor activity. We found that CpG did not significantly alter the infiltration of T cell subsets (CD8⁺, CD4⁺, and CD4⁺ Foxp3⁺) into tumors (**Fig 11a-b**). In addition, we detected no significant change in the expression of activation markers, including PD-1 and Tim3, by T cells after CpG treatment (**Fig 11c**). CpG-induced anti-tumor activity was also preserved in *Rag2*-deficient mice bearing PDAC.1 tumors, thereby excluding a role for lymphocytes (**Fig 12a**). Anti-tumor activity induced with CpG was also preserved in mice depleted of natural killer (NK) cells using the anti-NK1.1 antibody (**Fig 12c-d**).¹⁶¹ In addition, we found that depletion of dendritic cells (DC) using the CD11c-DTR/eGFP mouse model did not alter the anti-tumor

response stimulated by CpG (**Fig 13**).¹⁶² Collectively, these data indicate that T and B lymphocytes as well as DC and NK cells are not required for the anti-tumor response induced by CpG.

We have previously shown a role for peripheral blood myeloid cells in mediating anti-tumor activity against PDAC4. Thus, we investigated the expression of CSF1R on myeloid cell populations in the peripheral blood. We found that CSF1R was expressed by a subset of CD11b⁺ F4/80⁺ myeloid cells bearing high levels of the monocyte marker Ly6C (**Fig 14**), which marks a population of myeloid cells that have been previously shown to be recruited to PDAC tumors.^{32,163} Further, administration of an anti-CSF1R antibody significantly reduced the Ly6C^{hi} myeloid population in the peripheral blood (**Fig 14**). We also found, similar to CSF1Ri and anti-CSF1R treatment, that anti-Ly6C antibodies, which deplete the Ly6C^{hi} monocyte population *in vivo*,³² blocked both the accumulation of F4/80⁺ macrophages in tumors and the CpG-induced anti-tumor response (**Fig 14**). Together, these data implicate myeloid cells marked by expression of Ly6C and CSF1R in the anti-tumor activity induced by CpG.¹⁶⁴

CpG activation of macrophages bypasses inhibitory CD47 on PDAC cells

We next sought to understand the mechanism by which CpG stimulates macrophages with enhanced phagocytic and anti-tumor activity. We hypothesized that CpG may alter the capacity of macrophages to respond to CD47 as a negative regulatory signal. To test this, we assessed the impact of CpG on SIRP α expression. However, we observed no changes in SIRP α levels with increasing duration of CpG-activation (**Fig 15**). We also examined the effect of CpG-activation on macrophage-inhibitory signals

present *in vitro*. We found that CpG-BMDMs phagocytosed PDAC cells that either expressed or lacked CD47, indicating that CpG stimulates macrophages with anti-tumor activity that is independent, at least in part, of CD47 as a macrophage-inhibitory signal (**Fig 15**). This finding was generalizable as CpG-activation enabled macrophage engulfment of CD47-expressing syngeneic tumor cells derived from breast cancer, melanoma, colorectal cancer, glioblastoma, lung cancer and lymphoma (**Fig 16**). Interestingly, CD47-blockade alone also showed limited capacity to enhance macrophage phagocytosis in these tumors, except for EL4 lymphoma cells. However, despite limited activity by itself, we found that genetic ablation of CD47 in tumor cells (**Fig 15b**) as well as CD47 blockade (**Fig 16**) significantly enhanced the capacity of CpG-stimulated macrophages to phagocytose tumor cells *in vitro*, implying that appropriate macrophage-activation signals are critical for overcoming CD47 in non-hematopoietic tumors.

Prior studies have suggested that TLR agonists may promote phagocytic and anti-tumor activity by stimulating macrophages to produce calreticulin.⁵⁵ To test this possibility, we quantified calreticulin expression – including both membrane-bound and intracellular levels – but detected no differences between mock-BMDMs and CpG-BMDMs (**Fig 17**). Further, upon extended co-culture, CpG-BMDMs effectively eliminated PDAC cells, with loss of CD47 expression in tumor cells providing an additive benefit in anti-tumor activity (**Fig 15c**). However, the ability of CpG to promote anti-tumor activity by macrophages despite CD47 expression on tumor cells is in contrast with other TLR agonists, for which blockade of CD47 is critical for macrophage activity.⁵⁵

We then asked whether disruption of CD47 may enhance the *in vivo* anti-tumor activity of macrophages. Delivery of CpG to mice bearing control or CD47 knockout (CD47 KO) tumors produced similar increases in the relative abundance of tumor-associated macrophages (**Fig 15d-e**). The impact of CpG on tumor growth was also similar in tumors that expressed or lacked CD47 (Fig 3f). These findings underscore the dominant response elicited by CpG activation of macrophages *in vivo* that can overcome CD47 expressed by PDAC cells.

CpG induces a shift in macrophage metabolism

Pro-inflammatory cues can induce distinct phenotypes in macrophages. For example, the combination of lipopolysaccharide (LPS) and interferon- γ (IFN- γ) promote an M1 phenotype in macrophages, which is associated with pro-inflammatory and anti-tumor activity in cancer.^{51,62} In contrast, the combination of interleukin-4 (IL-4) and interleukin-13 (IL-13) endows macrophages with M2-polarity, which suppresses inflammation and promotes tumor growth. To study the direct effect of CpG on macrophage polarity, we evaluated CpG-BMDMs for expression of MHC-II and CD206, markers of M1 and M2 polarity, respectively. Surprisingly, we found that CpG did not induce a clear shift toward either M1 or M2 phenotypes, despite the pro-phagocytic and anti-tumor effects seen with CpG *in vitro* and *in vivo* (**Fig 18a**). Moreover, CpG induced production of pro-inflammatory cytokines (i.e. IL-6, IL-12, CCL2, and TNF- α) and anti-inflammatory cytokines (i.e. IL-10) relative to mock-treatment, indicating that CpG alone does not impart a clear M1 or M2 macrophage phenotype (**Fig 18b**). Further examination of activation markers revealed that CpG did not modulate CD80 or CD86, but

upregulated expression of FcγRIII and PD-L1 (**Fig 19a**). Expression of IL-4 receptor alpha, an M2 marker, was not altered.

In addition to phenotypical cell surface markers, macrophage metabolism can be modulated by pro-inflammatory stimuli.^{54,151} We sought to understand the impact of CpG-activation on the metabolic state of macrophages by assessing their ECAR (extracellular acidification rate) and OCR (oxygen consumption rate). We found that CpG and several other TLR agonists increased ECAR relative to mock-BMDMs, indicating an increase in glycolytic flux (**Fig 18c, Fig 20**). However, distinct from other TLR agonists, CpG elevated the basal OCR of macrophages, signifying higher rates of oxidative phosphorylation (**Fig 18d-e, Fig 20**). This metabolic change seen in CpG-stimulated macrophages is consistent with metabolic activation seen in dendritic cells in response to CpG34. Further, we observed that the basal OCR of macrophages increased with prolonged CpG stimulation (**Fig 18f**), and corresponded with reduced spare respiratory capacity (**Fig 18g**). Collectively, these findings demonstrate that CpG-activation confers a unique metabolic shift in macrophages that occurs without skewing toward a classical M1 or M2 polarization state.

Lipid metabolism is critical for anti-tumor functions induced by CpG

We next investigated the significance of elevated oxygen consumption in response to CpG activation by first assessing mitochondrial abundance in macrophages. CpG-BMDMs exhibited an increase in total mitochondria, in comparison to mock-BMDMs (**Fig 19b**). To further evaluate changes in mitochondrial function, we tested the contribution of FAO toward elevated oxygen consumption under normal culture

conditions, in the presence of serum and without other exogenous lipids. FAO was restricted using etomoxir, an irreversible inhibitor of the enzyme carnitine palmitoyltransferase 1A (CPT1A) that is involved in fatty acid breakdown. We found that FAO-inhibition blocked the CpG-induced increase in macrophage OCR without affecting the maximal respiratory capacity (**Fig 21a-b**). Furthermore, FAO inhibition with etomoxir attenuated the capacity of CpG-BMDMs to phagocytose PDAC cells, whether they expressed inhibitory CD47 or not (**Fig 21c-d**).

To test the role of FAO for the *in vivo* anti-tumor activity induced by CpG, etomoxir was administered daily to mice beginning on day 9 prior to initiating CpG treatment on day 10. We found that etomoxir treatment blocked the anti-tumor effect of CpG, whereas treatment with etomoxir alone had no significant impact on tumor outgrowth (**Fig 21e**). Importantly, etomoxir treatment also did not alter the abundance of F4/80+ macrophages in the tumor microenvironment, indicating that the inhibitory effect observed was not a result of depletion or exclusion of macrophages from the tumor microenvironment (**Fig 21f**). Rather, the inhibitory effect of etomoxir was associated with decreased engulfment of tumor cells by F4/80+ macrophages (**Fig 8**). Together, these data demonstrate a key role for FAO in macrophage-dependent anti-tumor activity induced with CpG.

***De novo* lipogenesis, but not exogenous fatty acids, are critical for CpG-activated anti-tumor activity**

To define the metabolic changes induced by CpG, we assessed the abundance of short chain coenzyme A (CoA) species in mock- and CpG-treated macrophages. We

hypothesized that an increase in FAO in CpG-BMDMs would require breakdown and incorporation of exogenous fatty acids into acetyl-CoA and TCA substrates. Surprisingly, we found that the incorporation of labeling from ^{13}C -palmitate into acetyl-CoA and succinyl-CoA was decreased in CpG-BMDMs, indicating that substrates other than exogenous palmitate likely serve as precursors for generating acetyl-CoA and succinyl-CoA in response to CpG stimulation (**Fig 22a-b**). We next investigated the impact of CpG on increased fatty acid uptake which is a key feature of M2 macrophages. We found that CpG-BMDMs did not upregulate fatty acid transporters such as CD36 which instead, was significantly downregulated in response to CpG stimulation (**Fig 19d**). In addition, CpG-BMDMs showed a limited increase in the uptake of BODIPY-labeled palmitate, indicating that utilization of exogenous fatty acids was not significantly altered in macrophages by CpG stimulation (**Fig 19c**). Together, these findings illustrate that while CpG-macrophages share several metabolic features with M2 macrophages, such as their oxidative phenotype, they differ significantly in their utilization of exogenous fatty acids.

We proceeded to examine alternative pathways that may support metabolic activation in CpG-BMDMs. Upon substitution of glucose or glutamine with ^{13}C -glucose or ^{13}C -glutamine in the media, the relative total pool sizes for acetyl-CoA, succinyl-CoA and HMG (hydroxymethylglutaryl)-CoA expanded in CpG-BMDMs compared to mock-BMDMs (**Fig 22c**). The percent of acetyl-CoA derived from glucose (M+2 isotopologue) increased in CpG-BMDMs relative to mock-BMDMs (Fig 6d). This shift was accompanied by a decreased percent of acetyl-CoA derived from glutamine (M+2 isotopologue) in CpG-BMDMs (**Fig 22d**). Conversely, incorporation of ^{13}C -glucose into succinyl-CoA (M+4 isotopologue) decreased upon CpG-stimulation, and was

accompanied by an increase in labeled, glutamine-derived succinyl-CoA (M+4 isotopologue) in CpG-BMDMs compared to mock-BMDMs (**Fig 22e**). Together, these data show that CpG activation of macrophages promotes a shift away from complete utilization of carbon from glucose and toward glutamine anaplerosis for generating TCA cycle intermediates such as succinyl-CoA.

The incorporation of glucose into acetyl-CoA and HMG-CoA (a precursor for the cholesterol synthesis pathway) seen in CpG-stimulated BMDMs was consistent with a shunting by ATP citrate lyase (ACLY) and de novo biosynthesis of cholesterol/lipids. As a result, we hypothesized that disruption of ACLY would directly impede the anti-tumor activity of CpG-activated macrophages. We found that inhibition of ACLY during macrophage activation attenuated the oxidative phenotype that was induced by CpG and abrogated the anti-tumor phagocytic activity of CpG-stimulated macrophages even with combined CD47 ablation (**Fig 22f-g**). Therefore, our findings demonstrate that CpG can impart macrophages with a metabolic state that is distinct from that produced by M1 or M2 polarization. CpG-activated macrophages exhibit a hybrid metabolism, with shared features of both M1 and M2 macrophages. This unique metabolic state defined by enhanced oxidative phosphorylation and a shunting of TCA cycle intermediates imparts macrophages with anti-tumor potential and the capacity to circumvent inhibitory signals received by CD47 expressed on malignant cells (**Fig 23**).

Discussion

Macrophages dominate the tumor microenvironment of many cancers, wherein they are directed toward a pro-tumor role and restricted in their anti-tumor potential. The

capacity of macrophages to engulf and kill tumor cells is countervailed by their phenotype as well as inhibitory signals that are present within their surrounding microenvironment, including the anti-phagocytic molecule CD47, which is overexpressed by many malignant cells.^{88,165} Our study identifies a critical role for the central carbon metabolism of macrophages in defining their anti-tumor functions, including the capacity to phagocytose tumor cells. We have found that redirection of macrophages toward an oxidative phenotype is essential for anti-tumor activity induced by CpG stimulation *in vitro* and *in vivo*. Furthermore, CpG-stimulated alterations in macrophage metabolism were necessary for circumventing inhibitory signals mediated by CD47. Together, our findings highlight the importance of rewiring macrophage metabolism – by promoting FAO and redirecting the use of TCA intermediates – as a mechanism to circumvent negative regulatory signals present on malignant cells and to endow macrophages with anti-tumor potential.

We found that inhibitory signals expressed by PDAC cells may not always be dominant in regulating anti-tumor activity by macrophages. Unlike findings in other cancers, we found that disruption of CD47 activity via antibody-blockade was not sufficient for inciting anti-tumor responses in an immunocompetent tumor model of PDAC. Deletion of tumor-expressed CD47 was also not sufficient for inducing *in vitro* phagocytosis of tumor cells or *in vivo* anti-tumor responses. The absence of macrophage activity in this setting was not due to a lack of pro-phagocytic signals as treatment with CD47-blocking antibodies, which contain Fc-domains for driving Fc receptor dependent pro-phagocytic signals in macrophages, also failed to elicit macrophage anti-tumor activity *in vitro* and *in vivo*. Further, in the absence of macrophage activation via CpG

stimulation, we found that CD47-blocking antibodies were insufficient for stimulating macrophage phagocytosis of multiple solid tumor types including colorectal, glioblastoma, melanoma, breast cancer, and lung cancer. Our findings are consistent with xenograft models of PDAC, where CD47-blockade as monotherapy has shown limited anti-tumor activity.⁹⁵ Interestingly, we also did not detect changes in cellular calreticulin in response to CpG stimulation, which has been shown in other settings to be critical for stimulating macrophages to engulf tumor cells.⁷³ Rather, our data support a conceptual model in which inhibitory signals, such as CD47, can be overcome by the activation state of macrophages, which is defined by core metabolic pathways that govern their anti-tumor potential. Consistent with this, we observed a significant role for CD47 in regulating macrophage anti-tumor activity *in vitro*, but only when macrophages were activated with CpG, which provides rationale for combining CD47 antagonists with myeloid agonists. However, this finding was not appreciated *in vivo* where CpG-induced anti-tumor activity was indistinguishable between tumors that expressed or lacked CD47. This may reflect the emergence of additional anti-phagocytic signals that are redundant with CD47 expressed by tumor cells or even the capacity of CpG to more effectively activate *macrophages in vivo* to circumvent inhibitory signals mediated by CD47.

Although M1 and M2 polarization is commonly used to describe macrophage activity in cancer and may underlie the mechanism of some macrophage-targeted therapies,¹⁶⁶ we found that the anti-tumor properties induced by CpG did not associate with a classical M1 or M2 phenotype. Even in the absence of M1-polarization, CpG stimulated macrophages to phagocytose and kill tumor cells, whether they expressed CD47 or not. These findings support a paradigm of plural activation states, in which

macrophages may adopt a wide spectrum of phenotypes that are distinguishable by changes in their functional and metabolic processes. Consistent with this premise, macrophage biology in microbial infection and obesity has been shown to be determined by their metabolic phenotype.¹⁶⁷ However, the functional consequences of metabolic changes in macrophages has remained poorly defined in cancer, despite findings to suggest that lipid metabolism has a pivotal role in governing the anti-tumor functions of several other immune cell types (e.g. myeloid-derived suppressor cells, dendritic cells, and T-cells).⁷⁰⁻⁷² Our findings substantiate the importance of lipid metabolism as a dominant regulator of anti-tumor activity by macrophages and in doing so, demonstrate that assessing M1 and M2 polarization is not always sufficient for delineating the anti-tumor potential of macrophages.

We found that the metabolic profile of CpG-activated macrophages exhibited a unique hybrid of M1 and M2 features, underscoring the need to understand the contribution of metabolism to macrophage phenotype beyond the M1 and M2 paradigm. We showed that, similar to M1 macrophages, CpG-activated macrophages redirected exogenous fatty acids and glucose toward acetyl-CoA generation and de novo lipid biosynthesis. Our findings are consistent with a known role for CpG in promoting foam cell formation by stimulating lipogenesis and cholesterol biosynthesis in macrophages.^{168,169} As seen in M2 macrophages, FAO and glutaminolysis were essential for the oxidative phenotype of CpG-activated macrophages.^{63,152} Notably, M2 macrophages are recognized to possess superior abilities than M1 macrophages in phagocytosing antibody-opsonized tumor cells,¹⁷⁰ suggesting an association between FAO and phagocytic capacity. However, even though inhibition of FAO in CpG-

activated macrophages wholly eliminated their ability to engulf PDAC cells expressing CD47, inhibition of CPT1A only partially inhibited phagocytosis of CD47 KO cells – suggesting that FAO was essential for overcoming tumor-expressed CD47, but dispensable for phagocytosis in the setting of CD47-inhibition. Functionally, FAO in anti-tumor macrophages may enable the breakdown of large lipid loads after engulfment of target cells or fulfill the metabolic demands for phagocytosis.¹⁷¹

Competition for limited nutrients can serve as a metabolic checkpoint that impinges on immune cell activation.¹⁷² If exogenous nutrients are limited, alternative biosynthetic pathways may support cellular metabolism by supplying glucose-derived fatty acids and reducing equivalents. Using metabolic tracers, we provide evidence of unique substrate partitioning in CpG-stimulated macrophages that promotes oxidation of ¹³C-glucose to acetyl-CoA. As acetyl-CoA is diverted into anabolic reactions supporting lipid biosynthesis, CpG-stimulated macrophages rely on glutamine to support TCA cycle anaplerosis in a futile cycle similar to that seen in M2-polarized macrophages and T-cells.^{63,70} Although speculative, increased glutamine flux may support utilization of spare respiratory capacity in CpG-stimulated macrophages, which could provide a contingency energy source for buffering against nutrient depletion and oxygen deprivation in hostile tumor environments.

Changes in the lipid metabolism of CpG-activated macrophages may also alter plasma membrane properties and in doing so, confer macrophages with an ability to phagocytose more effectively.¹⁵⁷ In turn, changes in membrane fluidity can critically regulate immunoreceptor signaling during activation of immune cells.^{173,174} Likewise in macrophages, CD47-SIRP α signaling and the formation of phagocytic synapses depend

on membrane rigidity and receptor-clustering.^{85,174} Macrophage activation by TLRs has been shown to promote lipid-modifying programs that can alter the abundance of ceramide and sphingolipid species. These changes in lipid metabolism may influence the membrane properties of macrophages, as well as their antimicrobial potential.¹⁷⁵ Analogously, CpG-activation can shift lipid metabolism in macrophages and consequently modulate their functions, including cytokine secretion.¹⁷⁶ Our data extend the functional role of TLR-activated changes in macrophage metabolism to include enhanced clearance of tumor cells, without need for engaging Fc-receptors or blocking CD47 activity. We speculate that additional mechanisms may operate downstream of CpG-activation. For example, distinct activation stimuli have been shown to induce macrophages with “trained memory” in immune functions, characterized by epigenetic changes with distinct patterns of histone acetylation.^{177,178} Key acetylation substrates that may shape the macrophage activation state include acetyl-CoA species derived from lipids.^{66,179,180} In CpG-activated macrophages, the dynamic contribution of glucose and fatty acids to acetyl-CoA pools may similarly support epigenetic changes that facilitate their anti-tumor role.

CpG is actively being investigated in clinical trials for the treatment of advanced cancer and our findings provide important insights. We show significant anti-tumor activity induced with repeated dosing of CpG as monotherapy. In contrast, clinical trials examining CpG as monotherapy, as well as in combination with immunotherapy and cytotoxic chemotherapy, have demonstrated limited efficacy in patients with advanced cancer.^{45,181,182} However, dosing schedule and route of CpG delivery differ significantly in these clinical investigations compared to our study. We administered CpG systemically

and repeatedly every 2 days for five doses with the intent of inciting robust and sustained macrophage activation. In contrast, most clinical studies evaluating CpG oligodeoxynucleotides have investigated subcutaneous delivery and weekly administration with the goal of stimulating dendritic cells and mobilizing T cell immunity. Our data suggest, though, that activation of these cell populations may not always be required for CpG-induced anti-tumor activity. Since intravenous delivery of CpG has demonstrated safety in patients,^{183,184} our findings support a role for sustained systemic dosing of CpG treatment to stimulate macrophage anti-tumor activity.

Macrophages have emerged as promising therapeutic targets for cancer. Although they most often adopt pro-tumor functions within tumors, their phenotype is inherently pliable such that they can be directed with anti-tumor activity. Our data highlight the implications of activating anti-tumor functions in distinct macrophage populations. Specifically, we found that CSF1R⁺ macrophages were necessary for mounting an anti-tumor response upon CpG-activation, despite this subset of macrophages being associated with immunosuppression.¹⁶⁶ This finding is consistent with reports from other studies showing the potential to redirect macrophages with anti-tumor properties.^{32,147,148} However, the mechanisms involved in shifting the role of macrophages from pro- to anti-tumor have remained poorly defined. Our findings show a role for core metabolic processes, which act in concert as a key regulator of macrophage anti-tumor activity. This finding also highlights the importance of the metabolic state of macrophages for potentiating CD47-based therapies that have, thus far, shown limited efficacy as monotherapy in PDAC and non-hematopoietic malignancies.^{95,150} Our study identifies

macrophage metabolism as a novel therapeutic target that must be appropriately wired to enable macrophages to carry out anti-tumor functions.

Figures

Figure 3: Macrophage activation via TLR agonists, but not disruption of CD47, induces anti-tumor activity in a model of pancreatic cancer.

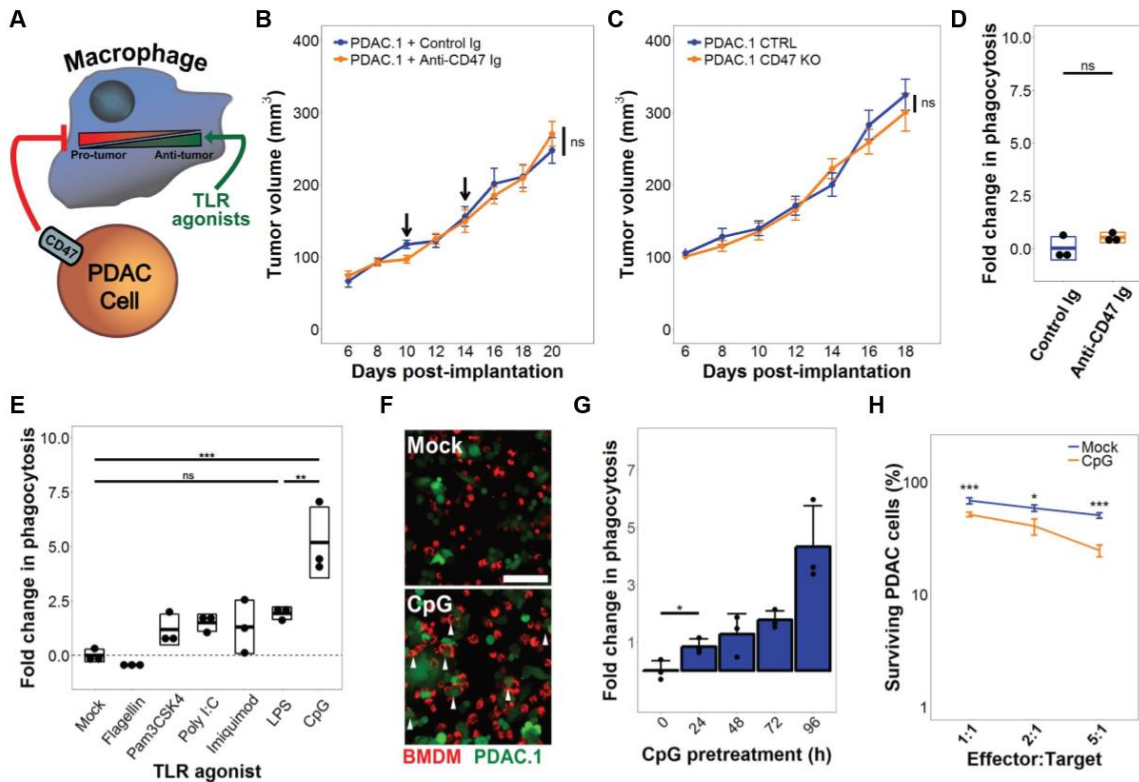


Figure 3: (a) Conceptual model showing a role for stimulatory (TLR agonists) and inhibitory (CD47) signals in regulating the anti-tumor activity of macrophages. (b) Syngeneic mice with established PDAC tumors were treated with 50 μ g isotype or anti-CD47 Ig on days 10 and 14 after tumor implantation (n=8). Arrows indicate intratumoral delivery of antibody; error bars represent standard error. (c) Syngeneic mice were challenged with PDAC tumors in which CD47 was knocked out (CD47 KO) versus control (CTRL) using CRISPR-Cas9 gene editing (n=5); error bars represent standard error. (d) *In vitro* phagocytosis of PDAC cells by BMDMs in the presence of isotype control or anti-CD47 Ig. (e) *In vitro* phagocytosis of PDAC cells by BMDMs stimulated with indicated TLR agonists for 24 hours. (f) Representative immunofluorescence images showing phagocytosis of PDAC cells (green) by macrophages (BMDM, red) pretreated

with vehicle (mock) or CpG for 24 hours. Arrows indicate phagocytic events. **(g)** *In vitro* phagocytosis of PDAC cells by BMDMs stimulated with CpG for increasing lengths of time (n=3), error bars represent standard error. **(h)** PDAC cell survival following 48-hour co-culture with macrophages pretreated with vehicle (Mock) or CpG for 96 hours (n=3), error bars represent standard error. Boxplots represent mean \pm SD. Two-tailed Student's *t*-test with Hochberg correction: ns (not significant); *, $p < 0.05$; **, $p < 0.01$; ***, $p < 0.001$. Results are representative of at least two independent experiments **(a-h)**.

Figure 4: CD47 expression in murine PDAC tumor cells.

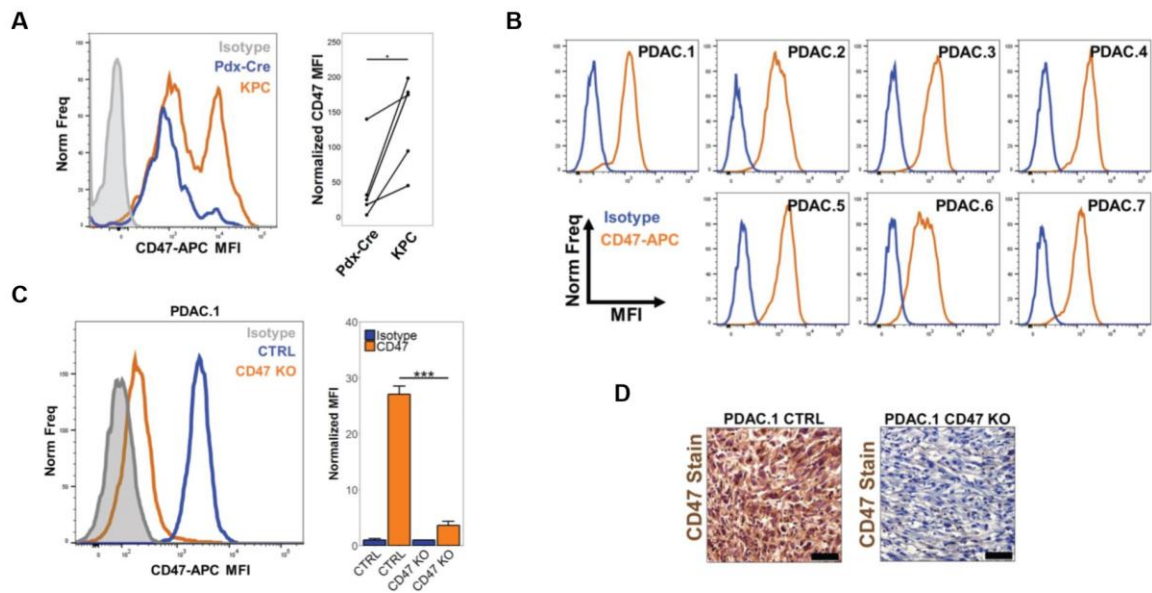


Figure 4: (a) Representative histograms of CD47 expression by live EpCAM+ cells in tumors and pancreata from age- and gender-matched KPC ($Kras^{LSL.G12D/+}; Trp53^{R172H/+}$; *Pdx-Cre*) and *Pdx-Cre* control mice. Significance determined by paired *t*-test of mean fluorescence intensity (MFI) normalized to isotype stain: ns (not significant); *, $p < 0.05$; **, $p < 0.01$; ***, $p < 0.001$. (b) Representative histograms of CD47 expression in distinct KPC-derived tumor cell lines cultured in vitro. (c) Histogram (left) of CD47 expression in control (CTRL) and CD47 knockout (CD47 KO) PDAC.1 cells after deletion of CD47 by CRISPR-Cas9 (left). Normalized MFI (right) relative to isotype stain (right). Significance determined by two-tailed Student's *t*-test of normalized MFI: ns (not significant); *, $p < 0.05$; **, $p < 0.01$; ***, $p < 0.001$. (d) Representative immunohistochemistry images showing CD47 expression detected in implanted tumors derived from PDAC.1 CTRL and CD47 KO cells. Scale bar represents 50 μ m. Error bars represent SD, and results are representative of at least two independent experiments (a-d).

Figure 5: CpG stimulates macrophage-dependent anti-tumor activity *in vivo*.

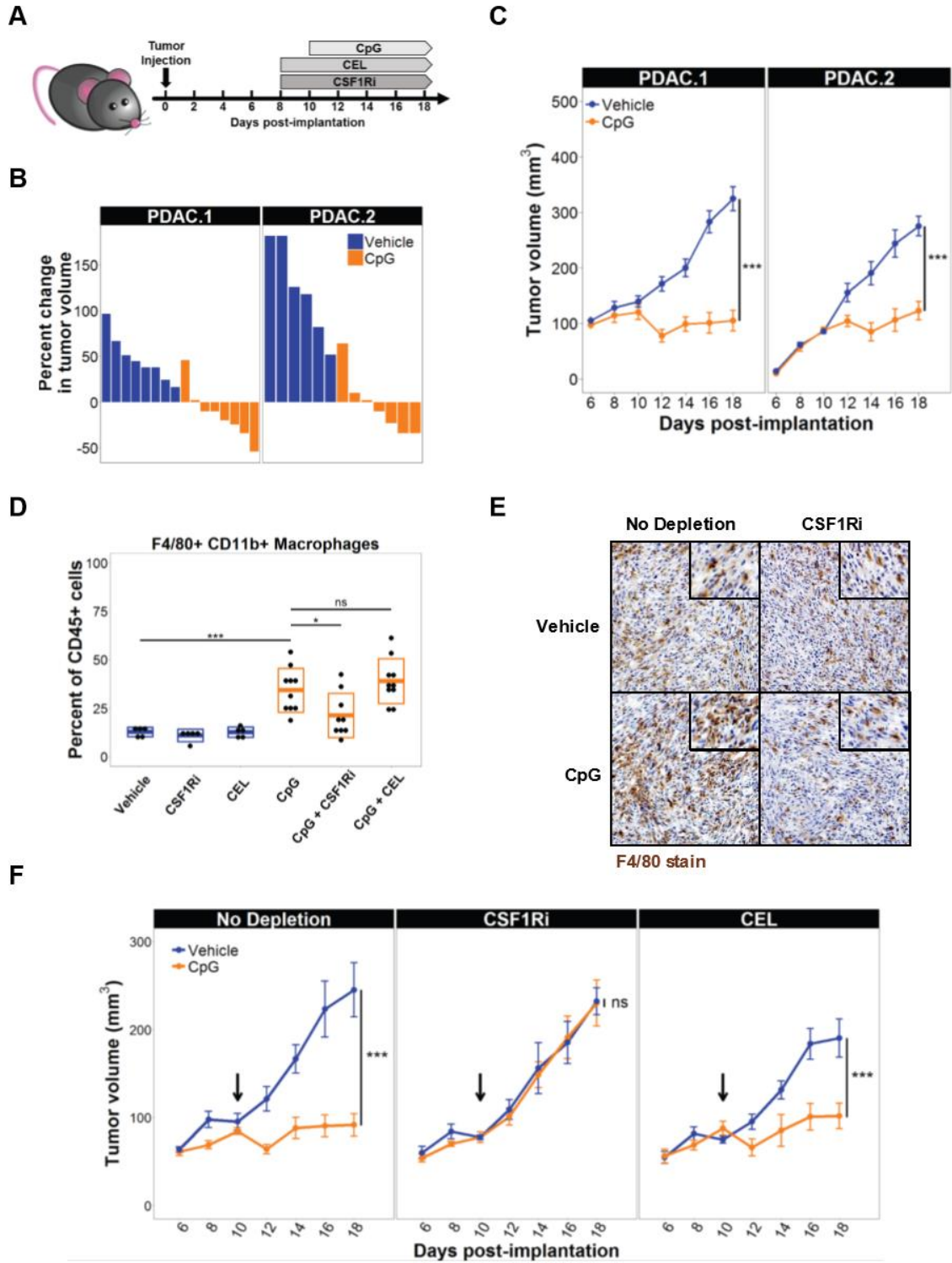
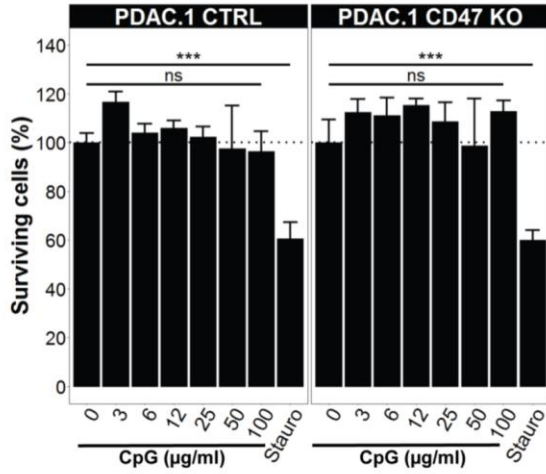


Figure 5: (a) Schematic showing implantation of PDAC tumor cells (day 0) and subsequent treatment schedule (beginning on day 8) for CpG and methods of macrophage depletion using clodronate encapsulated liposomes (CEL) and a CSF1R-inhibitor (CSF1Ri). (b) Two distinct syngeneic KPC-derived PDAC tumors (PDAC.1 and PDAC.2) were treated with vehicle or CpG beginning on day 10. Waterfall plots show percent change in tumor volume at day 14 relative to baseline prior to treatment (day 10). (c) Longitudinal growth curves for PDAC tumors treated with vehicle or CpG (n=6-8); error bars represent standard error. (d) Shown is frequency of CD11b⁺ F4/80⁺ macrophages among total CD45⁺ cells detected by flow cytometry in PDAC tumors at day 18, in mice treated with CpG, CSF1Ri, and CEL. Boxplots represent mean \pm SD. (e) Representative images of immunohistochemistry to detect F4/80⁺ macrophages in PDAC tumors after treatment with vehicle or CpG with or without CSF1Ri. (f) Longitudinal growth curves of PDAC.1 tumors treated with CpG and vehicle (no depletion), CSF1Ri, or clodronate encapsulated liposomes (CEL); error bars represent standard error. Arrows indicate the initiation of CpG treatment. Two-tailed Student's *t*-test with Hochberg correction: ns (not significant); *, $p < 0.05$; **, $p < 0.01$; ***, $p < 0.001$. Results are representative of at least two independent experiments (a-f).

Figure 6: Toxicity assessment of etomoxir and CpG in macrophages and PDAC cells.

A



B

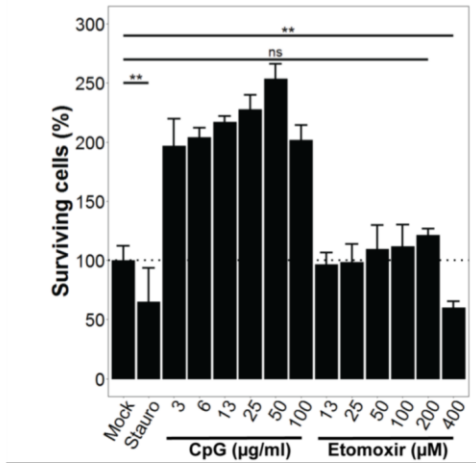
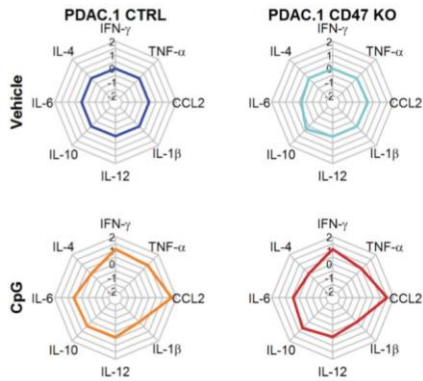


Figure 6: (a) Survival of PDAC cells with (CTRL) or without CD47 (CD47 KO) expression was detected by crystal violet stain, after treatment with vehicle (mock) for 48 hours, defined concentrations of CpG for 48 hours, or 10 mM staurosporine (Stauro) for 6 hours. **(b)** Survival of BMDMs detected by crystal violet stain, after treatment with vehicle (mock) for 48 hours, CpG and etomoxir for 48 hours, or 10 mM staurosporine (Stauro) for 6 hours. Error bars represent standard error, and results are representative of

at least two independent experiments (**a,b**). Significance determined by two-tailed Student's *t*-test: ns (not significant); *, $p < 0.05$; **, $p < 0.01$; ***, $p < 0.001$.

Figure 7: In vivo delivery of CpG to tumor-bearing mice induces systemic cytokine release.

A



B

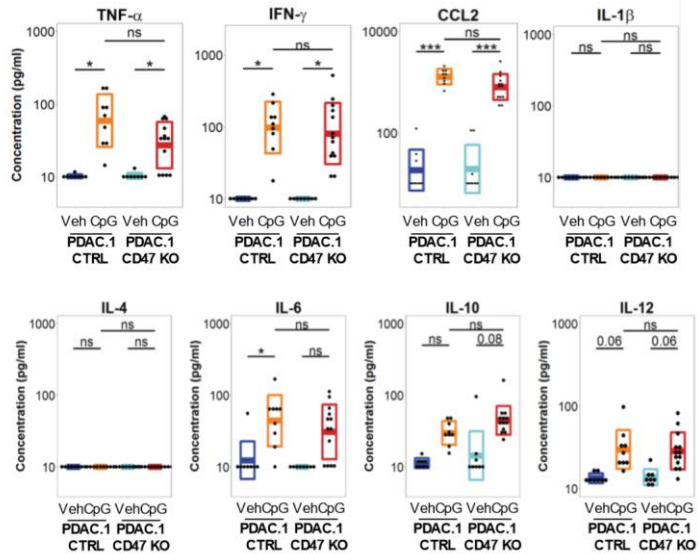


Figure 7: Syngeneic mice bearing PDAC.1 control (CTRL) or PDAC.1 CD47 KO tumors were treated with vehicle or CpG beginning on day 10 after tumor implantation. Peripheral blood cytokines were detected on day 14. Shown are (a) radar plots of fold change (radial axis) in cytokines detected in the peripheral blood, normalized to vehicle-treated mice bearing PDAC.1 control (CTRL) tumors and (b) box plots of cytokine concentrations detected in the peripheral blood. Two-tailed Student's *t*-test with Hochberg correction: ns (not significant); *, $p < 0.05$; **, $p < 0.01$; ***, $p < 0.001$. Results are representative of at least two independent experiments (a,b).

Figure 8: Macrophage engulfment of PDAC.1 cells *in vivo*.

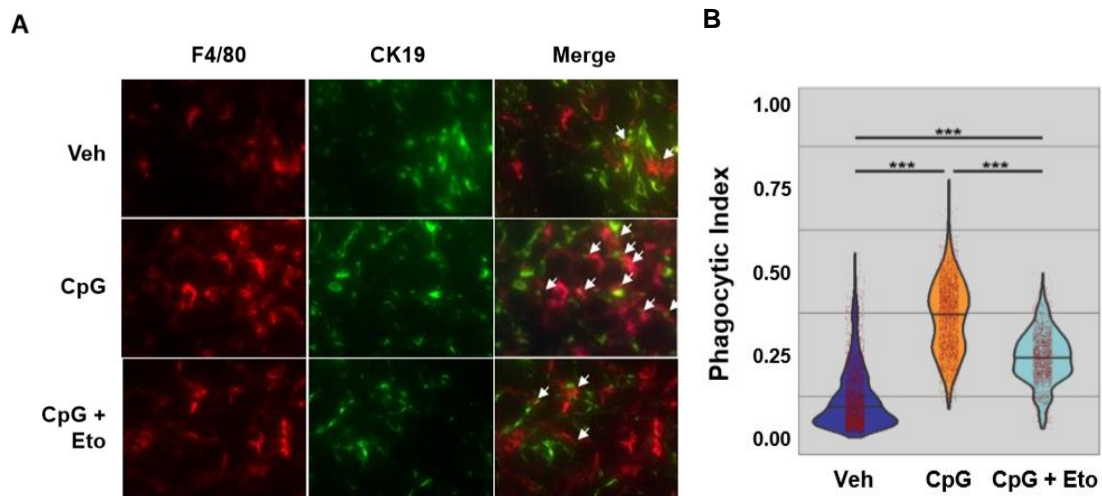


Figure 8: PDAC.1 tumors were harvested at day 14 post-implantation following treatment with vehicle (Veh), CpG, or CpG + Etomoxir (CpG + Eto) beginning on day 10. (a) Shown is representative images of immunofluorescent co-staining for F4/80⁺ (red) and cytokeratin 19 (CK19, green) in tumors treated as indicated. White arrows indicate macrophages that have engulfed/phagocytosed CK19⁺ tumor cells. (b) Phagocytic index was calculated as the intensity of CK19 signal in an F4/80⁺ macrophage, following normalization of the CK19 signal across treatment groups. Violin plots show the median, and every point represents an individual F4/80⁺ macrophage pooled from tumors in each treatment group (n = 4-5 tumors per group, four random 20x fields per tumor). Significance determined by ANOVA comparison of linear mixed effects models: ns (not significant); *, $p < 0.05$; **, $p < 0.01$; ***, $p < 0.001$

Figure 9: Depletion of tumor macrophages using anti-CSF1R antibody attenuates the anti-tumor response of CpG.

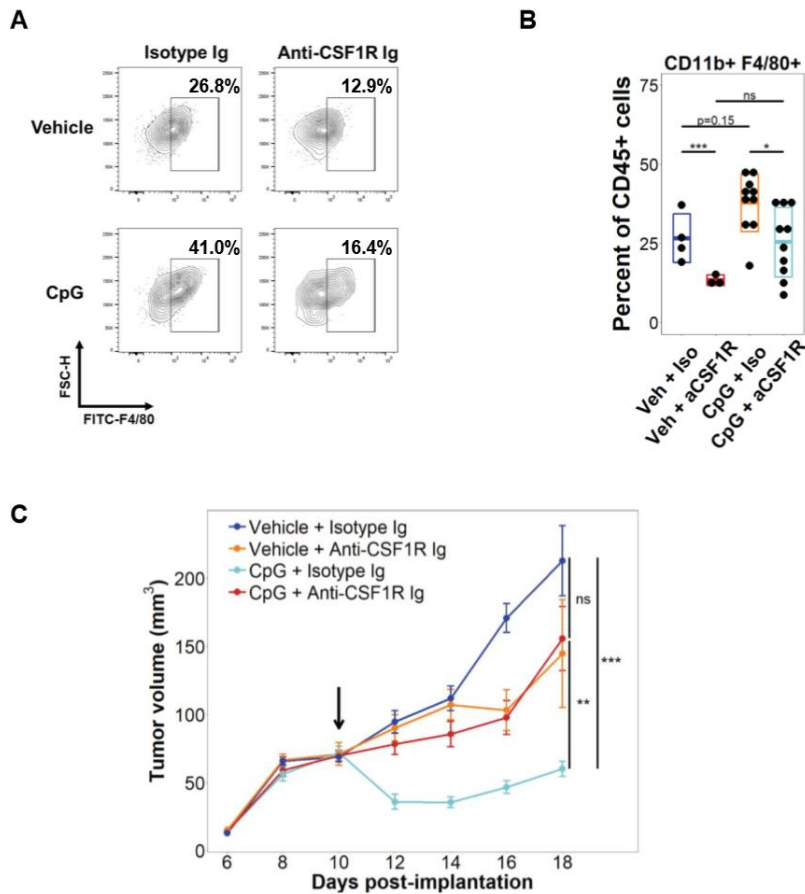


Figure 9: Mice bearing PDAC.1 tumors were treated with isotype (Iso) or anti-CSF1R (aCSF1R) antibody on days 8, 10, 13, 16; vehicle (Veh) or CpG was delivered beginning on day 10 and every two days thereafter. **(a)** Representative flow plots are shown of live F4/80⁺ CD11b⁺ CD45⁺ macrophages from tumors harvested on day 18. **(b)** Shown is frequency of F4/80⁺ CD11b⁺ macrophages among total CD45⁺ cells detected by flow cytometry in PDAC tumors at day 18, in mice treated with Veh + Iso, Veh + aCSF1R, CpG + Iso, and CpG + aCSF1R. Boxplots represent mean \pm SD. **(c)** Longitudinal growth curves of PDAC.1 tumors in mice treated with vehicle + isotype (n=4), vehicle + anti-CSF1R Ig (n=3), CpG + isotype (n=10), or CpG + anti+CSF1R Ig (n=10). Two-tailed Student's *t*-test with Hochberg correction: ns (not significant); *, $p < 0.05$; **, $p < 0.01$; ***, $p < 0.001$. Error bars indicate standard error.

Figure 10: Flow cytometric and histologic quantification of tumor-associated myeloid cells in mice treated with or without a CSF1R inhibitor (CSF1Ri).

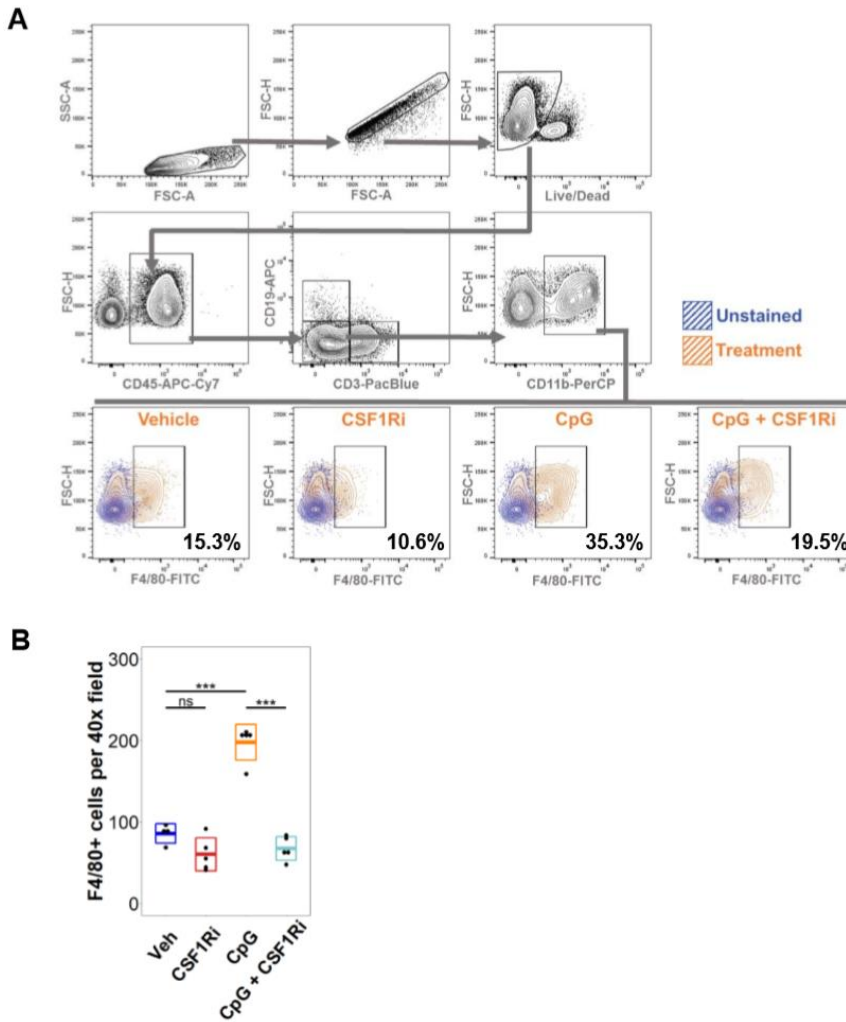


Figure 10: (a) Flow cytometric gating strategy for quantifying live (Amcyan^{neg}) CD45⁺ CD3^{neg} CD19^{neg} F4/80⁺ CD11b⁺ macrophages (orange) from singlet cells (gated by FSC-A and FSC-H) in tumor digest, compared to bulk unstained tumor cells (blue). Shown are representative flow cytometric dot plots for samples isolated from digest of PDAC.1 tumors on day 18 following tumor implantation, in mice treated with vehicle, CSF1Ri, CpG, or CpG + CSF1Ri beginning on day 10. Quantification is shown in Fig 2d. **(b)** Shown is quantification of F4/80⁺ macrophages detected by immunohistochemistry in PDAC tumors harvested on day 18, following treatment as indicated. Representative

images are shown in Fig 2e. Two-tailed Student's *t*-test with Hochberg correction: ns (not significant); *, $p < 0.05$; **, $p < 0.01$; ***, $p < 0.001$. Boxplots represent mean \pm SD.

Figure 11: CpG-treatment does not alter T cell activation or infiltration into tumors.

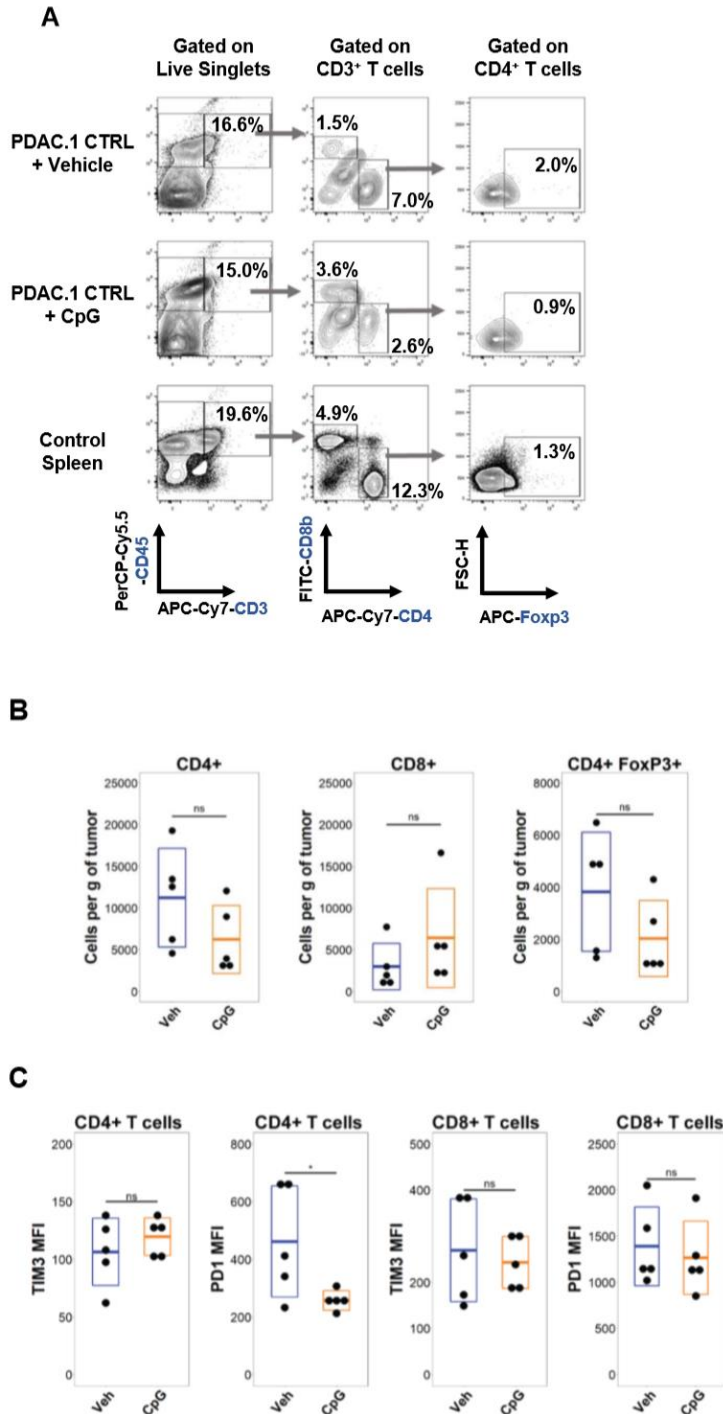


Figure 11: (a) Shown are representative flow cytometry dot plots of CD45⁺ CD3⁺ T cells from PDAC.1 tumors collected on day 18 post-implantation. Mice were treated as indicated with vehicle or CpG on days 10, 12, 14, 16, and 18 after tumor implantation. Splenocytes from untreated mice were included as a control. (b) Absolute number (per gram of tumor tissue) of CD4⁺, CD8⁺, and regulatory CD4⁺ Foxp3⁺ T cells detected in tumors from vehicle- or CpG-treated mice. (c) Mean fluorescence intensity (MFI) of Tim3 and PD1 activation markers on CD4⁺ and CD8⁺ T cells detected in tumors treated with vehicle or CpG. Boxplots represent mean \pm SD, significance was determined using two-tailed Student's *t*-test: ns (not significant); *, $p < 0.05$; **, $p < 0.01$; ***, $p < 0.001$.

Figure 12: T cells and natural killer (NK) cells are dispensable for CpG-induced anti-tumor activity.

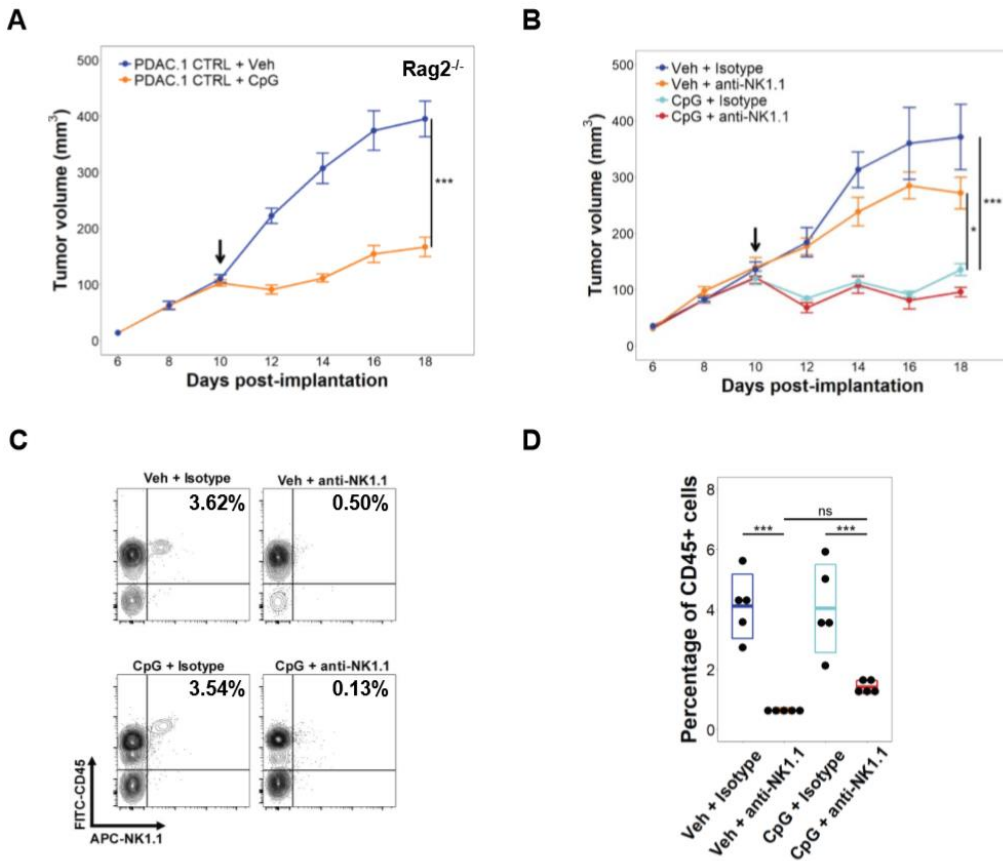


Figure 12: (a) Longitudinal growth curves of PDAC.1 CTRL tumors in syngeneic *Rag2*^{-/-} mice (n=8 per group) treated with vehicle (Veh) or CpG beginning on day 10 and repeated every 2 days for 4 doses. Results are representative of two independent experiments. **(b)** Longitudinal growth curves of PDAC.1 CTRL in syngeneic mice (n=5 per group) treated with Veh or CpG beginning on day 10 and repeated every 2 days., Mice also received isotype or anti-NK1.1 antibody delivered on days 8, 10, 13, and 16 after tumor implantation. **(c)** Representative flow cytometry dot plots and **(d)** quantification of percent CD45⁺ NK1.1⁺ NK cells detected in the peripheral blood on day 14 in mice treated as indicated. Arrows indicate the initiation of CpG treatment. Error bars represent standard error; boxplots represent mean ± SD. Two-tailed Student's *t*-test with Hochberg correction: ns (not significant); *, *p* < 0.05; **, *p* < 0.01; ***, *p* < 0.001.

Figure 13: Dendritic cells are not required for CpG-induced anti-tumor activity.

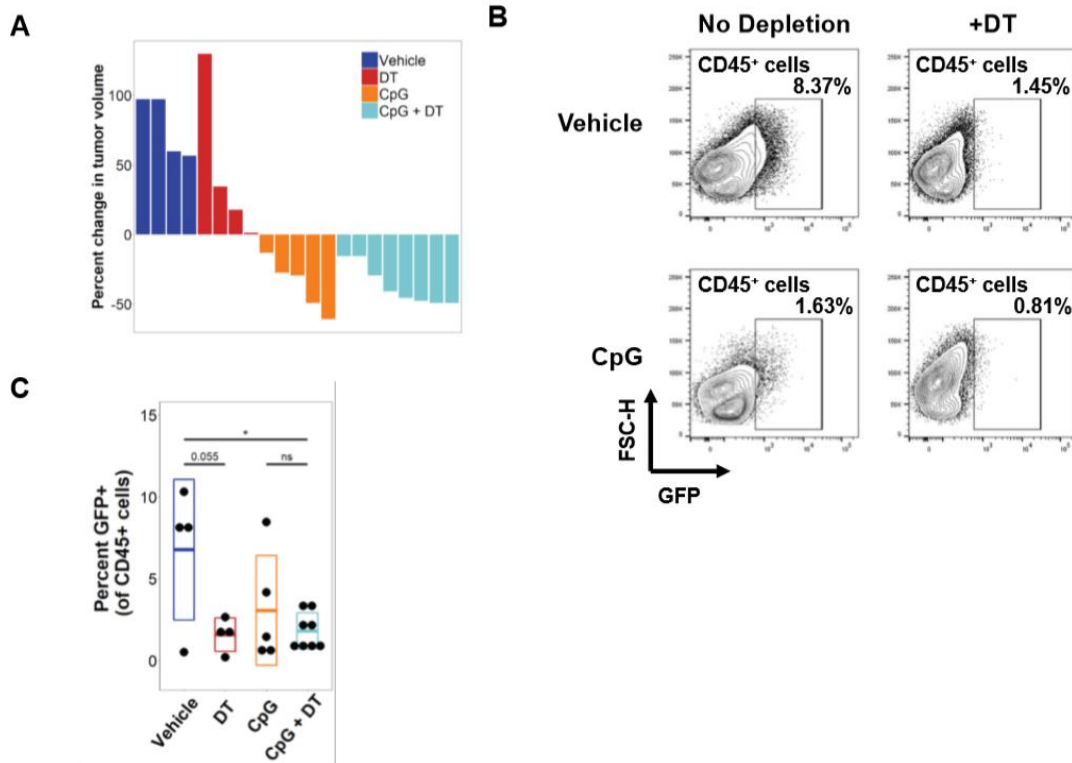


Figure 13: PDAC.1 CTRL tumors were implanted in syngeneic CD11c-DTR/eGFP mice and treated as indicated beginning on day 10 after tumor implantation. Diphtheria toxin (DT) was administered on day 10 and 12 at 12 hours prior to CpG dosing to deplete CD11c⁺ cells. (a) Waterfall plot showing percent change in tumor volume at day 13 relative to baseline (day 10), prior to CpG-treatment. (b) Representative flow cytometry dot plots to detect CD11c⁺ cells expressing GFP in tumor digests (gated on CD45⁺ singlets) (c) Shown is frequency of CD11c⁺ cells identified by GFP expression among total CD45⁺ cells detected by flow cytometry in PDAC tumors at day 13. Boxplots represent mean \pm SD. Two-tailed Student's *t*-test with Hochberg correction: ns (not significant); *, $p < 0.05$; **, $p < 0.01$; ***, $p < 0.001$.

Figure 14: CSF1R+ F4/80+ Ly6C+ macrophages are required for CpG-induced anti-tumor response.

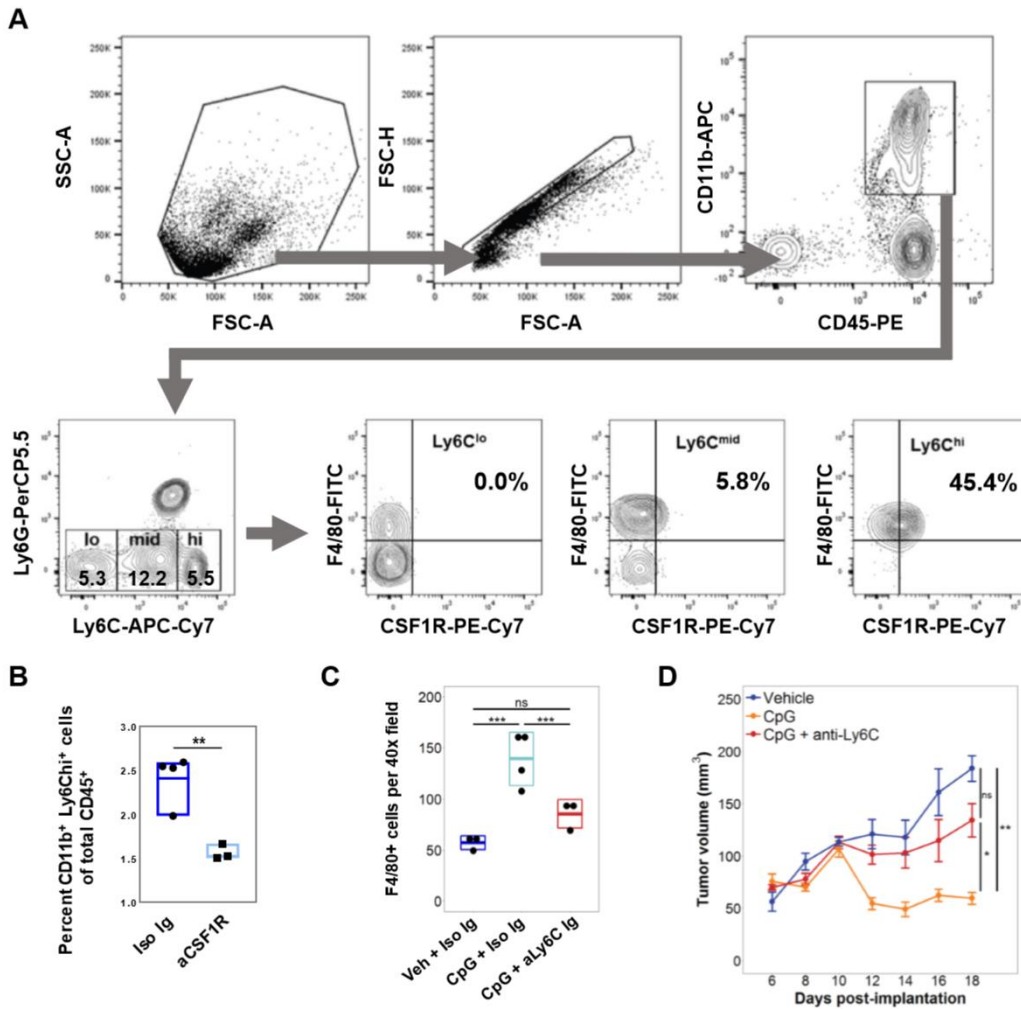


Figure 14: Mice bearing PDAC.1 tumors were treated with isotype (Iso) or anti-CSF1R (aCSF1R) antibody on days 8, 10, 13, 16 after tumor implantation; vehicle (Veh) or CpG was delivered on days 10, 12, 14, 16, 18. (a) Representative flow cytometric gating strategy for detecting CSF1R-expression on CD45⁺ F4/80⁺ CD11b⁺ macrophages in the peripheral blood. Shown are representative flow cytometric dot plots from a tumor-bearing mouse. (b) Quantification of Ly6C^{hi} monocytes in peripheral blood of tumor-bearing mice at day 14 after receiving isotype control (Iso Ig) or anti-CSF1R (aCSF1R) antibody. (c) Quantification by immunohistochemistry of F4/80⁺ cells in tumors of mice

on day 18 after treatment as indicated. **(d)** Longitudinal growth curves of PDAC.1 tumors in mice treated with vehicle, CpG, or CpG + anti-Ly6C antibody (Monts). Two-tailed Student's *t*-test with Hochberg correction: ns (not significant); *, $p < 0.05$; **, $p < 0.01$; ***, $p < 0.001$. Error bars indicate standard error. Results are representative of at least two independent experiments **(a,d)**

Figure 15: CpG stimulates macrophage anti-tumor activity *in vitro* and *in vivo* that is independent of the anti-phagocytic signal CD47 expressed on PDAC cells.

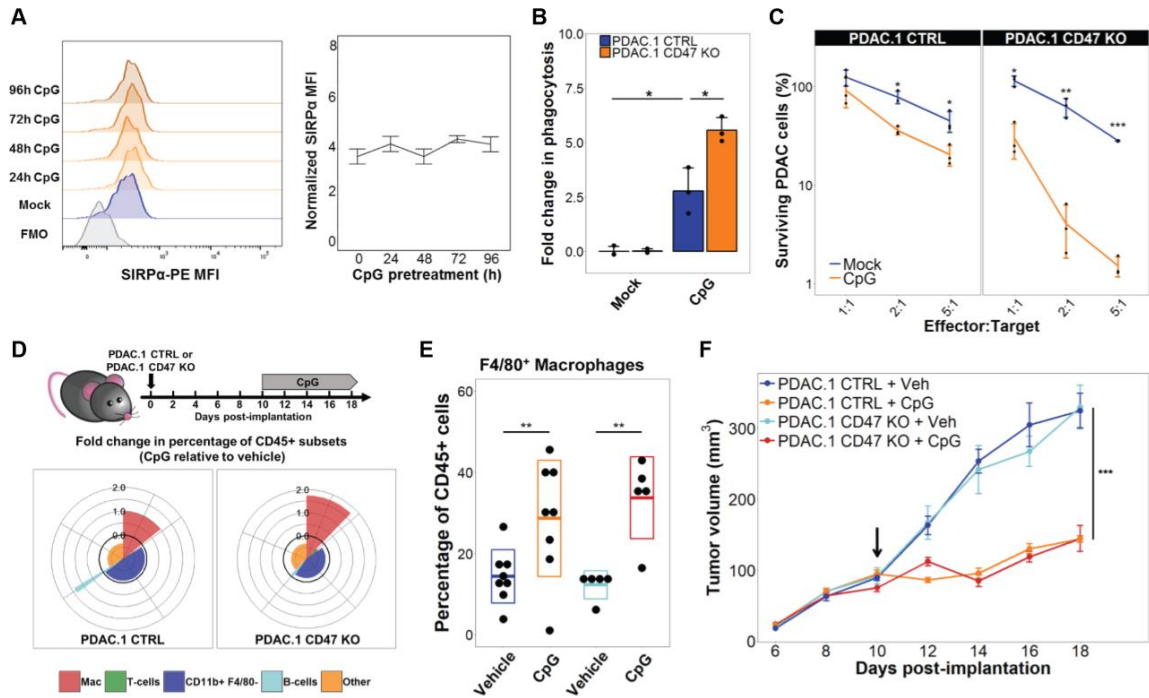


Figure 15: (a) Representative histogram plots of SIRP α expression (left) and normalized SIRP α expression (right) detected by flow cytometry on BMDMs after activation with CpG for 24-96 hours (n=3). **(b)** Vehicle (mock) versus CpG stimulated macrophage phagocytosis of PDAC cells in which CD47 was knocked out (CD47 KO) using CRISPR-Cas9 gene editing versus control (CTRL) (n=3). **(c)** Survival of PDAC.1 CTRL and CD47 KO cells following 48-hour co-culture with vehicle (mock) or CpG activated macrophages pretreated for 72 hours, using the indicated effector (macrophage) to target (tumor) ratios (n=3). **(d)** Coxcomb plots showing distribution and fold change in leukocyte subsets (as a percentage of CD45⁺ cells on day 18), for CpG treatment relative to vehicle treatment in control (left) and CD47 KO (right) PDAC tumors. Radial axis represents relative fold change in leukocyte subset percentage (n=5-8). **(e)** Percentage of CD11b⁺ F4/80⁺ macrophages in control and CD47 KO tumors following CpG treatment. Boxplot represents mean \pm SD. **(f)** Tumor volume of control and CD47 KO tumors treated with CpG (n=5-8); arrow indicates initiation of CpG; error bars represent standard error. Two-tailed Student's *t* test with Hochberg correction: ns (not significant); *, *p* <

0.05; **, $p < 0.01$; ***, $p < 0.001$. Results are representative of at least two independent experiments (**a-f**).

Figure 16: CpG-activation induces macrophage engulfment of tumor cells of multiple cancer types.

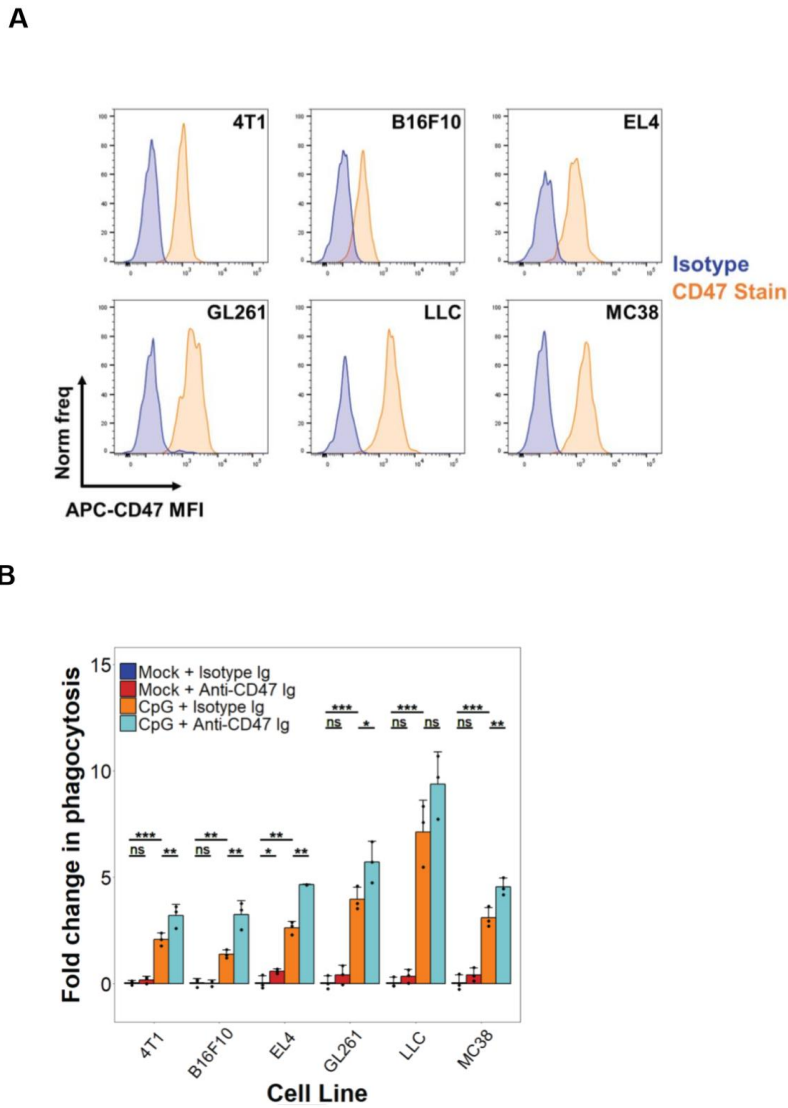


Figure 16: (a) Representative histograms showing CD47 expression on the cell surface of murine tumor cell lines, derived from breast cancer (4T1), melanoma (B16F10), T cell lymphoma (EL4), glioblastoma (GL261), lung cancer (LLC: Lewis Lung Carcinoma), and colorectal cancer (MC38) lines. **(b)** *In vitro* phagocytosis of syngeneic murine tumor cells treated with isotype or anti-CD47 antibody, and co-cultured with BMDMs stimulated with vehicle or CpG (n=3). Error bars represent standard error. Two-tailed

Student's t test with Hochberg correction: ns (not significant); *, $p < 0.05$; **, $p < 0.01$; ***, $p < 0.001$.

Figure 17: Calreticulin abundance in Mock- and CpG-BMDMs.

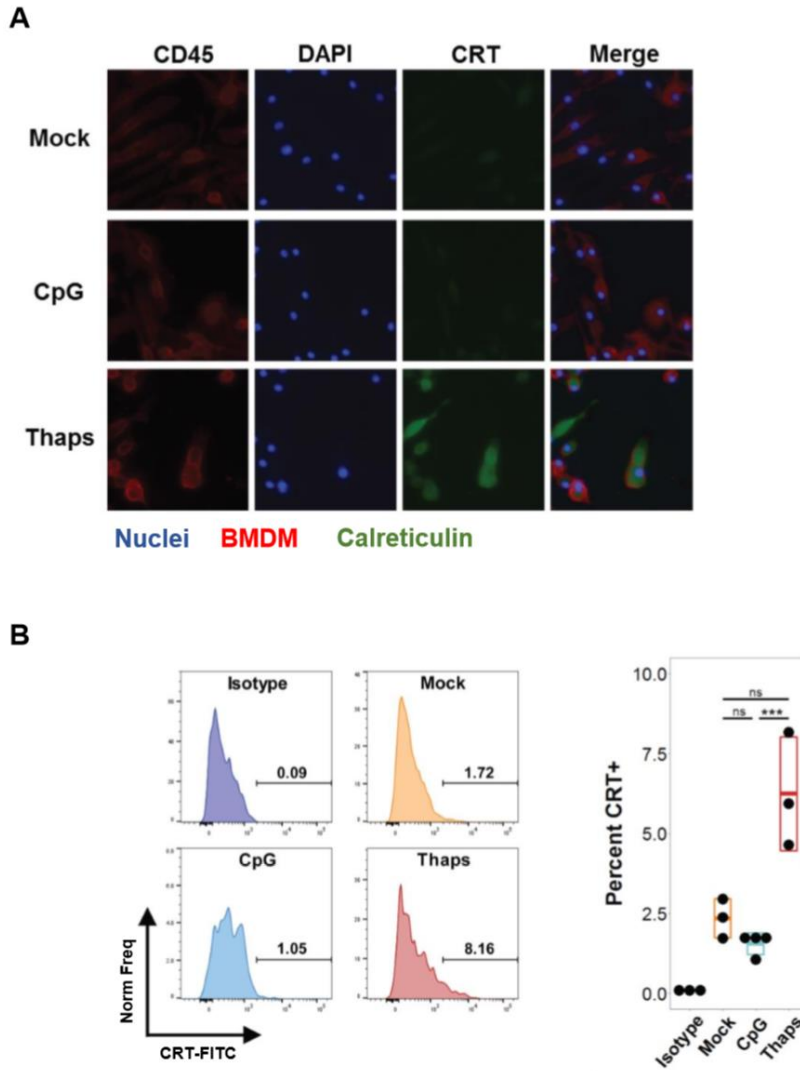


Figure 17: (a) Representative immunofluorescence stain to detect calreticulin (CRT, green) expression by CD45⁺ BMDMs (red) treated with vehicle (mock) or CpG for 96 hours, or thapsigargin (Thaps) for 6 hours. Nuclei are stained with DAPI (blue). **(b)** Representative histograms showing calreticulin expression by BMDMs detected by flow cytometry (left) with quantification (right), showing percentage of BMDMs expressing CRT after treatment with vehicle (mock), CpG, or thapsigargin. Two-tailed Student's *t* test with Hochberg correction: ns (not significant); *, *p* < 0.05; **, *p* < 0.01; ***, *p* < 0.001. Boxplots represent mean ± SD. Results are representative of at least two independent experiments **(a,b)**.

Figure 18: CpG evokes metabolic changes in macrophages without polarization to M1 or M2.

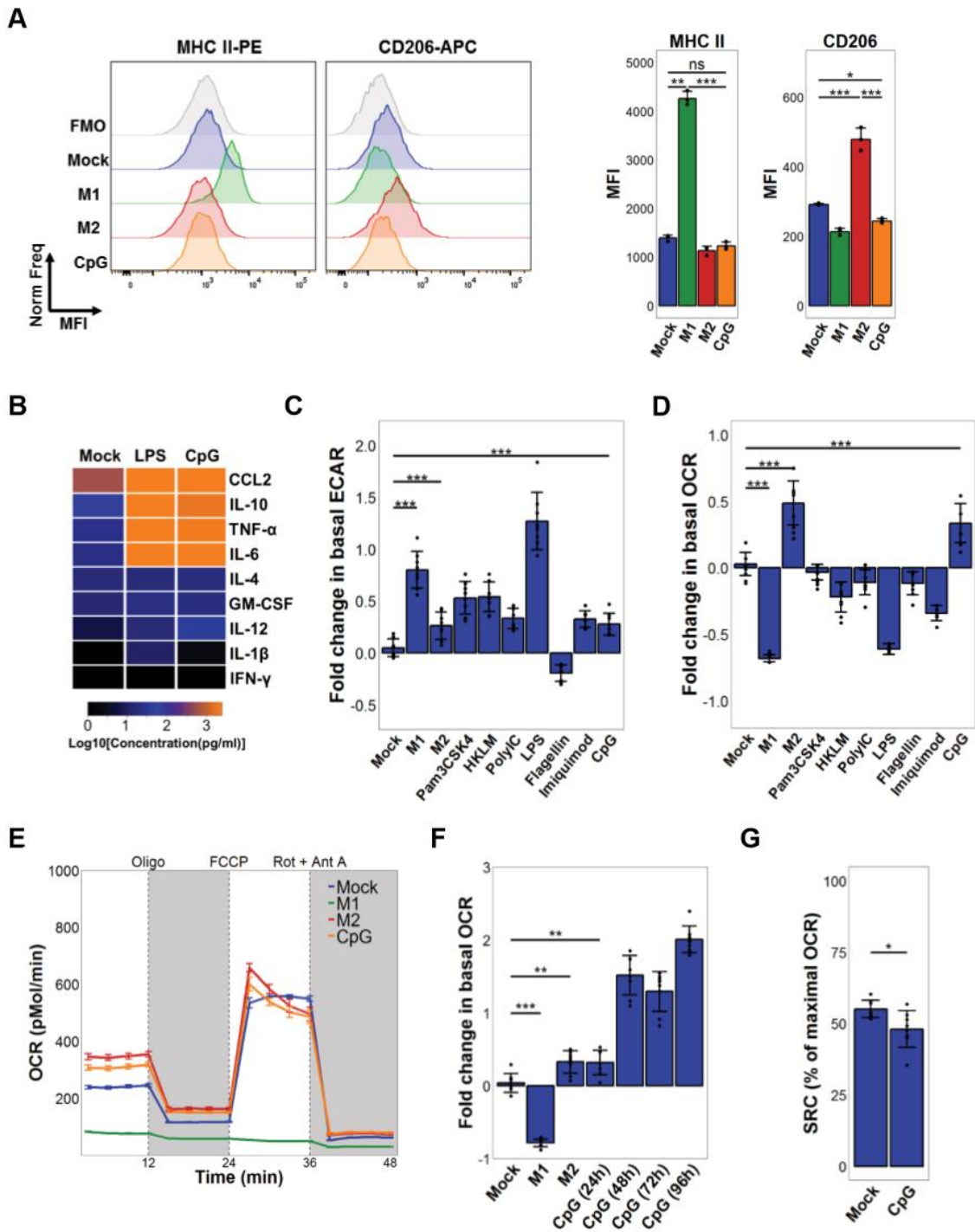


Figure 18: (a) Representative histogram plots of MHCII and CD206 expression (left) and mean fluorescence intensity (right) for BMDMs pretreated with vehicle (mock) or CpG for 96 hours, compared with M1 and M2 BMDMs (n=3). (b) Heatmap of cytokine concentrations produced *in vitro* by BMDMs treated with vehicle (mock), LPS, or CpG for 48 hours (n=3), scaled to Log10(Concentration in pg/ml). (c) Extracellular acidification rate (ECAR) of BMDMs after 24-hour activation with indicated TLR agonists (n=8), relative to mock-treated baseline. (d) Basal oxygen consumption rate (OCR) of BMDMs after 24-hour activation with indicated TLR agonists (n=8), relative to mock-treated baseline. (e) Profile of OCR in BMDMs pretreated for 24 hours with vehicle (mock) or CpG, in comparison to M1 and M2 BMDMs (n=8). OCR was measured as picomoles of O₂ per minute upon sequential administration with oligomycin, FCCP, and Rotenone + Antimycin A. (f) Basal OCR of BMDMs following activation with CpG for increasing durations (n=8), relative to mock-treated baseline. (g) Spare respiratory capacity of BMDMs treated with vehicle (mock) or CpG for 96 hours (n=8), shown as the difference between basal OCR and maximal OCR (after addition of FCCP). Two-tailed Student's *t* test with Hochberg correction: ns (not significant); *, $p < 0.05$; **, $p < 0.01$; ***, $p < 0.001$. Results are representative of at least two independent experiments (a-g).

Figure 19: Phenotypic differences in mock- and CpG-treated macrophages.

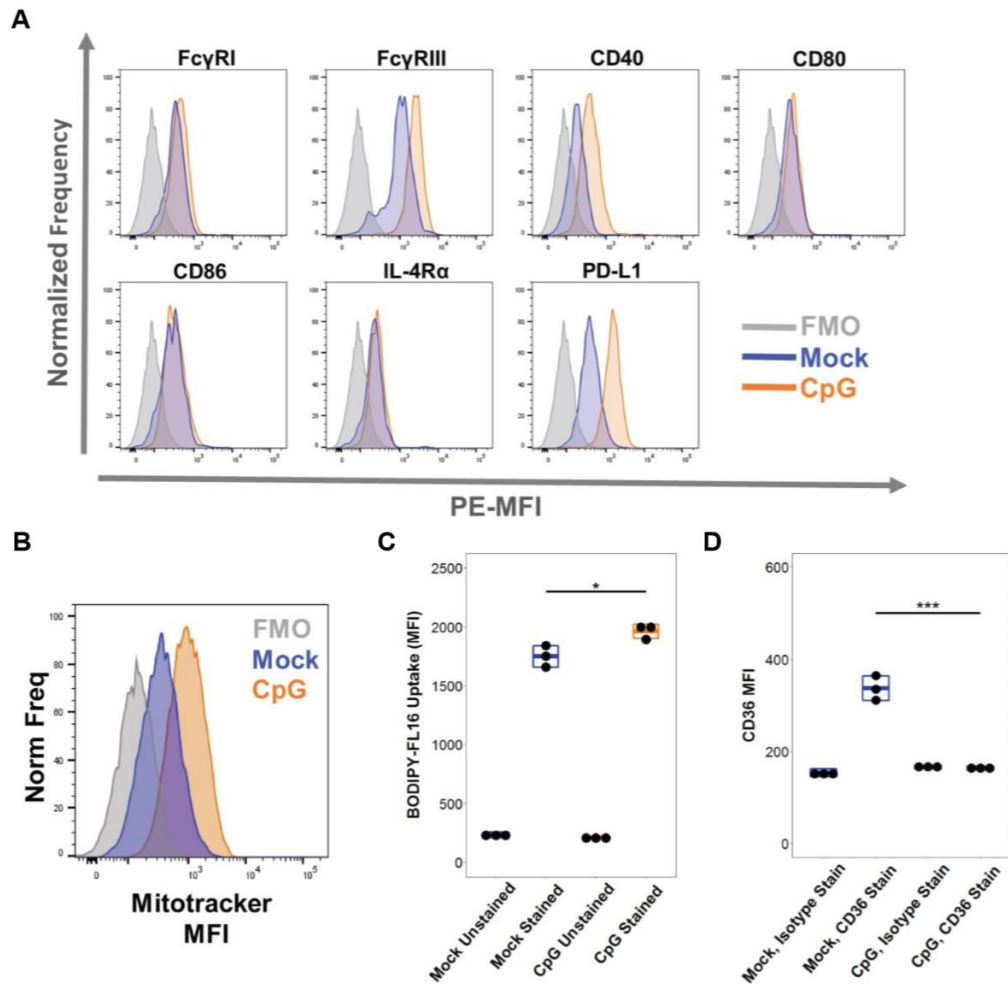


Figure 19: (a) Mean fluorescence intensity (MFI) of activation markers for BMDMs treated for 96 hours with vehicle (mock) or CpG, in relation to fluorescence minus one (FMO). Representative histogram plots are shown (n=3). (b) Mitochondrial abundance, measured as MFI of mitotracker staining, in BMDMs treated for 96 hours with vehicle (mock) or CpG, in relation to FMO. Representative histogram plots shown for n=3. (c) Fatty acid uptake of BODIPY-FL16 stain by BMDMs pretreated for 24 hours with vehicle (mock) or CpG (n=3). (d) Mean fluorescence intensity of CD36 expression in BMDMs treated with vehicle (mock) or CpG (n=3). Boxplots represent mean \pm SD, significance determined using Two-tailed Student's *t*-test: ns (not significant); *, $p <$

0.05; **, $p < 0.01$; ***, $p < 0.001$. Results are representative of at least two independent experiments (**a-d**).

Figure 20: Extracellular acidification and oxygen consumption rates in TLR-activated BMDMs.

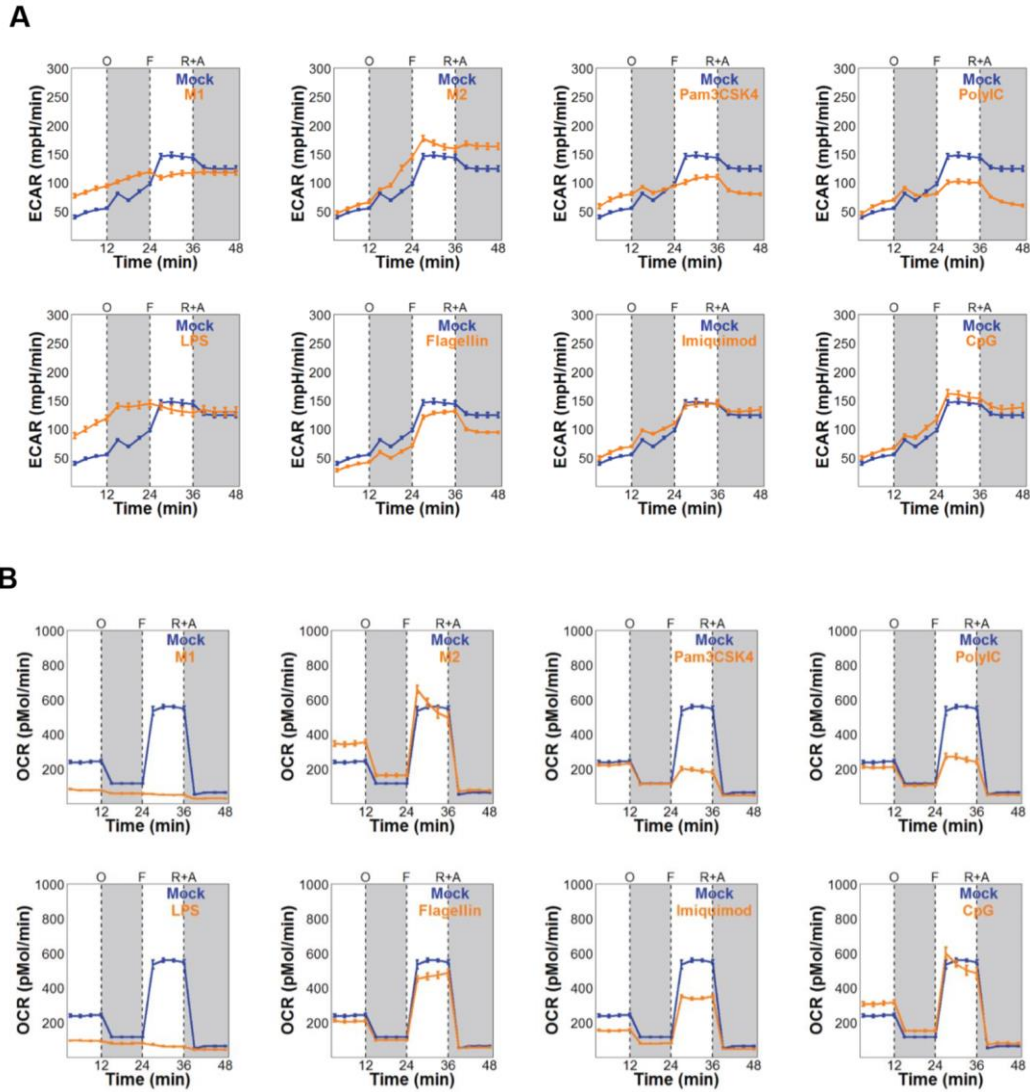


Figure 20: (a) Profiles of extracellular acidification rate (ECAR) of BMDMs pretreated with TLR agonists for 24 hours (n=8), upon sequential administration with oligomycin (O), FCCP (F), and Rotenone + Antimycin A (R+A); measured as mpH per minute. **(b)** Profiles of oxygen consumption rate (OCR) of BMDMs pretreated with TLR agonists for 24 hours (n=8), upon sequential administration with oligomycin (O), FCCP (F), and Rotenone + Antimycin A (R+A); measured as picomoles of O₂ per minute. Error bars

represent standard error, and results are representative of at least two independent experiments (**a,b**).

Figure 21: Fatty acid oxidation induced by CpG is essential for macrophage anti-tumor activity.

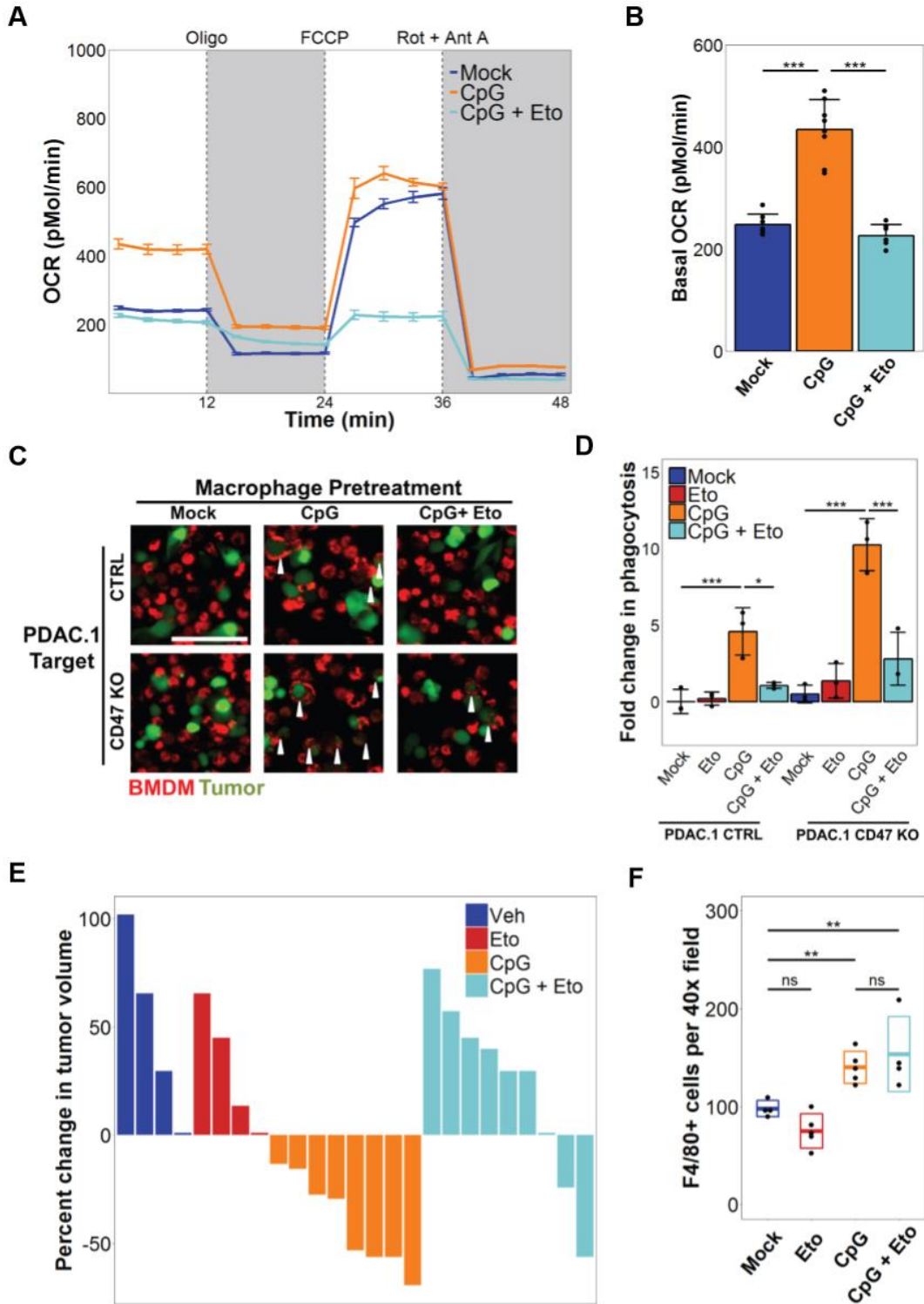


Figure 21: (a) Profile of oxygen consumption rate (OCR) in BMDMs treated with vehicle (mock), CpG, or CpG + etomoxir for 96 hours (n=8). Shown is OCR measured as picomoles of O₂ per minute upon sequential administration with oligomycin, FCCP, and Rotenone + Antimycin A. (b) Basal OCR of BMDMs treated with vehicle (mock), CpG, and CpG + etomoxir for 96 hours (n=8). (c) Representative immunofluorescence images showing phagocytosis of PDAC.1 control (CTRL) or CD47 KO cells (green) after co-culture with macrophages (BMDM, red) pretreated with vehicle (mock), CpG, or CpG + etomoxir for 96 hours. Arrows indicate phagocytic events. (d) *In vitro* phagocytosis of PDAC.1 CTRL or CD47 KO cells following co-culture with BMDMs pretreated with vehicle (mock), CpG, or CpG + etomoxir for 96 hours. (e) Treatment of PDAC.1 CTRL tumors with vehicle, etomoxir, CpG, or CpG + etomoxir beginning on day 10 after tumor implantation. Waterfall plot shows percent change in tumor volume at day 14 relative to baseline prior to CpG-treatment (day 10). (f) Quantification by immunohistochemistry of F4/80⁺ macrophages in PDAC tumors on day 14, following treatment with vehicle (mock), etomoxir, CpG, or CpG + etomoxir. Two-tailed Student's *t* test with Hochberg correction: ns (not significant); *, $p < 0.05$; **, $p < 0.01$; ***, $p < 0.001$. Boxplots represent mean \pm SD. Results are representative of at least two independent experiments (a-f).

Figure 22: Metabolic rewiring of TCA cycle supports the oxidative phenotype and anti-tumor activity of CpG-activated macrophages.

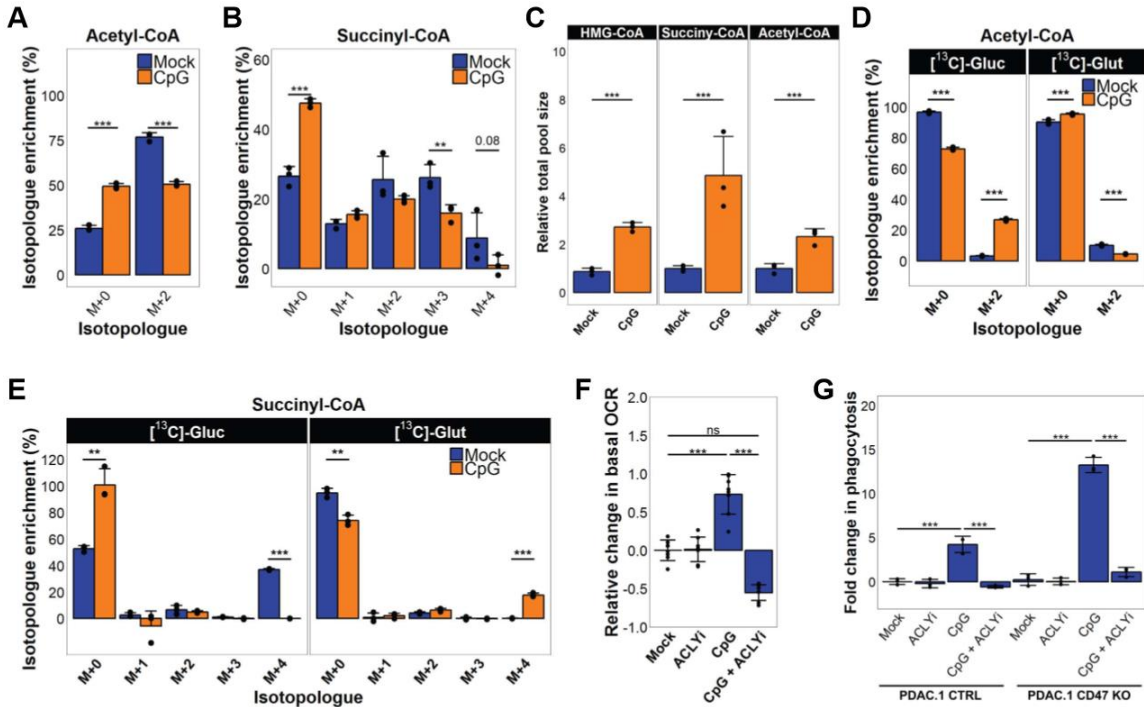


Figure 22: BMDMs were pretreated with CpG or vehicle for 96 hours, plated, and then labeled (i) with the addition of 100 μM ^{13}C -palmitate for 4 hours (n=3) (**a,b**) or (ii) in the presence of 25 mM ^{13}C -glucose or 4 mM ^{13}C -glutamine for 2 hours (n=3) (**c-e**). (**a**) Percent isotopologue enrichment of acetyl-CoA with addition of ^{13}C -palmitate. (**b**) Percent isotopologue enrichment of succinyl-CoA with addition of ^{13}C -palmitate. (**c**) Relative total pool size of HMG-CoA, succinyl-CoA, and acetyl-CoA after labeling with tracers (^{13}C -glucose or ^{13}C -glutamine). (**d**) Percent isotopologue enrichment of acetyl-CoA from ^{13}C -glucose and ^{13}C -glutamine. (**e**) Percent isotopologue enrichment of succinyl-CoA from ^{13}C -glucose and ^{13}C -glutamine. (**f**) Basal oxygen consumption of BMDMs pretreated as indicated (n=8). (**g**) *In vitro* phagocytosis of PDAC.1 CTRL or CD47 KO cells by BMDMs pretreated as indicated (n=3). Two-tailed Student's *t* test with Hochberg correction: ns (not significant); *, $p < 0.05$; **, $p < 0.01$; ***, $p < 0.001$. Results are representative of at least two independent experiments (**f,g**).

Figure 23: CpG-activation of macrophage metabolism leads to CD47-independent anti-tumor activity.

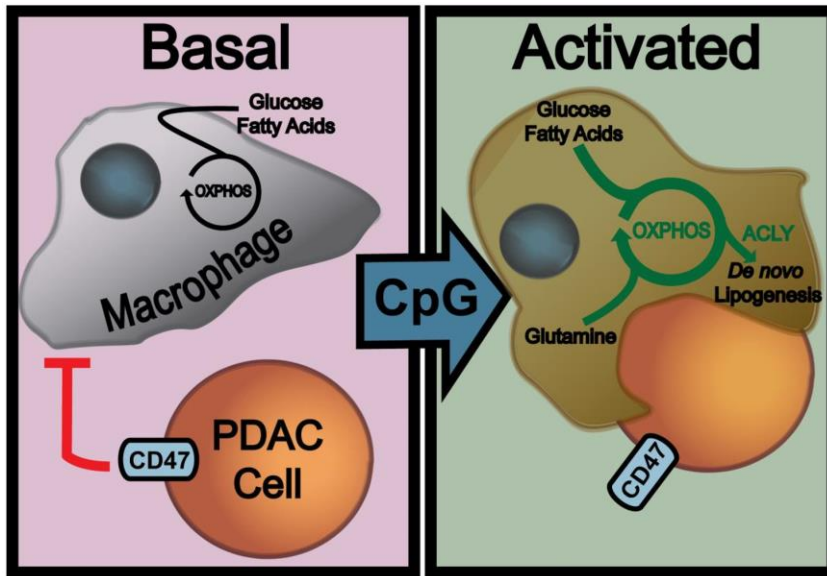


Figure 23: A conceptual model showing the oxidative phenotype induced by CpG, and the multiple metabolic pathways that are essential for supporting CD47-independent phagocytosis and anti-tumor activity by macrophages.

Chapter 4: Summary and Future Directions

Summary

In our studies, we identify macrophage metabolism to be a novel and important determinant of anti-tumor function. Despite the ability of macrophages to engulf and kill tumor cells, macrophages can be restricted in their ability to execute these functions, even upon complete loss of anti-phagocytic CD47-receptor on tumor cells. However, macrophage activation by CpG restored the anti-tumor potential of macrophages *in vitro* and *in vivo*. We found that CpG did not activate a classical M1 or M2 phenotypes associated with anti- and pro-tumor roles, but stimulated a hybrid of M1 and M2 metabolic features, which proved critical for phagocytosis and anti-tumor activity. Our findings not only highlight key considerations about CD47-based therapies and combination strategies for redirecting macrophage activity, but also reveal new directions for understanding the functional programming of macrophages under physiological and disease settings – beyond the M1 and M2 paradigm.

Optimizing phagocytic program for engulfing and degrading tumor cells.

Macrophage phagocytosis requires coordination of multiple cellular processes, which includes engagement of target cells, internalization of cargo into phagosomes, phagosomal maturation, degradation of cargo, etc.¹⁸⁵ Though CpG enables macrophages to overcome anti-phagocytic CD47 present on the surface of tumor cells, there may lie downstream processes that remain rate-limiting for phagocytic flux. Understanding how each of these steps responds to CpG-activation will be essential for maximizing the

phagocytic function of tumor macrophages and essential for advancing the therapeutic potential of this approach.

For example, macrophage stimulation through immune sensing pathways induces cellular features of distinct phagocytic programs. Select TLR pathways (e.g. TLR1/2, TLR 2/3, and TLR4) induce LC3-associated phagocytosis (LAP), which promotes immunologically silent clearance of apoptotic cells.⁵⁷ Likewise, TLR9 stimulation augments macrophage function by inducing formation of LC3-associated endosomes for production of type I interferons.⁵⁹ Examining whether CpG-activated engulfment of PDAC cells in our experimental model induces LAP apparatuses may provide additional insight into the mechanisms underlying anti-tumor activity. If CpG-activated engulfment of PDAC cells does not require LAP, then there may be multiple modes of phagocytosis that can be harnessed for a cooperative effect. If CpG-activated engulfment of PDAC cells induces features of LAP, then it will be critical to overcome the immunologically silent nature of LAP. Doing so will activate a more comprehensive anti-tumor response involving adaptive immunity and other immune effectors, which we have found to be muted in the CpG-induced responses observed in our immunocompetent model.

Macrophage clearance of engulfed cells may intrinsically be immunogenically silent.¹⁸⁶ Enhancing the immunogenicity of macrophage-engulfed tumor cells will thus require stimulation of orthogonal signaling pathways. One such pathway is through STING (STimulator of INterferon Genes), which responds to cyclic dinucleotides in the cytoplasm as well as clinical agents in development for cancer immunotherapy.¹⁸⁷⁻¹⁸⁹ Degradation of DNA fragments released from engulfed cells, by DNases in the macrophage cytoplasm, restricts the capacity of macrophages to process tumor cell

components for antigen presentation.¹⁹⁰ STING agonists allow macrophages to overcome this barrier and may provide additive benefit to the pro-phagocytic effect of CpG-activation by enhancing downstream pathways.

Additional treatment combinations that deserve experimental evaluation include targeting immunogenic and pro-phagocytic determinants – such as calreticulin-regulators and MerTK (Mer Tyrosine Kinase).^{73,191,192} Although we did not observe CpG to induce macrophage production of calreticulin as a pro-phagocytic signal,⁵⁵ instigating cellular stress in the endoplasmic reticulum of tumor cells and macrophages may be sufficient for calreticulin translocation to the cell membrane.⁷⁴ Alternatively, engaging established pro-phagocytic pathways such as MerTK could activate phagocytic programs that complement the effect of CpG-induced activity.⁸³ Together, examining these pathways will not only reveal potential anti-tumor targets for therapy, but also provide tools for integrating potentially distinct phagocytic programs.

Overcoming resistance to CpG-induced anti-tumor activity: Completing the cancer immunity cycle

Although CpG induces potent anti-tumor activity in our PDAC model, tumors ultimately relapse, suggesting the development of treatment resistance. One possible mechanism is the gradual loss of macrophage activity following stimulation. Indeed, tonic activation of PRR pathways leads to functional tolerance in macrophages.^{193,194} Loss of effector functions is similarly observed in other immune cells such as T cells following prolonged inflammation (e.g. viral infection, cancer, etc), leading to metabolic impairment and functional exhaustion.^{195,196} Whether macrophages undergo similar loss

of anti-tumor functions is unknown; thus, their metabolic and functional states should be assessed during periods of tumor relapse. If macrophages expression of PD-1(programmed death-1) activation markers indeed signify functional exhaustion,¹⁹⁷ it may be possible to rescue their activity, as demonstrated with immune checkpoint modulation in T cells. Other experimental strategies for overcoming the hurdle of tonic activation include drug holidays during CpG-dosing, clinical agents for enhancing myelopoiesis (e.g. granulocyte monocyte colony-stimulating factor), or identification of unique cellular pathways in tolerized cells. Drug holidays or targeting these cellular pathways in tolerized cells may permit macrophages to ‘reset’ following tonic activation. Alterations induced by CpG may nonetheless persist, and production and mobilization of naïve macrophages could be necessary to sustain CpG anti-tumor activity.

An alternative mechanism supporting tumor outgrowth after extended CpG treatment may be the induction of additional anti-phagocytic pathways during treatment, including macrophage-expressed PD-1 and tumor-expressed MHC I expressed.^{94,197} To address this possibility, it may be necessary to inhibit these pathways together using a combination strategy – which has proven effective for inciting T cell responses in pancreatic and other cancers.^{35,198} A major challenge to this approach will be efficiently identifying pleiotropic inhibitory pathways and which cell populations that they are expressed on; if inhibitory receptors are selectively expressed by specific cell populations in the tumor microenvironment, then depletion of these cell populations may represent a strategy for ablating anti-phagocytic pathways.

A third strategy for preventing tumor relapse would be to stimulate a consummate immune response involving other immune effectors, such as cytotoxic T cells. Indeed,

CD47-blockade effectively enhances antigen presentation by dendritic cells and macrophages, in a manner that leads to improved anti-tumor activity by T cells.^{93,145,199} Similarly, CpG provides an adjuvant effect that bolsters T cell responses with appropriate co-stimulation (e.g. OX40 agonist).⁴⁶ Together, these studies indicate that the addition of other immunostimulatory agents may complete the cancer immunity cycle by also engaging adaptive immune cells to enact cancer immunosurveillance.

Integrating metabolism of effector cells, tumor microenvironment, and hosts

Immune activation rewires macrophage metabolism, but macrophage-extrinsic regulators of metabolism include the hostile microenvironment of tumors as well as cachexia commonly found in patients. These conditions can subvert macrophage function – and potentially suppress phagocytosis of tumor cells – by depriving macrophages of critical substrates. For example, hypoxic conditions in tumors sequester macrophages and supports tumor-promoting functions (i.e. angiogenesis), or drive expression of anti-phagocytic CD47 on tumor cells.^{200–202} Likewise, the metabolic demand for tumor cell growth drives consumption of essential nutrients, such as glucose and amino acids, that are also essential for macrophage bioenergetics and function.¹⁷² In turn, tumor cells produce metabolites such as lactate that redirect macrophages toward a pro-tumor phenotype.²⁰³ Under appropriate activation conditions or with metabolic rewiring, immune cells such as T cells can utilize lactate as a fuel source as well (unpublished data). Understanding how CpG-activated macrophages harness fuel sources beyond glucose and fatty acids will reveal opportunities for improving CpG-induced anti-tumor activity.

Upon engulfing an apoptotic cell or tumor cell, macrophages effectively double their lipid content.¹⁷¹ Whether altered lipid metabolism in macrophages serves to meet bioenergetic demands for executing phagocytosis, or whether these changes are reactionary to catabolizing a large lipid load remains unclear. For exogenous lipids (e.g. long chain fatty acids, cholesterol, etc) imported into macrophages and other immune cells, breakdown products are used to generate epigenetic substrates, such as histone acetyl groups, and incorporated into components of cellular membranes.^{157,179,180} Studying the metabolic fate and cellular fate of phagocytosed cargo may reveal essential conditions underpinning phagocytosis. In particular, assessing CpG-induced changes in membrane composition and epigenetic landscape of macrophages may provide important insight into the ontology of their phagocytic programming.

Therapeutic opportunities beyond the primary tumor

Pancreatic cancer is a systemic condition, with approximately 80% of patients with disseminated disease at the time of diagnosis, with the most common site of metastasis being the liver.²⁴ The liver is also profoundly affected by repeated systemic administration of CpG, which induces extramedullary hematopoiesis.¹⁵⁹ Whether extramedullary hematopoiesis instigated by CpG sufficiently generates functional immune cells for cancer immunosurveillance will need to be assessed. If so, lymphocytes arising in the liver may represent an important pool of effectors that can be readily primed by macrophage antigen presentation, and harnessed for sustained anti-tumor activity.

Targeting specific immune populations with CpG administration, however, will remain a challenge, because systemic treatments often give rise inflammatory responses that consequently to adverse events. To mitigate this risk, it may be necessary to enhance the therapeutic index of clinical agents such as CpG when administered systemically. One approach is conjugation of immune agonists to cell-specific antibodies that target specific sites while concomitantly modulating other immune pathways.^{204,205} Another strategy for macrophage-based therapy is adoptive transfer of engineered or conditioned macrophages, which is an approach that has shown efficacy in preclinical models for restoring the function of pulmonary macrophages in hereditary pulmonary alveolar proteinosis.^{206,207} Together, these methods represent promising methods for therapeutic targeting of macrophage metabolism across multiple diseases.

We study a role for cellular metabolism in regulating macrophage function in pancreatic cancer, but our findings may apply to other diseases as well. Aberrant functions in macrophages manifest as clinical conditions such as hemophagocytic lymphohistiocytosis or chronic granulomatous disease – which are respectively characterized by hyperactivation leading to fulminant inflammation and hypofunction leading to recurrent infections.^{159,208,209} Exploiting metabolic pathways or conditions in these diseases could offer therapeutic benefit for modulating macrophage activity and restoring normal function. In other diseases, macrophages subsets (e.g. osteoclasts and microglia) serve as critical mediators of bone homeostasis and clearance of protein aggregates. Perturbation of physiological functions can contribute to osteoporosis or neurological disease;²¹⁰⁻²¹² hence, improving our understanding of cellular metabolism and its role in other macrophage types could elucidate broader therapeutic opportunities.

Chapter 5: Materials and Methods

Experimental Model and Subject Details

Mice

C57BL/6, *Rag2*^{-/-} (B6(Cg)-*Rag2*^{tm1.1Cgn}/J), CD11c-DTR/eGFP (B6.FVB-1700016L21RikTg(*Itgax*-DTR/EGFP)57Lan/J) mice were obtained from Jackson Laboratories. CD11c-DTR/eGFP heterozygotes were enrolled for tumor studies. Animal protocols were reviewed and approved by the Institute of Animal Care and Use Committee (IACUC) of the University of Pennsylvania, and conducted in compliance with the guidelines for animal research by the National Institutes of Health.

Method Details

Reagents.

TLR agonists were resuspended in PBS (phosphate buffered saline, Thermo Scientific Fisher) prior to addition to cell culture media at final concentrations of: 1 µg/ml Pam3CSK4 (Invivogen), 1 µg/ml PolyI:C (Invivogen), 1 µg/ml E. coli LPS (Invivogen), 1 µg/ml flagellin (Invivogen), 1 µg/ml imiquimod (Invivogen), 100 µg/ml ODN1826 CpG DNA (Invivogen and Integrated DNA Technologies). Etomoxir (Sigma) was reconstituted in DMSO (Sigma) and supplemented into media at a 200 µM concentration; BMS 303141 (Tocris) was reconstituted in DMSO and added into media at 50 µM concentration. Thapsigargin (Sigma) and staurosporine (Sigma) were reconstituted in DMSO and added into media at 10 nM and 1 mM, respectively. For mock-treatment, PBS or DMSO vehicles were utilized as controls when appropriate.

Tissue Culture.

Tumor cells were cultured in DMEM (Dulbecco's Modified Eagle's Media, Thermo Scientific Fisher) supplemented with 10% v/v FCS (fetal calf serum, Gemini and VWR), 2 mM glutamax (Thermo Scientific Fisher), and 10 ng/ml gentamicin (Thermo Scientific Fisher). Cell cultures and *in vitro* co-cultures were maintained at 37°C and 5% CO₂. Cell counts were determined using a hemacytometer. For *in vitro* experiments, PDAC cells were below passage 15, and for *in vivo* experiments, cells were below passage 10.

Generation of BMDMs.

BMDMs were derived by isolating bone marrow from mice euthanized with CO₂ overexposure. Following treatment with ACK lysis buffer (Thermo Scientific Fisher). Bone marrow cells were then cultured in Iscove's Modified Eagle's Media (Thermo Scientific Fisher) supplemented with 10% v/v FCS, 2 mM glutamax, 10 ng/ml gentamicin, and 10 ng/ml M-CSF (Peprotech) for 7-10 days. Prior to use in experiments, BMDMs were removed from M-CSF and pretreated with TLR agonists or inhibitors for indicated durations.

Cell lines.

PDAC.1 (152 PDA) and PDAC.2 (69 PDA) cell lines were derived from PDAC tumors, as previously described⁴, which arose spontaneously in *Kras*^{LSL.G12D/+}; *Trp53*^{R172H/+}; *Pdx-Cre* mice backcrossed onto the C57BL/6 background (Jackson Labs). Cell line authentication was performed as previously described⁴. Isogenic PDAC lines were established by cloning single cells for *in vitro* and *in vivo* experiments. PDAC knockout lines were generated as previously described (**Table 5**)²¹³: 1x10⁶ tumor cells

from isogenic lines were transiently transfected with guide RNAs targeting GFP (5'-GTGAACCGCATCGAGCTGAA-3') or CD47 (5'-GGAGCCATCCTTCTCATCCC-3') sequences. Guide RNAs were inserted into TOPO-plasmids (Qiagen) per manufacturer instructions, and mixed 1:1 with LentiCRISPR V2 plasmid (Addgene). The plasmid mix was combined with Lipofectamine 2000 (Thermo Scientific Fisher) and Opti-MEM (Thermo Scientific Fisher) for transfection mixture. Tumor cells were transfected for 6 hours; at 24 hours post-transfection, cells were treated with 1 µg/ml puromycin (Invivogen) for 2 days. Following selection, tumor cells were stained for CD47 and purified as CD47⁺ and CD47⁻ populations by fluorescence-activated cell sorting. Reporter cell lines were generated for phagocytosis and anti-tumor assays by transduction with lentivirus encoding GFP and Click Beetle Green luciferase, joined by a T2A signal peptide. After expansion, GFP-expressing PDAC cells were isolated using fluorescence-activated cell sorting.

Flow Cytometry.

PDAC Tumor cell cultures were treated with trypsin (Thermo Scientific Fisher) and prepared as a single-cell suspension for flow cytometric analysis; BMDMs in culture were incubated in cell dissociation buffer (Thermo Scientific Fisher) prior to mechanical detachment and resuspension. For intracellular stains, cells were permeabilized in 0.1% Triton-X (Sigma) for 15 min. For tumors, samples were harvested upon necropsy, mechanically separated, and digested in 1 mg/ml collagenase (Sigma) and 100 µUnits/ml DNase I (Roche). Tumor digests were filtered and resuspended as single cell suspensions. Cells were treated with Fc-block (BD Pharmingen), then stained with Amcyan live/dead dye (Thermo Scientific Fisher). For antibody staining (**Table 3**), cells were washed with

PBS containing 2% FCS, and stained on ice. Flow analysis was performed using FACS Canto (BD Biosciences), and singlets were gated on using FSC-H versus FSC-A.

BODIPY-C16 labeling.

BMDMs were seeded at 1×10^5 cells/well into a 96-well plate and stimulated with vehicle or 10 $\mu\text{g/ml}$ CpG for 18 hours. Following stimulation, media was replaced with fresh DMEM supplemented with 10% v/v FCS, 2 mM glutamax, 10 ng/ml gentamicin, and 1 $\mu\text{g/ml}$ BODIPY-C16 (Thermo Scientific Fisher) for 1 hour. After labeling, cells were washed, detached, and analyzed by flow cytometry on a FACS Canto.

Phagocytosis assay.

Pretreated BMDMs were mechanically detached and labeled with 5 μM DiI (Life Technologies), then seeded into a transparent 96-well tissue culture plate at 5×10^4 cells/well. GFP-labeled PDAC cells were harvested as a single cell suspension and seeded at 5×10^4 cells/well. For other tumor cell lines, cell suspensions were labeled with 5 μM DiO (Life Technologies) and washed prior to being seeded at 5×10^4 cells/well. Following 4-hour co-culture, samples were washed and fixed in 4% PFA (paraformaldehyde, Sigma) for 15 min, prior to image collection. For antibody blockade, PDAC tumor cell suspensions were incubated with 10 $\mu\text{g/ml}$ isotype (2A3, BioXcell) or rat-anti-mouse anti-CD47 (MiapIAP301, BioXcell) antibodies for 20 min, prior to being washed and co-incubated with macrophages. Multiple random fields were collected per replicate, using an Olympus IX83 microscope, and the number of phagocytic events were scored and averaged for each replicate.

Anti-tumor activity assay.

Luciferase-labeled PDAC cells were harvested as a single cell suspension and seeded into a 96-well tissue culture plates at 5×10^4 cells/well. Pretreated BMDMs were harvested by mechanical detachment and seeded at 0:1, 1:1, 2:1, 5:1 macrophage-to-tumor ratios. After 48-hour co-culture, tumor cell survival was determined using Luciferase assay system (Promega). Luminescence measurements were performed using a SpectraMax M3 reader (Molecular Devices). Tumor cell survival was determined by normalizing luminescence to tumor-only controls.

Immunohistochemistry.

Cryosectioned murine PDAC tumors were fixed in 4% PFA and treated with 0.1% hydrogen peroxide (Sigma). Samples were blocked in 10% goat serum (Vector Laboratories) in PBS and treated overnight with primary antibodies (**Table 4**). Secondary antibody was applied for 1 hour, and samples were stained with ABC HRP kit (Vectastain) per manufacturer instructions. Samples were then treated with DAB (3, 3 - diaminobenzidine) HRP substrate (Vector Labs) prior to counterstaining with hematoxylin (Sigma) and dehydration. Images were captured using the Olympus BX-43 microscope.

Immunofluorescence microscopy.

Treated BMDMs were harvested by mechanical detachment and seeded into glass chamber slides (Nunc). Samples were then fixed in 4% PFA, permeablized in 0.1% Triton-X for 15 min, and blocked with 10% goat serum (Vector Laboratories) in PBS. Primary antibodies and isotype control were applied overnight and washed; secondary antibody was applied for 1 hour and washed. Samples were stained with DAPI for 15 min

and mounted prior to image acquisition. Images were captured using the Olympus IX83 microscope.

Tumor growth studies.

PDAC cells were harvested from culture, washed, and prepared as a single cell suspension for implantation into the subcutis of C57Bl/6 mice. Rat-anti-mouse anti-CD47 (MIAP301, BioXcell) and isotype control antibodies (2A3, BioXcell) were diluted in saline, and 50 µg of each antibody was delivered intratumorally on days 10 and 14 after tumor implantation, as previously described (**Table 5**).⁹³ Tumor-bearing mice were treated with vehicle (PBS) or 50 µg CpG by intraperitoneal injection every other day, beginning on day 10. For macrophage depletion: 200 µl of clodronate-encapsulated liposomes (clodronateliposomes.org) was delivered by retroorbital injection into mice, 400 µg of anti-CSF1R Ig (AFS98, BioXcell) diluted in saline was delivered by intraperitoneal injection, or GW2580 (AdooQ) was delivered daily at 160 mg/kg by oral gavage. For natural killer cell depletion, 200 µg anti-NK1.1 Ig (PK136, BioXcell) diluted in saline was delivered by intraperitoneal injection; diphtheria toxin (Sigma) was administered by intraperitoneal injection at 8 ng/gram body weight. Etomoxir (Sigma) was resuspended in PBS and delivered daily at 40 mg/kg by intraperitoneal injection as previously described (**Table 5**)²¹⁴. Tumor volume was monitored by caliper measurement and calculated using a formula for an ellipsoid: $\text{Volume} = 1/2 \times (\text{Length}) \times (\text{Width})^2$.

ECAR and OCR measurements.

BMDMs were pretreated with TLR agonists or inhibitors and seeded into XF96-well plates (Agilent) at 1×10^5 cells/well. Prior to measurements, samples were washed and incubated in Seahorse media (Agilent) supplemented with 0.5 mM D-glucose

(Sigma). The mitostress kit (Agilent) was prepared per manufacturer instructions by loading 1.5 μ M oligomycin 1.5 μ M FCCP, and 1 μ M rotenone/antimycin A into injection ports. Measurements were made using an XF96 Extracellular Flux Analyzer (Agilent) and results processed with Wave v2.2.0 software.

Cytotoxicity studies.

BMDMs and tumor cells were seeded at 1×10^5 cells/well into a 96-well plate and treated with inhibitors diluted in Dulbecco's Modified Eagle's Media supplemented with 10% v/v fetal calf serum, 2 mM glutamax, and 10 ng/ml gentamicin. After 4 hours, the media was removed, and samples were stained with 0.05% w/v crystal violet (Sigma) in 20% ethanol/80% H₂O. Samples were then washed and optical density measured at 570 nm using a Spectramax M3 spectrophotometer. Cell viability was determined by normalizing optical density of treated conditions to mock-treated controls.

¹³C metabolite tracing.

After pretreatment with CpG or vehicle for 96 hours, macrophages were counted and seeded at 4×10^6 cells per sample. For glucose and glutamine labeling, U-¹³C-glucose and U-¹³C-glutamine (Cambridge Isotope Laboratories) were substituted into DMEM supplemented with 10% v/v dialyzed FCS (Life Technologies), 4 mM L-glutamine (Sigma), and 25 mM glucose (Sigma). Cells were incubated at 37 °C in labeled media for 2 hours prior to harvest. For palmitate labeling, cells were cultured in DMEM supplemented with 100 μ M U-¹³C-palmitate (Cambridge Isotope Laboratories), 10% v/v charcoal-stripped FCS (Life Technologies), 4 mM L-glutamine (Sigma), and 25 mM glucose (Sigma) for 4 hours. Both tracer experiments included unlabeled control samples not exposed to ¹³C-labeled substrates. After incubation, cells harvested and placed on

ice. Samples were then pelleted, washed in cold PBS, and harvested in 750 μ l of ice-cold 10% trichloroacetic acid (Sigma-Aldrich, St. Louis, MO cat. #T6399) and internal standard containing $^{13}\text{C}^{15}\text{N}_1$ -labeled acyl-CoAs generated in pan6-deficient yeast culture were added to each sample in equal amounts.²¹⁵ Acyl-CoA thioester were analyzed by LC-MS/HRMS using an Ultimate 3000 autosampler coupled to a Thermo Q Exactive Plus instrument in positive ESI mode using the settings described previously.²¹⁶ Isotopologue enrichment in cells exposed to ^{13}C labeled substrates was calculated using unlabeled control samples not exposed to ^{13}C substrate as previously described.²¹⁷ For relative total pool quantitation, the total AUC for each acyl-CoA species (sum of all relevant isotopologues) was normalized to the AUC for the $^{13}\text{C}^{15}\text{N}_1$ -labeled internal standard specific for that species. As previously described (**Table 5**),^{215,218} samples were centrifuged at 1,200xg for 10 min at 4 °C and pulse-sonicated with a probe sonicator (Fisher Scientific). Lysates were centrifuged at 15,000xg for 15 min, and the supernatants were further purified by solid-phase extraction using (OASIS HLB) columns. Supernatants were then applied, and columns were washed with 1 ml H₂O. Analytes were eluted in 25 mM ammonium acetate in methanol and evaporated to dryness overnight by N₂ gas. Samples were resuspended in 50 μ l of 5% 5-sulfosalicylic acid and 10 μ l injections were applied in LC/ESI/MS/MS analysis. Isotopologues were designated as unlabeled (M+0), containing one ^{13}C isotope (M+1), two ^{13}C isotopes (M+2), etc following tracer labeling.

***In vivo* phagocytosis.**

Frozen sections of PDAC tumors were fixed for 20 min in 4% PFA, followed by permeabilization in ice-cold methanol for 20 min. Samples were blocked for 1 hr in 10%

goat serum and stained for 4 hr in primary antibodies (rabbit-anti-mouse cytokeratin, rat-anti-mouse F4/80). After washing, secondary antibody (488 goat-anti-rabbit, 568 goat-anti-rat) was applied for 1 hr. Samples were washed, and images were captured using an Olympus IX83 microscope. Background reduction was performed in CellSens software (Olympus) and images were subsequently processed using EBIImage software analysis in R to perform color deconvolution, adaptive thresholding of F4/80 signal, gaussian blur, and binarization of signal. Size exclusion was applied to remove particles with a radius less than 10 pixels or greater than 200 pixels. The green (CK) signal was normalized intrinsically for each image to minimize variability in staining intensity. The phagocytic index was determined by calculating the normalized green (CK) intensity within each F4/80+ cells, and the normalized phagocytic index was calculated by taking the ratio of normalized green (CK) intensity to cell size.

Cytokine analysis.

Peripheral blood was collected by tail vein bleed on day 14, and the serum fraction was isolated following centrifugation at 10,000xg for 15 min. For *in vitro* experiments, 1×10^6 macrophages were cultured in 1 ml of media. Supernatant was collected following 48 hour activation with cytokines and TLR agonists. Serum and supernatants were analyzed per manufacturer instructions using cytokine bead array kits (BD Biosciences) for IL-1 β , IL-4, IL-6, IL-1 β , IL-12, IFN- γ , TNF- α , and CCL2. Beads were analyzed using a FACS Canto II.

Statistics and software analysis.

P-values were calculated using a two-tailed unpaired Student's t-test and Hochberg correction for multiple comparison testing, unless stated otherwise. Linear

mixed effects models (LMEM) were built to include random effects for each cell and image fields; statistical differences between treatment conditions were determined by ANOVA comparison of LMEM models. P-values of 0.05 or less were considered significant. Error bars indicate standard deviation unless stated otherwise. Data analysis and graphical design was performed using R software (v3.4.3), R-studio, and additional R-packages: ggplot2, dplyr, reshape2, EBimages, lme4, and heatmap.2 (**Fig 5**). Flow cytometric analysis was completed using FlowJo (v10.3), and figure design utilized Adobe Illustrator CS6.

Tables: Reagents

Table 3: Flow cytometry and immunohistochemistry antibodies.

Flow cytometry and immunohistochemistry antibodies		
Antibody	Manufacturer	Clone
FITC anti-mouse F4/80	eBioscience	BM8
FITC anti-mouse CD8b	Biologend	YTS156.7.7
PE anti-mouse I-A/I-E	BD Pharmingen	M5/114.15.2
PE anti-mouse SIRP α	eBioscience	P84
PE anti-mouse CD16/32	eBioscience	93
PE anti-mouse CD36	Biologend	101306
PE anti-mouse CD40	BD Pharmingen	3/23
PE anti-mouse CD64	BD Pharmingen	X54-5/7.1.1
PE anti-mouse CD80	BD Pharmingen	16-10A1
PE anti-mouse CD86	BD Pharmingen	GL1
PE anti-mouse PD-L1	BD Pharmingen	MIH5
PE anti-mouse CD366 (TIM3)	Biologend	RMT3-23
PerCP-Cy5.5 anti-mouse CD11b	BD Pharmingen	M1/70
PerCP-Cy5.5 anti-mouse CD3a	BD Biosciences	145-2C11
APC anti-mouse CD19	Biologend	6D5
APC anti-mouse CD206	Biologend	C068C2
APC anti-mouse NK1.1	R&D Systems	FAB7614R
APC anti-mouse CD115 (CSF1R)	eBioscience	AFS98
APC anti-mouse FoxP3	Biologend	FJK-16s
APC anti-mouse F4/80	eBiosciences	BM8
APC anti-mouse CD47	Biologend	Miap301
APC-Cy7 anti-mouse CD45	BD Pharmingen	30-F11
APC-Cy7 anti-mouse Ly6C	BD Pharmingen	AL-21
PE-Cy7 anti-mouse CD45	BD Biosciences	30-F11
PE-Cy7 anti-mouse PD1	Biologend	RMP1-30
PacBlue anti-mouse CD3	Biologend	17A2
PacBlue anti-mouse CD4	eBiosciences	RM4.5
PE rat IgG2a Isotype	BD Biosciences	N/A
APC rat IgG2a Isotype	BD Biosciences	N/A

Table 4: Immunohistochemistry and immunofluorescence antibodies.

Immunohistochemistry/Immunofluorescence antibodies		
Antibody	Manufacturer	Clone
Rat anti-F4/80 Ig	eBioscience	BM8
Rat anti-CD47 Ig	eBioscience	Miap301
Rabbit anti-Cytokeratin	Abcam	EPNCIR127B
Rabbit anti-Calreticulin Ig	Abcam	EPR3924
Rat anti-CD45 Ig	BD Pharmingen	30-F11
Rabbit isotype Ig	Santa Cruz Biotechnology	Sc-3888
Biotin goat-anti-rat Ig	BD Pharmingen	N/A
488 goat-anti-rabbit Ig	Life Technologies	N/A
568 goat-anti-rabbit Ig	Life Technologies	N/A

Table 5: Methods and software references.

Methods References	
Method	Pubmed Central ID & References
Delivery of CD47-antibody	PMC4598283
CRISPR/Cas9 expression	PMC3712628
Etomoxir dosing	PMC4892846
¹³ C metabolite tracing	PMC3802537
<i>Lme4</i> package	Douglas Bates, Martin Maechler, Ben Bolker, Steve Walker (2015). Fitting Linear Mixed-Effects Models Using lme4. Journal of Statistical Software, 67(1), 1-48.
<i>EbImage</i> package	Gregoire Pau, Florian Fuchs, Oleg Sklyar, Michael Boutros, and Wolfgang Huber (2010): EBImage - an R package for image processing with applications to cellular phenotypes. Bioinformatics, 26(7), pp. 979-981, 10.1093/bioinformatics/btq046
<i>ggplot2</i> package	H. Wickham. ggplot2: Elegant Graphics for Data Analysis. Springer-Verlag New York, 2009.
<i>dplyr</i> package	Hadley Wickham (2011). The Split-Apply-Combine Strategy for Data Analysis. Journal of Statistical Software, 40(1), 1-29.
<i>reshape2</i> package	Hadley Wickham (2007). Reshaping Data with the reshape Package. Journal of Statistical Software, 21(12), 1-20.
<i>heatmap.2</i> package	Gregory R. Warnes et al. Schwartz and Bill Venables (2016). gplots: Various R Programming Tools for Plotting Data. R package version 3.0.1.

References

1. Dvorak, H. F. Tumors: Wounds That Do Not Heal. *N. Engl. J. Med.* **315**, 1650–1660 (1986).
2. Fridman, W. H., Pagès, F., Sauts-Fridman, C. & Galon, J. The immune contexture in human tumours: Impact on clinical outcome. *Nat. Rev. Cancer* **12**, 298–306 (2012).
3. Hanahan, D. & Weinberg, R. A. Hallmarks of Cancer: The Next Generation. *Cell* **144**, 646–74 (2011).
4. Dunn, G. P., Bruce, A. T., Ikeda, H., Old, L. J. & Schreiber, R. D. Cancer immunoediting: From immunosurveillance to tumor escape. *Nat. Immunol.* **3**, 991–998 (2002).
5. Burnet, M. Cancer; a biological approach. I. The processes of control. *Br. Med. J.* **1**, 779–86 (1957).
6. Chen, D. S. & Mellman, I. Oncology meets immunology: The cancer-immunity cycle. *Immunity* **39**, 1–10 (2013).
7. Clark, W. M. *et al.* Improved survival with ipilimumab in patients with metastatic melanoma. *N. Engl. J. Med.* **363**, 711–723 (2012).
8. Hodi, F. & O’Day, S. Improved survival with ipilimumab in patients with metastatic melanoma. *N. Engl. J. Med.* **363**, 711–723 (2010).
9. Lichty, B. D., Breitbach, C. J., Stojdl, D. F. & Bell, J. C. Going viral with cancer immunotherapy. *Nat. Rev. Cancer* **14**, 559–567 (2014).
10. Drake, C. G., Lipson, E. J. & Brahmer, J. R. Breathing new life into immunotherapy: Review of melanoma, lung and kidney cancer. *Nat. Rev. Clin. Oncol.* **11**, 24–37 (2014).
11. Sharma, P., Hu-Lieskovan, S., Wargo, J. A. & Ribas, A. Primary, Adaptive, and Acquired Resistance to Cancer Immunotherapy. *Cell* **168**, 707–723 (2017).
12. Kandoth, C. *et al.* Mutational landscape and significance across 12 major cancer types. *Nature* **502**, 333–339 (2013).
13. Pardoll, D. M. The blockade of immune Slide checkpoints in cancer immunotherapy. *Nat Rev Cancer.* **12**, 252–264 (2012).
14. McGranahan, N. *et al.* Clonal neoantigens elicit T cell immunoreactivity and sensitivity to immune checkpoint blockade. *Science (80-.).* **351**, 1463–1469 (2016).
15. Rizvi, N. A. *et al.* Mutational landscape determines sensitivity to PD-1 blockade in non – small cell lung cancer. *Science (80-.).* **348**, 124 (2016).
16. Joyce, J. A. & Fearon, D. T. T cell exclusion, immune privilege, and the tumor microenvironment. *Science (80-.).* **348**, 74–80 (2015).
17. Teng, M. W. L., Ngiow, S. F., Ribas, A. & Smyth, M. J. Classifying cancers basedon T-cell infiltration and PD-L1. *Cancer Res.* **75**, 2139–2145 (2015).
18. Haanen, J. B. A. G. Converting Cold into Hot Tumors by Combining Immunotherapies. *Cell* **170**, 1055–1056 (2017).
19. Kershaw, M. H. & Smyth, M. J. Immunology. Making macrophages eat cancer. *Science* **341**, 41–2 (2013).

20. Noy, R. & Pollard, J. W. Tumor-Associated Macrophages: From Mechanisms to Therapy. *Immunity* **41**, 49–61 (2014).
21. Mantovani, A., Marchesi, F., Malesci, A., Laghi, L. & Allavena, P. Tumour-associated macrophages as treatment targets in oncology. *Nat. Rev. Clin. Oncol.* **14**, 399–416 (2017).
22. MacDonald, K. P. a *et al.* An antibody against the colony-stimulating factor 1 receptor depletes the resident subset of monocytes and tissue- and tumor-associated macrophages but does not inhibit inflammation. *Blood* **116**, 3955–63 (2010).
23. Mitchem, J. B. *et al.* Targeting tumor-infiltrating macrophages decreases tumor-initiating cells, relieves immunosuppression, and improves chemotherapeutic responses. *Cancer Res.* **73**, 1128–1141 (2013).
24. NCI. SEER Cancer Stat Facts.
25. Conroy, T. & *et al.* FOLFIRINOX versus gemcitabine for metastatic pancreatic cancer. *N. Engl. J. Med.* **364**, 1817–25 (2011).
26. Von Hoff, D. D. *et al.* Increased survival in pancreatic cancer with nab-paclitaxel plus gemcitabine. *N. Engl. J. Med.* **369**, 1691–703 (2013).
27. Le, D. T. *et al.* Mismatch repair deficiency predicts response of solid tumors to PD-1 blockade. *Science* **357**, 409–413 (2017).
28. Le, D. T. *et al.* PD-1 Blockade in Tumors with Mismatch-Repair Deficiency. *N. Engl. J. Med.* **372**, 2509–2520 (2015).
29. Balachandran, V. P. *et al.* Identification of unique neoantigen qualities in long-term survivors of pancreatic cancer. *Nature* **551**, S12–S16 (2017).
30. Vonderheide, R. H. *et al.* Clinical activity and immune modulation in cancer patients treated with CP-870,893, a novel CD40 agonist monoclonal antibody. *J. Clin. Oncol.* **25**, 876–883 (2007).
31. Beatty, G. L. *et al.* CD40 agonists alter tumor stroma and show efficacy against pancreatic carcinoma in mice and humans. *Science* **331**, 1612–6 (2011).
32. Long, K. B. *et al.* IFN γ and CCL2 cooperate to redirect tumor-infiltrating monocytes to degrade fibrosis and enhance chemotherapy efficacy in pancreatic carcinoma. *Cancer Discov.* **6**, 400–413 (2016).
33. Olive, K. P. *et al.* Inhibition of Hedgehog signaling enhances delivery of chemotherapy in a mouse model of pancreatic cancer. *Science* **324**, 1457–61 (2009).
34. Provenzano, P. P. *et al.* Enzymatic targeting of the stroma ablates physical barriers to treatment of pancreatic ductal adenocarcinoma. *Cancer Cell* **21**, 418–29 (2012).
35. Winograd, R. *et al.* Induction of T-cell Immunity Overcomes Complete Resistance to PD-1 and CTLA-4 Blockade and Improves Survival in Pancreatic Carcinoma. *Cancer Immunol. Res.* **3**, 399–411 (2015).
36. Coley, W. B. THE TREATMENT OF INOPERABLE SARCOMA WITH THE MIXED TOXINS OF ERYSIPELAS AND THE BACILLUS PRODIGIOSUS. *Lancet* **167**, 1407–1408 (1906).
37. Alexander, C. & Rietschel, E. T. Invited review: Bacterial lipopolysaccharides and innate immunity. *J. Endotoxin Res.* **7**, 167–202 (2001).
38. Geisse, J. *et al.* Imiquimod 5% cream for the treatment of superficial basal cell

- carcinoma: Results from two phase III, randomized, vehicle-controlled studies. *J. Am. Acad. Dermatol.* **50**, 722–733 (2004).
39. Love, W. E. . B. Topical imiquimod or fluorouracil therapy for basal and squamous cell carcinoma: a systematic review. *Arch. Dermatol.* **145**, 1431–1438 (2009).
 40. Kawai, T. & Akira, S. TLR signaling. *Cell Death Differ.* **13**, 816–825 (2006).
 41. Gordon, S. Pattern recognition receptors: Doubling up for the innate immune response. *Cell* **111**, 927–930 (2002).
 42. Belani, C. P. *et al.* Phase 2 trial of erlotinib with or without PF-3512676 (CPG 7909, a Toll-like receptor 9 agonist) in patients with advanced recurrent EGFR-positive non-small cell lung cancer. *Cancer Biol. Ther.* **14**, 557–563 (2013).
 43. Weber, J. S. *et al.* Randomized phase 2/3 trial of CpG oligodeoxynucleotide PF-3512676 alone or with dacarbazine for patients with unresectable stage III and IV melanoma. *Cancer* **115**, 3944–3954 (2009).
 44. Brody, J. D. *et al.* In situ vaccination with a TLR9 agonist induces systemic lymphoma regression: A phase I/II study. *J. Clin. Oncol.* **28**, 4324–4332 (2010).
 45. Hirsh, V. *et al.* Randomized phase III trial of paclitaxel/carboplatin with or without PF-3512676 (toll-like receptor 9 agonist) as first-line treatment for advanced non-small-cell lung cancer. *J. Clin. Oncol.* **29**, 2667–2674 (2011).
 46. Sagiv-Barfi, I. *et al.* Eradication of spontaneous malignancy by local immunotherapy. *Sci. Transl. Med.* **10**, (2018).
 47. Guiducci, A., Sangaletti, S., Trinchieri, G., Colombo, M. & Christiana, V. Redirecting in vivo elicited tumor infiltrating macrophages and dendritic cells towards tumor rejection. *Cancer Res.* **65**, 3437–3446 (2005).
 48. Dinapoli, M. R., Calderon, C. L. & Lopez, D. M. The altered tumoricidal capacity of macrophages isolated from tumor-bearing mice is related to reduce expression of the inducible nitric oxide synthase gene. *J. Exp. Med.* **183**, 1323–9 (1996).
 49. Chang, C. I., Liao, J. C. & Kuo, L. Macrophage arginase promotes tumor cell growth and suppresses nitric oxide-mediated tumor cytotoxicity. *Cancer Res.* **61**, 1100–1106 (2001).
 50. Munn, D. H. *et al.* Inhibition of T Cell Proliferation by Macrophage Tryptophan Catabolism. *J. Exp. Med.* **189**, 1363–1372 (1999).
 51. Mantovani, A., Sozzani, S., Locati, M., Allavena, P. & Sica, A. Macrophage polarization: Tumor-associated macrophages as a paradigm for polarized M2 mononuclear phagocytes. *Trends Immunol.* **23**, 549–555 (2002).
 52. Glass, C. K. & Natoli, G. Molecular control of activation and priming in macrophages. *Nat. Immunol.* **17**, 26–33 (2015).
 53. Mosser, D. M. & Edwards, J. P. Exploring the full spectrum of macrophage activation. *Nat. Rev. Immunol.* **8**, 958–69 (2008).
 54. Sanjuan, M. A. *et al.* Toll-like receptor signalling in macrophages links the autophagy pathway to phagocytosis. *Nature* **450**, 1253–7 (2007).
 55. Feng, M. *et al.* Macrophages eat cancer cells using their own calreticulin as a guide: Roles of TLR and Btk. *Proc. Natl. Acad. Sci.* **112**, 201424907 (2015).
 56. Galon, J. *et al.* Cancer classification using the Immunoscore: a worldwide task force. *J. Transl. Med.* **10**, 205 (2012).

57. Heckmann, B. L., Boada-Romero, E., Cunha, L. D., Magne, J. & Green, D. R. LC3-Associated Phagocytosis and Inflammation. *J. Mol. Biol.* **429**, 3561–3576 (2017).
58. Martinez, J., Verbist, K., Wang, R. & Green, D. R. The relationship between metabolism and the autophagy machinery during the innate immune response. *Cell Metab.* **17**, 895–900 (2013).
59. Henault, J. *et al.* Noncanonical Autophagy Is Required for Type I Interferon Secretion in Response to DNA-Immune Complexes. *Immunity* **37**, 986–997 (2012).
60. Palsson-McDermott, E. M. *et al.* Pyruvate Kinase M2 Regulates Hif-1 α Activity and IL-1 β Induction and Is a Critical Determinant of the Warburg Effect in LPS-Activated Macrophages. *Cell Metab.* **21**, 65–80 (2015).
61. O’Neill, L. A. J. & Pearce, E. J. Immunometabolism governs dendritic cell and macrophage function. *J. Exp. Med.* jem.20151570 (2015). doi:10.1084/jem.20151570
62. Biswas, S. K. & Mantovani, A. Orchestration of metabolism by macrophages. *Cell Metab.* **15**, 432–7 (2012).
63. Huang, S. C.-C. *et al.* Cell-intrinsic lysosomal lipolysis is essential for alternative activation of macrophages. *Nat. Immunol.* 1–12 (2014). doi:10.1038/ni.2956
64. Nomura, M. *et al.* Fatty acid oxidation in macrophage polarization. *Nat. Immunol.* **17**, 216–217 (2016).
65. Jha, A. K. *et al.* Network integration of parallel metabolic and transcriptional data reveals metabolic modules that regulate macrophage polarization. *Immunity* **42**, 419–430 (2015).
66. Arts, R. J. W. *et al.* Glutaminolysis and Fumarate Accumulation Integrate Immunometabolic and Epigenetic Programs in Trained Immunity. *Cell Metab.* 1–13 (2016).
67. Zhao, E. *et al.* Cancer mediates effector T cell dysfunction by targeting microRNAs and EZH2 via glycolysis restriction. *Nat. Immunol.* **17**, 95–103 (2015).
68. Balmer, M. L. *et al.* Memory CD8⁺ T Cells Require Increased Concentrations of Acetate Induced by Stress for Optimal Function. *Immunity* 1–13 (2016). doi:10.1016/j.immuni.2016.03.016
69. Xu, X., Araki, K., Li, S., Han, J. & Ye, L. Autophagy is essential for effector CD8⁺ T cell survival and memory formation. *Nat. ...* **15**, (2014).
70. O’Sullivan, D. *et al.* Memory CD8(+) T Cells Use Cell-Intrinsic Lipolysis to Support the Metabolic Programming Necessary for Development. *Immunity* **41**, 75–88 (2014).
71. Hossain, F. *et al.* Inhibition of Fatty Acid Oxidation Modulates Immunosuppressive Functions of Myeloid-Derived Suppressor Cells and Enhances Cancer Therapies HHS Public Access. *Cancer Immunol Res* **3**, 1236–1247 (2015).
72. Wu, D. *et al.* Type 1 Interferons Induce Changes in Core Metabolism that Are Critical for Immune Function. *Immunity* **44**, 1325–1336 (2016).
73. Gardai, S. J. *et al.* Cell-surface calreticulin initiates clearance of viable or apoptotic cells through trans-activation of LRP on the phagocyte. *Cell* **123**, 321–334 (2005).

74. Obeid, M. *et al.* Calreticulin exposure dictates the immunogenicity of cancer cell death. *Nat. Med.* **13**, 54–61 (2007).
75. Boross, P., Jansen, J. H. M., Pastula, A., van der Poel, C. E. & Leusen, J. H. W. Both activating and inhibitory Fc gamma receptors mediate rituximab-induced trogocytosis of CD20 in mice. *Immunol. Lett.* **143**, 44–52 (2012).
76. Overdijk, M. B. *et al.* Epidermal growth factor receptor (EGFR) antibody-induced antibody-dependent cellular cytotoxicity plays a prominent role in inhibiting tumorigenesis, even of tumor cells insensitive to EGFR signaling inhibition. *J. Immunol.* **187**, 3383–90 (2011).
77. Okazawa, H. *et al.* Negative regulation of phagocytosis in macrophages by the CD47-SHPS-1 system. *J. Immunol.* **174**, 2004–2011 (2005).
78. Olsson, M. & Oldenborg, P. A. CD47 on experimentally senescent murine RBCs inhibits phagocytosis following Fcγ receptor-mediated but not scavenger receptor-mediated recognition by macrophages. *Blood* **112**, 4259–4267 (2008).
79. Segawa, K. *et al.* Caspase-mediated cleavage of phospholipid flippase for apoptotic phosphatidylserine exposure. 2–7 (2014).
80. Miyanishi, M. *et al.* Identification of Tim4 as a phosphatidylserine receptor. *Nature* **450**, 435–439 (2007).
81. Tietjen, G. T. *et al.* Molecular mechanism for differential recognition of membrane phosphatidylserine by the immune regulatory receptor Tim4. *Proc. Natl. Acad. Sci. U. S. A.* **111**, E1463-72 (2014).
82. Seitz, H. M., Camenisch, T. D., Lemke, G., Earp, H. S. & Matsushima, G. K. Macrophages and Dendritic Cells Use Different Axl/Mertk/Tyro3 Receptors in Clearance of Apoptotic Cells. *J. Immunol.* **178**, 5635–5642 (2007).
83. Graham, D. K., Deryckere, D., Davies, K. D. & Earp, H. S. The TAM family: Phosphatidylserine-sensing receptor tyrosine kinases gone awry in cancer. *Nat. Rev. Cancer* **14**, 769–785 (2014).
84. Chao, M. P. *et al.* Calreticulin is the dominant pro-phagocytic signal on multiple human cancers and is counterbalanced by CD47. *Sci. Transl. Med.* **2**, 63ra94 (2010).
85. Sosale, N. G. *et al.* Cell rigidity and shape override CD47's 'Self' signaling in phagocytosis by hyperactivating Myosin-II. *Blood* (2014).
86. Soto-Pantoja, D. R., Ridnour, L. a, Wink, D. a & Roberts, D. D. Blockade of CD47 increases survival of mice exposed to lethal total body irradiation. *Sci. Rep.* **3**, 1038 (2013).
87. Kaur, S. *et al.* Thrombospondin-1 signaling through CD47 inhibits self-renewal by regulating c-Myc and other stem cell transcription factors. *Sci. Rep.* **3**, 1673 (2013).
88. Majeti, R. *et al.* CD47 is an adverse prognostic factor and therapeutic antibody target on human acute myeloid leukemia stem cells. *Cell* **138**, 286–99 (2009).
89. Willingham, S. B. *et al.* The CD47-signal regulatory protein alpha (SIRPα) interaction is a therapeutic target for human solid tumors. *Proc. Natl. Acad. Sci. U. S. A.* **109**, 6662–7 (2012).
90. Weiskopf, K. *et al.* Engineered SIRPα variants as immunotherapeutic adjuvants to anticancer antibodies. *Science* **341**, 88–91 (2013).

91. Chao, M. P. *et al.* Anti-CD47 antibody synergizes with rituximab to promote phagocytosis and eradicate non-Hodgkin lymphoma. *Cell* **142**, 699–713 (2010).
92. Zhang, M. *et al.* Anti-CD47 treatment stimulates phagocytosis of glioblastoma by M1 and M2 polarized macrophages and promotes M1 polarized macrophages in vivo. *PLoS One* **11**, 1–21 (2016).
93. Liu, X. *et al.* CD47 blockade triggers T cell-mediated destruction of immunogenic tumors. *Nat. Med.* **21**, 1209–1215 (2015).
94. Barkal, A. A. *et al.* Engagement of MHC class i by the inhibitory receptor LILRB1 suppresses macrophages and is a target of cancer immunotherapy article. *Nat. Immunol.* **19**, 76–84 (2018).
95. Cioffi, M. *et al.* Inhibition of CD47 effectively targets pancreatic cancer stem cells via dual mechanism. *Clin. Cancer Res.* **21**, 2325–37 (2015).
96. Ferrone, C. & Dranoff, G. Dual roles for immunity in gastrointestinal cancers. *J. Clin. Oncol.* **28**, 4045–4051 (2010).
97. Qian, B. Z. & Pollard, J. W. Macrophage Diversity Enhances Tumor Progression and Metastasis. *Cell* **141**, 39–51 (2010).
98. Seruga, B., Zhang, H., Bernstein, L. J. & Tannock, I. F. Cytokines and their relationship to the symptoms and outcome of cancer. *Nat. Rev. Cancer* **8**, 887–899 (2008).
99. McMillan, D. C. The systemic inflammation-based Glasgow Prognostic Score: A decade of experience in patients with cancer. *Cancer Treat. Rev.* **39**, 534–540 (2013).
100. Dreyer, S. B. *et al.* The Pretreatment Systemic Inflammatory Response is an Important Determinant of Poor Pathologic Response for Patients Undergoing Neoadjuvant Therapy for Rectal Cancer. *Ann. Surg. Oncol.* **24**, 1295–1303 (2017).
101. Hurwitz, H. I. *et al.* Randomized, double-blind, phase II study of ruxolitinib or placebo in combination with capecitabine in patients with metastatic pancreatic cancer for whom therapy with gemcitabine has failed. *J. Clin. Oncol.* **33**, 4039–4047 (2015).
102. Hurwitz, H. *et al.* JANUS 1: A phase 3, placebo-controlled study of ruxolitinib plus capecitabine in patients with advanced or metastatic pancreatic cancer (mPC) after failure or intolerance of first-line chemotherapy. *J Clin Oncol* **33**, abstr TPS4147 (2015).
103. Templeton, A. J. *et al.* Prognostic role of neutrophil-to-lymphocyte ratio in solid tumors: A systematic review and meta-analysis. *J. Natl. Cancer Inst.* **106**, (2014).
104. Chua, W., Charles, K. A., Baracos, V. E. & Clarke, S. J. Neutrophil/lymphocyte ratio predicts chemotherapy outcomes in patients with advanced colorectal cancer. *Br. J. Cancer* **104**, 1288–1295 (2011).
105. Kaneko, M. *et al.* Elevated neutrophil to lymphocyte ratio predicts poor prognosis in advanced colorectal cancer patients receiving oxaliplatin-based chemotherapy. *Oncol.* **82**, 261–268 (2012).
106. Ojerholm, E. *et al.* Neutrophil-to-lymphocyte ratio as a bladder cancer biomarker: Assessing prognostic and predictive value in SWOG 8710. *Cancer* **123**, 794–801 (2017).
107. Galon, J. Type, Density, and Location of Immune Cells Within Human Colorectal

- Tumors Predict Clinical Outcome. *Science* (80-.). **313**, 1960–1964 (2006).
108. Galon, J. *et al.* Cancer classification using the Immunoscore: a worldwide task force. *J. Transl. Med.* **10**, 205 (2012).
 109. Mlecnik, B. *et al.* Integrative Analyses of Colorectal Cancer Show Immunoscore Is a Stronger Predictor of Patient Survival Than Microsatellite Instability. *Immunity* **44**, 698–711 (2016).
 110. Tumeh, P. C. *et al.* PD-1 blockade induces responses by inhibiting adaptive immune resistance. *Nature* **515**, 568–571 (2014).
 111. Beatty, G. L. Overcoming Therapeutic Resistance by Targeting Cancer Inflammation. *ASCO Educational B.* 168–173 (2016). doi:10.14694/EDBK_158948
 112. Namboodiri Mohan M, H. C. W. T. M. J. Aspirin use and reduced risk for fatal colon cancer. *NEJM* **325**, 1593–1596 (1991).
 113. Burn, J. *et al.* Long-term effect of aspirin on cancer risk in carriers of hereditary colorectal cancer: An analysis from the CAPP2 randomised controlled trial. *Lancet* **378**, 2081–2087 (2011).
 114. Ait Ouakrim, D. *et al.* Aspirin, Ibuprofen, and the Risk of Colorectal Cancer in Lynch Syndrome. *J. Natl. Cancer Inst.* **107**, 1–11 (2015).
 115. Rothwell, P. M. *et al.* Effect of daily aspirin on long-term risk of death due to cancer: Analysis of individual patient data from randomised trials. *Lancet* **377**, 31–41 (2011).
 116. Terry, M. B., Gammon, M. D., Teitelbaum, S. L., Britton, J. A. & Neugut, A. I. Association of Frequency and Duration With Breast Cancer Risk. *JAMA* **291**, 2433–2440 (2004).
 117. Bains, S. J. *et al.* Aspirin as secondary prevention in patients with colorectal cancer: An unselected population-based study. *J. Clin. Oncol.* **34**, 2501–2508 (2016).
 118. Arber, N. *et al.* Celecoxib for the prevention of colorectal adenomatous polyps. *N. Engl. J. Med.* **355**, 885–95 (2006).
 119. Bertagnolli, M. M. *et al.* Five-year efficacy and safety analysis of the adenoma prevention with celecoxib trial. *Cancer Prev. Res.* **2**, 310–321 (2009).
 120. Steinbach, G. *et al.* The effect of celecoxib, a cyclooxygenase-2 inhibitor, in familial adenomatous polyposis. *N. Engl. J. Med.* **342**, 1946–52 (2000).
 121. Gupta, S. *et al.* NCCN guidelines@insights: Genetic/Familial High-Risk Assessment: Colorectal, version 3.2017 featured updates to the NCCN Guidelines. *JNCCN J. Natl. Compr. Cancer Netw.* **15**, 1465–1475 (2017).
 122. Jiang, H. *et al.* Targeting focal adhesion kinase renders pancreatic cancers responsive to checkpoint immunotherapy. *Nat. Med.* **22**, 851–860 (2016).
 123. Kalbasi, A. *et al.* Tumor-derived CCL2 mediates resistance to radiotherapy in pancreatic ductal adenocarcinoma. *Clin. Cancer Res.* **23**, 137–148 (2017).
 124. DeNardo, D. G. *et al.* Leukocyte complexity predicts breast cancer survival and functionally regulates response to chemotherapy. *Cancer Discov.* **1**, 54–67 (2011).
 125. Nywening, T. M. *et al.* Targeting tumour-associated macrophages with CCR2 inhibition in combination with FOLFIRINOX in patients with borderline resectable and locally advanced pancreatic cancer: a single-centre, open-label, dose-finding, non-randomised, phase 1b trial. *Lancet Oncol.* **17**, 651–662 (2016).

126. Lesina, M. *et al.* Stat3/Socs3 activation by IL-6 transsignaling promotes progression of pancreatic intraepithelial neoplasia and development of pancreatic cancer. *Cancer Cell* **19**, 456–69 (2011).
127. Nagathihalli, N. S. *et al.* Signal Transducer and Activator of Transcription 3, Mediated Remodeling of the Tumor Microenvironment Results in Enhanced Tumor Drug Delivery in a Mouse Model of Pancreatic Cancer. *Gastroenterology* **149**, 1932–1943.e9 (2015).
128. Ireland, L. *et al.* Chemoresistance in pancreatic cancer is driven by stroma-derived insulin-like growth factors. *Cancer Res.* **76**, 6851–6863 (2016).
129. Beatty, G. L. & Gladney, W. L. Immune escape mechanisms as a guide for cancer immunotherapy. *Clin. Cancer Res.* **21**, 687–692 (2015).
130. Topalian, S. L., Drake, C. G. & Pardoll, D. M. Immune checkpoint blockade: A common denominator approach to cancer therapy. *Cancer Cell* **27**, 451–461 (2015).
131. Munn, D. H. & Mellor, A. L. IDO in the Tumor Microenvironment: Inflammation, Counter-Regulation, and Tolerance. *Trends Immunol.* **37**, 193–207 (2016).
132. Long, K. B. & Beatty, G. L. Harnessing the antitumor potential of macrophages for cancer immunotherapy. *Oncoimmunology* **2**, e26860 (2013).
133. Llosa, N. J. *et al.* The vigorous immune microenvironment of microsatellite instable colon cancer is balanced by multiple counter-inhibitory checkpoints. *Cancer Discov.* **5**, 43–51 (2015).
134. Kusmartsev, S. *et al.* All- trans -Retinoic Acid Eliminates Immature Myeloid Cells from Tumor-bearing Mice and Improves the Effect of Vaccination All- trans -Retinoic Acid Eliminates Immature Myeloid Cells from Tumor-bearing Mice and Improves the Effect of Vaccination. 4441–4449 (2003).
135. Ding, Z. C. *et al.* Immunosuppressive myeloid cells induced by chemotherapy attenuate antitumor cd4 t-cell responses through the PD-1-PD-L1 axis. *Cancer Res.* **74**, 3441–3453 (2014).
136. Zhu, Y. *et al.* CSF1/CSF1R blockade reprograms tumor-infiltrating macrophages and improves response to T-cell checkpoint immunotherapy in pancreatic cancer models. *Cancer Res.* **74**, 5057–5069 (2014).
137. Kimura, T. *et al.* MUC1 vaccine for individuals with advanced adenoma of the colon: A cancer immunoprevention feasibility study. *Cancer Prev. Res.* **6**, 18–26 (2013).
138. Topalian, S. L., Taube, J. M., Anders, R. A. & Pardoll, D. M. Mechanism-driven biomarkers to guide immune checkpoint blockade in cancer therapy. *Nat. Rev. Cancer* **16**, 275–287 (2016).
139. Ying, H. *et al.* Oncogenic Kras maintains pancreatic tumors through regulation of anabolic glucose metabolism. *Cell* **149**, 656–70 (2012).
140. Ying, H. *et al.* PTEN is a major tumor suppressor in pancreatic ductal adenocarcinoma and regulates an NF- κ B-cytokine network. *Cancer Discov.* **1**, 158–169 (2011).
141. Yu, H., Pardoll, D. & Jove, R. STATs in cancer inflammation and immunity: A leading role for STAT3. *Nat. Rev. Cancer* **9**, 798–809 (2009).
142. Spear, P., Barber, A., Rynda-Apple, A. & Sentman, C. L. Chimeric Antigen

- Receptor T Cells Shape Myeloid Cell Function within the Tumor Microenvironment through IFN- and GM-CSF. *J. Immunol.* **188**, 6389–6398 (2012).
143. Crusz, S. M. & Balkwill, F. R. Inflammation and cancer: Advances and new agents. *Nat. Rev. Clin. Oncol.* **12**, 584–596 (2015).
 144. Chao, M. P., Majeti, R. & Weissman, I. L. Programmed cell removal: A new obstacle in the road to developing cancer. *Nat. Rev. Cancer* **12**, 58–67 (2012).
 145. Sockolosky, J. T. *et al.* Durable antitumor responses to CD47 blockade require adaptive immune stimulation. *Proc. Natl. Acad. Sci.* **113**, E2646–E2654 (2016).
 146. Colegio, O. R. *et al.* Functional polarization of tumour-associated macrophages by tumour-derived lactic acid. *Nature* (2014).
 147. Pyonteck, S. M. *et al.* CSF-1R inhibition alters macrophage polarization and blocks glioma progression. *Nat. Med.* **19**, 1264–72 (2013).
 148. Guerriero, J. L. *et al.* Class IIa HDAC inhibition reduces breast tumours and metastases through anti-tumour macrophages. *Nature* **543**, 428–432 (2017).
 149. Oldenborg, P.-A., Gresham, H. D. & Lindberg, F. P. Cd47-Signal Regulatory Protein α (Sirp α) Regulates Fc γ and Complement Receptor-Mediated Phagocytosis. *J. Exp. Med.* **193**, 855–862 (2001).
 150. Chen, J. *et al.* SLAMF7 is critical for phagocytosis of haematopoietic tumour cells via Mac-1 integrin. *Nature* **544**, 493–497 (2017).
 151. Xue, J. *et al.* Transcriptome-Based Network Analysis Reveals a Spectrum Model of Human Macrophage Activation. *Immunity* **40**, 274–288 (2014).
 152. Liu, P.-S. *et al.* A-Ketoglutarate Orchestrates Macrophage Activation Through Metabolic and Epigenetic Reprogramming. *Nat. Immunol.* (2017). doi:10.1038/ni.3796
 153. Vats, D. *et al.* Oxidative metabolism and PGC-1 β attenuate macrophage-mediated inflammation. *Cell Metab.* **4**, 13–24 (2006).
 154. Herber, D. L. *et al.* Lipid accumulation and dendritic cell dysfunction in cancer. *Nat. Med.* **16**, 880–6 (2010).
 155. Kelly, B. & O'Neill, L. A. Metabolic reprogramming in macrophages and dendritic cells in innate immunity. *Cell Res.* **25**, 771–84 (2015).
 156. Sastry, P. S. & Hokin, L. E. Studies on the role of phospholipids in phagocytosis. *J. Biol. Chem.* **241**, 3354–3361 (1966).
 157. Lokesh, BR; Wrann, M. Incorporation of palmitic acid or oleic acid into macrophage membrane lipids exerts differential effects on the function of normal mouse peritoneal macrophages. *Biochim. Biophys. Acta* **792**, 141–148 (1984).
 158. Hingorani, S. R. *et al.* Trp53R172H and KrasG12D cooperate to promote chromosomal instability and widely metastatic pancreatic ductal adenocarcinoma in mice. *Cancer Cell* **7**, 469–83 (2005).
 159. Behrens, E. M. *et al.* Repeated TLR9 stimulation results in macrophage activation syndrome-like disease in mice. *J. Clin. Invest.* **121**, 2264–2277 (2011).
 160. Beatty, G. L. *et al.* Exclusion of T Cells From Pancreatic Carcinomas in Mice Is Regulated by Ly6C^{low} F4/80⁺ Extratumoral Macrophages. *Gastroenterology* **149**, 201–210 (2015).
 161. Harshan, K. V & Gangadharam, P. R. In vivo depletion of natural killer cell

- activity leads to enhanced multiplication of *Mycobacterium avium* complex in mice. *Infect. Immun.* **59**, 2818–21 (1991).
162. Jung, S. *et al.* In vivo depletion of CD11c+dendritic cells abrogates priming of CD8+T cells by exogenous cell-associated antigens. *Immunity* **17**, 211–220 (2002).
 163. Sanford, D. E. *et al.* Inflammatory monocyte mobilization decreases patient survival in pancreatic cancer: A role for targeting the CCL2/CCR2 axis. *Clin. Cancer Res.* **19**, 3404–3415 (2013).
 164. Sabatel, C. *et al.* Exposure to Bacterial CpG DNA Protects from Airway Allergic Inflammation by Expanding Regulatory Lung Interstitial Macrophages. *Immunity* **46**, 457–473 (2017).
 165. Jaiswal, S. *et al.* CD47 is upregulated on circulating hematopoietic stem cells and leukemia cells to avoid phagocytosis. *Cell* **138**, 271–85 (2009).
 166. Mitchem, J. B. *et al.* Targeting tumor-infiltrating macrophages decreases tumor-initiating cells, relieves immunosuppression, and improves chemotherapeutic responses. *Cancer Res.* **73**, 1128–41 (2013).
 167. Biswas, S. K. Metabolic Reprogramming of Immune Cells in Cancer Progression. *Immunity* **43**, 435–449 (2015).
 168. Lee, J. G. *et al.* A combination of Lox-1 and Nox1 regulates TLR9-mediated foam cell formation. *Cell. Signal.* **20**, 2266–2275 (2008).
 169. LI, K. *et al.* Effects of CpG-ODN on gene expression in formation of foam cells. *Acta Pharmacol. Sin.* **26**, 1359–1364 (2005).
 170. Leidi, M. *et al.* M2 Macrophages Phagocytose Rituximab-Opsonized Leukemic Targets More Efficiently than M1 Cells In Vitro. *J. Immunol.* **182**, 4415–4422 (2009).
 171. Han, C. Z. & Ravichandran, K. S. Metabolic connections during apoptotic cell engulfment. *Cell* **147**, 1442–1445 (2011).
 172. Chang, C. H. *et al.* Metabolic Competition in the Tumor Microenvironment Is a Driver of Cancer Progression. *Cell* **162**, 1229–1241 (2015).
 173. Swamy, M. *et al.* A Cholesterol-Based Allosteric Model of T Cell Receptor Phosphorylation. *Immunity* **44**, 1091–1101 (2016).
 174. Ha, B. *et al.* ‘Clustering’ SIRP α into the Plasma Membrane Lipid Microdomains Is Required for Activated Monocytes and Macrophages to Mediate Effective Cell Surface Interactions with CD47. *PLoS One* **8**, 1–13 (2013).
 175. Heinz, L. X. *et al.* The Lipid-Modifying Enzyme SMPDL3B Negatively Regulates Innate Immunity. *Cell Rep.* **11**, 1919–1928 (2015).
 176. Köberlin, M. S. *et al.* A Conserved Circular Network of Coregulated Lipids Modulates Innate Immune Responses. *Cell* **162**, 170–183 (2015).
 177. Ishii, M. *et al.* Epigenetic regulation of the alternatively activated macrophage phenotype Epigenetic regulation of the alternatively activated macrophage phenotype. **114**, 3244–3254 (2013).
 178. Novakovic, B. *et al.* β -Glucan Reverses the Epigenetic State of LPS-Induced Immunological Tolerance. *Cell* **167**, 1354–1368.e14 (2016).
 179. McDonnell, E. *et al.* Lipids Reprogram Metabolism to Become a Major Carbon Source for Histone Acetylation. *Cell Rep.* **17**, 1463–1472 (2016).

180. Covarrubias, A. J. *et al.* Akt-mTORC1 signaling regulates Acly to integrate metabolic input to control of macrophage activation. *Elife* **5**, 1–19 (2016).
181. Krieg, A. M. Review series Development of TLR9 agonists for cancer therapy. **117**, (2007).
182. Manegold, C. *et al.* Randomized phase II trial of a toll-like receptor 9 agonist oligodeoxynucleotide, PF-3512676, in combination with first-line taxane plus platinum chemotherapy for advanced-stage non-small-cell lung cancer. *J. Clin. Oncol.* **26**, 3979–3986 (2008).
183. Oligodeoxynucleotide, B. C. *et al.* Induction of Systemic T H 1-Like Innate Immunity in Normal Volunteers Following Subcutaneous but Not Intravenous Administration of CPG 7909 , a Synthetic. **27**, 460–471 (2004).
184. Zent, C. S. *et al.* Phase I clinical trial of CpG oligonucleotide 7909 (PF-03512676) in patients with previously treated chronic lymphocytic leukemia. *Leuk. Lymphoma* **53**, 211–217 (2012).
185. Flannagan, R. S., Jaumouillé, V. & Grinstein, S. The Cell Biology of Phagocytosis. *Annu. Rev. Pathol. Mech. Dis.* **7**, 61–98 (2012).
186. Roberts, A. W. *et al.* Tissue-Resident Macrophages Are Locally Programmed for Silent Clearance of Apoptotic Cells. *Immunity* **47**, 913–927.e6 (2017).
187. Burdette, D. L. *et al.* STING is a direct innate immune sensor of cyclic di-GMP. *Nature* **478**, 515–518 (2011).
188. Ishikawa, H. & Barber, G. N. STING is an endoplasmic reticulum adaptor that facilitates innate immune signalling. *Nature* **455**, 674–678 (2008).
189. Chen, Q., Sun, L. & Chen, Z. J. Regulation and function of the cGAS-STING pathway of cytosolic DNA sensing. *Nat. Immunol.* **17**, 1142–1149 (2016).
190. Ahn, J., Xia, T., Rabasa Capote, A., Betancourt, D. & Barber, G. N. Extrinsic Phagocyte-Dependent STING Signaling Dictates the Immunogenicity of Dying Cells. *Cancer Cell* **33**, 862–873.e5 (2018).
191. Scott, R. S. *et al.* Phagocytosis and clearance of apoptotic cells is mediated by MER. *Nature* **411**, 207–211 (2001).
192. Zagórska, A., Través, P. G., Lew, E. D., Dransfield, I. & Lemke, G. Diversification of TAM receptor tyrosine kinase function. *Nat. Immunol.* **15**, (2014).
193. Ifrim, D. C. *et al.* Trained immunity or tolerance: Opposing functional programs induced in human monocytes after engagement of various pattern recognition receptors. *Clin. Vaccine Immunol.* **21**, 534–545 (2014).
194. Weaver, L. K., Chu, N. & Behrens, E. M. TLR9-mediated inflammation drives a Ccr2-independent peripheral monocytopoiesis through enhanced extramedullary monocytopoiesis. *Proc. Natl. Acad. Sci.* **113**, 10944–10949 (2016).
195. Wherry, E. J. T cell exhaustion. *Nat. Immunol.* **12**, 492–499 (2011).
196. Wherry, E. J. *et al.* Molecular Signature of CD8+T Cell Exhaustion during Chronic Viral Infection. *Immunity* **27**, 670–684 (2007).
197. Gordon, S. R. *et al.* PD-1 expression by tumour-associated macrophages inhibits phagocytosis and tumour immunity. *Nature* **545**, 495–499 (2017).
198. Victor, C. T.-S. *et al.* Radiation and dual checkpoint blockade activate non-redundant immune mechanisms in cancer. *Nature* (2015).

doi:10.1038/nature14292

199. Tseng, D. *et al.* Anti-CD47 antibody-mediated phagocytosis of cancer by macrophages primes an effective antitumor T-cell response. *Proc. Natl. Acad. Sci. U. S. A.* **110**, 11103–8 (2013).
200. Zhang, H. *et al.* HIF-1 regulates CD47 expression in breast cancer cells to promote evasion of phagocytosis and maintenance of cancer stem cells. *Proc. Natl. Acad. Sci.* **112**, E6215–E6223 (2015).
201. Casazza, A. *et al.* Article Impeding Macrophage Entry into Hypoxic Tumor Areas by Sema3A / Nrp1 Signaling Blockade Inhibits Angiogenesis and Restores Antitumor Immunity. *Cancer Cell* **24**, 695–709 (2013).
202. Mazziere, R. *et al.* Targeting the ANG2/TIE2 Axis Inhibits Tumor Growth and Metastasis by Impairing Angiogenesis and Disabling Rebounds of Proangiogenic Myeloid Cells. *Cancer Cell* **19**, 512–526 (2011).
203. Colegio, O. R. *et al.* Functional polarization of tumour-associated macrophages by tumour-derived lactic acid. *Nat. ...* **513**, 559–563 (2014).
204. Kortylewski, M. *et al.* In vivo delivery of siRNA to immune cells by conjugation to a TLR9 agonist enhances antitumor immune responses. *Nat. Biotechnol.* **27**, 925–932 (2009).
205. Schettini, J. *et al.* Intratumoral delivery of CpG-conjugated anti-MUC1 antibody enhances NK cell anti-tumor activity. *Cancer Immunol. Immunother.* **61**, 2055–2065 (2012).
206. Happel, C. *et al.* Pulmonary transplantation of macrophage progenitors as effective and long-lasting therapy for hereditary pulmonary alveolar proteinosis. *Sci. Transl. Med.* **6**, (2014).
207. Suzuki, T. *et al.* Pulmonary macrophage transplantation therapy. *Nature* **514**, 450–454 (2014).
208. Pollock, J. D. *et al.* Mouse model of X-linked chronic granulomatous disease, an inherited defect in phagocyte superoxide production. *Nat. Genet.* **9**, 202–209 (1995).
209. Morgenstern, D. E., Gifford, M. a, Li, L. L., Doerschuk, C. M. & Dinauer, M. C. Absence of respiratory burst in X-linked chronic granulomatous disease mice leads to abnormalities in both host defense and inflammatory response to *Aspergillus fumigatus*. *J. Exp. Med.* **185**, 207–218 (1997).
210. Wei, S., Dai, X.-M. & Stanley, E. R. Transgenic expression of CSF-1 in CSF-1 receptor-expressing cells leads to macrophage activation, osteoporosis, and early death. *J. Leukoc. Biol.* **80**, 1445–53 (2006).
211. Streit, W. J. & Graeber, M. B. & Kreutzberg, G. W. Functional plasticity of microglia: A review. *Glia* **1**, 301–307 (1988).
212. Janda, E., Boi, L. & Carta, A. R. Microglial Phagocytosis and Its Regulation: A Therapeutic Target in Parkinson’s Disease? *Front. Mol. Neurosci.* **11**, 144 (2018).
213. Mali, P. *et al.* RNA-Guided Human Genome Engineering via Cas9 Prashant. *Science (80-.)*. **339**, 823–826 (2013).
214. Renier, N. *et al.* Inhibition of fatty acid oxidation as a therapy for MYC-overexpressing triple-negative breast cancer. **165**, 1789–1802 (2017).
215. Snyder, N. W. *et al.* Production of stable isotope-labeled acyl-coenzyme A

- thioesters by yeast stable isotope labeling by essential nutrients in cell culture. *Anal. Biochem.* **474**, 59–65 (2015).
216. Frey, A. J. *et al.* LC-quadrupole/Orbitrap high-resolution mass spectrometry enables stable isotope-resolved simultaneous quantification and ¹³C-isotopic labeling of acyl-coenzyme A thioesters. *Anal. Bioanal. Chem.* **408**, 3651–3658 (2016).
 217. Trefely, S., Ashwell, P. & Snyder, N. W. FluxFix: automatic isotopologue normalization for metabolic tracer analysis. *BMC Bioinformatics* **17**, 485 (2016).
 218. Basu, S. S. & Blair, I. A. SILEC: a protocol for generating and using isotopically labeled coenzyme A mass spectrometry standards. *Nat. Protoc.* **7**, 1–12 (2011).